

AD-A113 644

SINGER CO FAIRFIELD NJ KEARFOTT DIV

F/G 17/7

NEW SENSOR CONCEPTS: LOW COST VIBRATING BEAM ACCELEROMETER.(U)

DEC 81 W C ALBERT

F33615-80-C-1218

UNCLASSIFIED

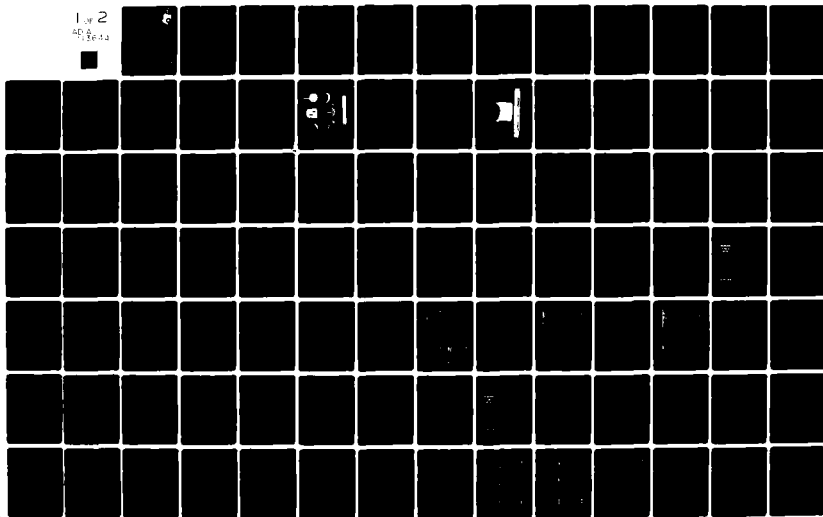
KD-81-27

AFWAL-TR-81-1229

NL

1 of 2

AD-A113 644



AD A113644

AFWAL-TR-81-1229



NEW SENSOR CONCEPTS

LOW COST VIBRATING BEAM ACCELEROMETER

Author: W. C. Albert

The Singer Company
Kearfott Division
1150 McBride Ave.
Little Falls, NJ 07424

December 1981

Final Report for Period September 1980 to
September 1981

Approved for public release; distribution unlimited

DTIC FILE COPY

AVIONICS LABORATORY
AIR FORCE WRIGHT AERONAUTICAL LABORATORIES
AIR FORCE SYSTEMS COMMAND
WRIGHT-PATTERSON AFB OH 45433

DTIC
ELECTE
S APR 21 1982 D
D

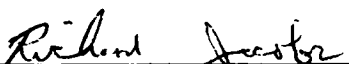
82 04 21 065

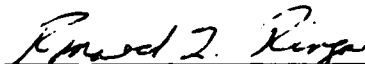
NOTICE

When Government drawings, specifications, or other data are used for any purpose other than in connection with a definitely related Government procurement operation, the United States Government thereby incurs no responsibility nor any obligation whatsoever; and the fact that the government may have formulated, furnished, or in any way supplied the said drawings, specifications, or other data, is not to be regarded by implication or otherwise as in any manner licensing the holder or any other person or corporation, or conveying any rights or permission to manufacture use, or sell any patented invention that may in any way be related thereto.

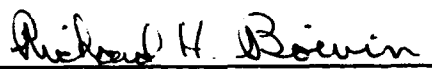
This report has been reviewed by the Office of Public Affairs (ASD/PA) and is releasable to the National Technical Information Service (NTIS). At NTIS, it will be available to the general public, including foreign nations.

This technical report has been reviewed and is approved for publication.


RICHARD W. JACOBS, Project Engineer
Reference Systems Technology Group
Reference Systems Branch


RONALD L. RINGO, Chief
Reference Systems Branch
System Avionics Division

FOR THE COMMANDER


RICHARD H. BOIVIN, Colonel, USAF
Chief, System Avionics Division
Avionics Laboratory

"If your address has changed, if you wish to be removed from our mailing list, or if the addressee is no longer employed by your organization please notify AFWAL/AAAN-2, W-PAFB, OH 45433 to help us maintain a current mailing list."

Copies of this report should not be returned unless return is required by security considerations, contractual obligations, or notice on a specific document.

Unclassified

SECURITY CLASSIFICATION OF THIS PAGE (When Data Entered)

REPORT DOCUMENTATION PAGE		READ INSTRUCTIONS BEFORE COMPLETING FORM
1. REPORT NUMBER AFWAL-TR-81-1229	2. GOVT ACCESSION NO. DA113 644	3. RECIPIENT'S CATALOG NUMBER
4. TITLE (and Subtitle) New Sensor Concepts Low Cost Vibrating Beam Accelerometer		5. TYPE OF REPORT & PERIOD COVERED Final Report 9/80 to 9/81
7. AUTHOR(s) W. C. Albert		6. PERFORMING ORG. REPORT NUMBER KD-81-27
9. PERFORMING ORGANIZATION NAME AND ADDRESS The Singer Co. - Kearfott Div. 90 New Dutch Lane Fairfield, NJ 07006		8. CONTRACT OR GRANT NUMBER(s) F33615-80-C-1218
11. CONTROLLING OFFICE NAME AND ADDRESS Air Force Systems Command Aeronautical Systems Div./PMREP Wright Patterson AFB, Ohio 45433		10. PROGRAM ELEMENT, PROJECT, TASK AREA & WORK UNIT NUMBERS 6095 12 24
14. MONITORING AGENCY NAME & ADDRESS (if different from Controlling Office)		12. REPORT DATE December 1981
		13. NUMBER OF PAGES 127
		15. SECURITY CLASS. (of this report) Unclassified
		15a. DECLASSIFICATION/DOWNGRADING SCHEDULE
16. DISTRIBUTION STATEMENT (of this Report) Approved for public release; distribution unlimited		
17. DISTRIBUTION STATEMENT (of the abstract entered in Block 20, if different from Report)		
18. SUPPLEMENTARY NOTES		
19. KEY WORDS (Continue on reverse side if necessary and identify by block number) Accelerometer - inertial guidance systems Strapdown - digital output - quartz crystal		
20. ABSTRACT (Continue on reverse side if necessary and identify by block number) Engineering model accelerometers have been assembled and tested to assess their potential for use in future strapped down inertial systems. The accelerometer concept investigated uses vibrating quartz crystal beams as the basic force sensing element. This concept has an inherent digital output and the potential for meeting the performance goals of bias stability of less than 100ug, scale factor stability less than 100ppm, input range at least 10g, bias temperature sensitivity on the order of 1ug/°C		

DD FORM 1 JAN 73 1473

EDITION OF 1 NOV 65 IS OBSOLETE i

Unclassified

SECURITY CLASSIFICATION OF THIS PAGE (When Data Entered)

20. (Continued)

and scale factor temperature sensitivity on the order of 1ppm/°C. The accelerometer mechanization utilizes two force sensing crystals in a push pull arrangement to enhance the scale factor and cancel non-linear and thermal effects. Test data on engineering units is presented and recommendations for future development tasks are made.

PREFACE

This report documents the development work conducted under USAF Contract No. F33615-80-C-1218 during the period September, 1980 to September, 1981. The work was performed by The Singer Company - Kearfott Division, of Little Falls, New Jersey under the direction of W.C. Albert. The work was performed for the Air Force Systems Command, Aeronautical Systems Division/PMREP Wright Patterson AFB, Ohio with Mr. R. Jacobs serving as contract monitor.

Accession For		
NTIS	GRA&I	<input checked="" type="checkbox"/>
DTIC	TAB	<input type="checkbox"/>
Unannounced		<input type="checkbox"/>
Justification		
By		
Distribution/		
Availability Codes		
Dist	Avail and/or Special	
A		



TABLE OF CONTENTS

	<u>PARAGRAPH</u>	<u>PAGE</u>
Section I - Introduction and Summary		1
Background	1	1
Performance Goals and Accomplishment Summary	2	2
Section II - VBA Basic Operation		3
Basic Mechanization	1	3
Vibrating Beam Force Transducer (Resonator)	2	3
Dual Beam VBA Mechanization	3	3
Section III - Low Cost VBA Design Approach		6
VBA Technology Baseline	1	6
Low-Cost Tactical VBA Approach	2	6
Increased Sensitivity	3	6
Proof Mass Damping Mechanism	4	7
Compliant Resonator	5	7
Accelerometer Design Approach	6	10
Section IV - Test Results		13
Nominal Bias and Scale Factor	1	13
Bias Stability	2	13
Bias Thermal Sensitivity	3	16
Scale Factor Stability	4	16
Scale Factor Temperature Sensitivity	5	20
Nonlinearity	6	20
Alignment Stability	7	21
Vibration Tests	8	21
Resonator-Gas Effects	9	24
Section V - Oscillator Electronics		26
Background	1	26
Design Approach	2	26
Theory of Operation	3	26
Temperature Compensation	4	28
Experimental Results	5	32
Recommended Future Activities	6	32
Section VI - VBA Reliability/Maintainability Prediction		34
Introduction	1	34
Results and Conclusions	2	34
Discussion	3	34
Section VII - Future Development Areas		40
Glass Frit	1	40
All-Welded Assembly	2	40
Gas Damping	3	40
Miniaturization	4	40
Hybrid Oscillator	5	42
Resonator Geometry Improvement	6	42
Finite Element Analysis	7	42
Non-Prismal Resonator Geometry	8	42
Linearity Improvement	9	42

TABLE OF CONTENTS (Cont'd)

	<u>PARAGRAPH</u>	<u>PAGE</u>
Appendix A - Vibrating Flexure Beam in Tension Math Model		44
Introduction	1	47
Beam Analysis Considering Flexure, Tension & Linear	2	48
Appendix B - Squeeze Film Gas Damping for the Low Cost VBA		68
Introduction	1	71
Damping Gap Design	2	72
Frequency Effects of Squeeze Film Damping	3	75
Conclusions	4	80
References	5	81
Appendix C - Resonator Mode Frequency Analysis		82
Appendix D - Dual Beam VBA Four Position Test		85
Appendix E - Bias Temperature Sensitivity Model		88
Appendix F - Dual Beam VBA Cross Axis Sensitivity		91
Appendix G - Low Cost VBA - Parabolic Temperature Compensation		94

LIST OF ILLUSTRATIONS

<u>Figure No.</u>	<u>Title</u>	<u>Page No.</u>
1	Schematic of Dual Beam VBA Approach	4
2	Damping Gap Geometry Schematic	8
3	Breadboard Accelerometer Piece Parts	9
4	Assembled Breadboard Accelerometer	12
5	Low Cost VBA Short Term Bias Stability Individual Resonator	14
6	Low Cost VBA Individual Resonator and Difference Frequency	15
7	Low Cost VBA Bias Stability	17
8	Bias Temperature Sensitivity Compensation Experiment	18
9	Low Cost VBA Vibration Test	22
10	Transmissibility vs Absolute Pressure for Various Gases	23
11	Resonator Gas Effects	25
12	Barkhausen's Criterion for S.S. Oscillation	27
13	Saturating Oscillator Schematic	27
14	Low Cost VBA Brassboard Schematic	29
15	Glass Frit Joint	41

APPENDIX A

2-1	Beam Deflection Curves For Modes 1 through 5	49
2-2	Mode 1 Characteristics	53
2-3	Mode 2 Characteristics	55
2-4	Mode 3 Characteristics	57
2-5	Bending Moment Effect	58
2-6	Tension Effect	59
2-7	Linear Momentum Effect	60

APPENDIX B

2-1	Second Order System	72
2-2	Damping Mechanism	73
3-1	Gas Spring Effects	75
3-2	Gas Spring Effects on Coefficients	78
3-3	Gas Spring Effects on Transmissibility	79

APPENDIX D

D-1	Dual Beam VBA 4 Position Test	86
-----	-------------------------------	----

APPENDIX E

E-1	Resonator Bias Frequency vs Temperature	88
-----	---	----

APPENDIX F

F-1	Dual Beam VBA Cross Axis Sensitivity	92
-----	--------------------------------------	----

LIST OF TABLES

<u>Table No.</u>	<u>Title</u>	<u>Page No.</u>
1	Reliability Prediction Analysis Results for Single VBA	35
2	Parts and (Failure Rate) Source of Data	36
3	Environment - Airborne, Inhab, FTR	37
4	Environment - Airborne, Uninhab, FTR	38

APPENDIX A

2-1	Boundary Conditions for Modes of Operation	50
2-2	Mode 1 Characteristic	52
2-3	Mode 2 Characteristics	54
2-4	Mode 3 Characteristics	56
2-5	Integral Values	64
2-6	Coefficients of Equation	65
2-7	Beam Frequency-Tension Coefficients	67

SECTION I INTRODUCTION AND SUMMARY

1. BACKGROUND

This document is the final report of contract F33615-80-C-1218, NEW SENSOR CONCEPTS. The objective of this effort was to assess the feasibility of promising new strapdown inertial sensors, using innovative approaches. The scope of the effort included theoretical and experimental investigations, laboratory experiments, the building and testing of breadboard accelerometers and recommendations for further work needed to improve the potential of the concept.

This program focused on developing an accelerometer which utilizes force-sensitive vibrating quartz beams as the basic sensing elements. This approach results in a device that is virtually a solid state accelerometer with an inherent digital output. The sensor also has good potential for low cost.

The Kearfott approach in the application of quartz crystals to accelerometers has been to use flexure-mode resonators in a beam configuration. The behavior of a vibrating beam in tension is somewhat like a string in tension; an increase in tension will cause the resonant frequency to increase. The beam, however, has several advantages over the string:

- requires no bias tension
- responds to compression
- frequency change with tension is more linear than the string
- achieves usable full-scale force induced frequency change of up to $\pm 10\%$ resulting in high instrument scale factor
- scale factor temperature sensitivity less than $10 \text{ ppm}/^{\circ}\text{C}$
- predictable and hence modelable temperature sensitivity, an advantage for heaterless operation over wide temperature range.

In an accelerometer application, the crystal resonator and oscillator circuit replaces the torquer coils, torquer magnets, pickoff and capture electronics of a conventional force rebalance accelerometer. This results in the following advantages:

- the accelerometer becomes virtually solid-state
- the mechanical assembly becomes very simple for low cost and high reliability
- the electronics (oscillator) becomes very simple for low cost, low power and high reliability with an inherently digital output (no pulse capture or A/D conversion)
- higher performance-to-cost ratio per acceleration sensing channel.

The most successful applications of the quartz vibrating beam have been the High Accuracy Vibrating Beam Accelerometer (VBA), for strategic missile and gravity measurement applications, and a commercially available pressure sensor. In each of the above applications the force-sensitive crystal technology, which is about 15 years old, is successfully competing against the conventional electromagnetic force rebalance technology (D'Arsonval galvanometer mechanism) which is about 100 years old.

Because this force-sensitive crystal concept has been very successful in both ultraprecise as well as commercial use, its application to tactical systems, with accuracy requirements between these two extremes, appears a natural choice.

2. PERFORMANCE GOALS AND ACCOMPLISHMENT SUMMARY

Below is a goal-by-goal review of what has been accomplished and what this program indicates can be accomplished on future units.

- Bias stability: 100 μg Goal - Short term bias stabilities of less than 1 μg have been demonstrated. Long term stability is currently limited by trending, but we recommended several ways to eliminate this trending and achieve 100 μg long term stability.
- Bias Temperature Sensitivity: 1 $\mu\text{g}/^{\circ}\text{C}$ (0°C to 60°C) Goal - Unmodeled bias temperature sensitivity of 2 $\mu\text{g}/^{\circ}\text{C}$ has been demonstrated. Improvements along with modeling have the potential of achieving 1 $\mu\text{g}/^{\circ}\text{C}$ sensitivity.
- Scale Factor Linearity: 0.001% Goal - Test data and analysis indicate that a method of matching and trimming to achieve the goal appears feasible.
- Scale Factor Stability: 100 ppm Goal - Analysis and test data indicate that scale factor stability achieved is on the order of 0.1 ppm.
- Scale Factor Temperature Sensitivity: 1 ppm/ $^{\circ}\text{C}$ Goal - Scale factor temperature sensitivity on the order of 1 ppm/ $^{\circ}\text{C}$ has been achieved, however, sensitivities of 10 ppm/ $^{\circ}\text{C}$ are expected to be more typical. This sensitivity will be very repeatable and can be modeled and compensated to 1 ppm/ $^{\circ}\text{C}$.
- Dynamic Range: $\pm 10\text{ g}$ Goal - A +10 g range was easily achieved; we recommend that future units have a greater full scale input.
- Reaction Time: 1 min Goal - Accelerometer reaction is virtually instant on with an ultimate goal of no temperature control.
- Scale Factor Symmetry: 2 $\mu\text{g/g}$ Goal - The approach taken is not a pulsed device. Therefore, this requirement is not applicable.
- Threshold: 50 μg Goal - Thresholds of less than 1 μg have been demonstrated.

SECTION II VBA BASIC OPERATION

1. BASIC MECHANIZATION

The basic acceleration sensing element in the VBA is a pendulously supported proof mass constrained along its axis of freedom by a crystal vibrating beam force transducer. These transducers change their natural frequency in a highly systematic way with force; the frequency increasing with tension and decreasing with compression. The transducer is used as the resonating element in an oscillator circuit. The frequency of the oscillator is thereby a sensitive function of input acceleration.

2. VIBRATING BEAM FORCE TRANSDUCER (RESONATOR)

The behavior of a vibrating beam in tension is described in Appendix A. The analysis describes the relationship between beam geometry, material physical properties, boundary conditions and their effect on the instrument's bias frequency and frequency-force sensitivity. This behavior is most conveniently expressed as a power series used in Equations (1) through (3).

The quartz beam material has a unique combination of mechanical, chemical and thermal properties needed for frequency standards. In addition, quartz is piezoelectric which affords a very convenient way to sustain the oscillations.

The beam vibrates in flexure as a fixed-fixed beam, described analytically in Appendix A, and illustrated schematically in Figure 1.

The crystals are driven piezoelectrically by means of electrode pairs arranged to provide an electric field across the minimum dimension of the beam and induce the desired flexure stresses.

The resonators themselves are low cost items of which thousands have been manufactured. The raw material, quartz crystal, is relatively abundant, in both its natural and synthetic form, and is used extensively in the frequency control and communication industries. Machining techniques have been developed to produce them in large quantities at low cost. Many of the machining, plating, and other manufacturing processes used are similar to those used to make the quartz crystals used in wristwatches. Wristwatch crystals also vibrate in flexure in a tuning fork or free-free beam configuration. In large quantities, they cost watch manufacturers less than two dollars each.

3. DUAL BEAM VBA MECHANIZATION

A schematic representation of the dual beam VBA is presented in Figure 1.

The two beams and two proof masses used are arranged so that an input acceleration places one beam in tension and the other in compression. The VBA output is then taken as the difference frequency between the two beams.

This two-beam mechanization is described analytically by Equations (1) through (3). Note that these equations express the frequency behavior of the individual beams as a power series. The K terms are the product of the proof mass and the appropriate K terms of Table 2-7 of Appendix A.

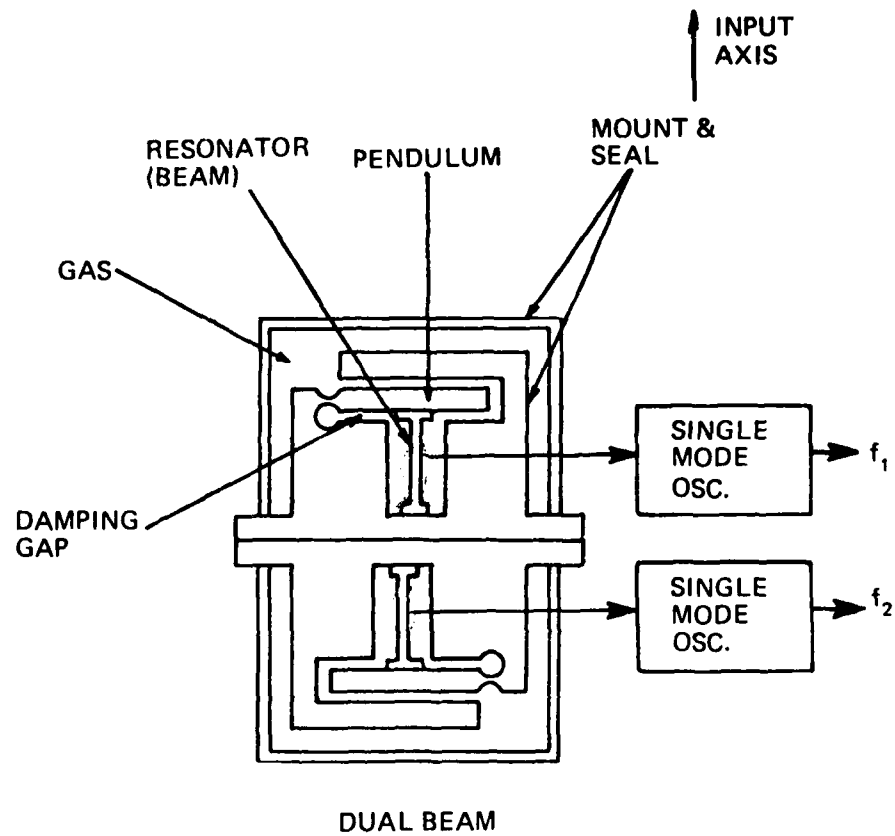


FIGURE 1. SCHEMATIC OF DUAL BEAM VBA APPROACH

BEAM 1 OUTPUT

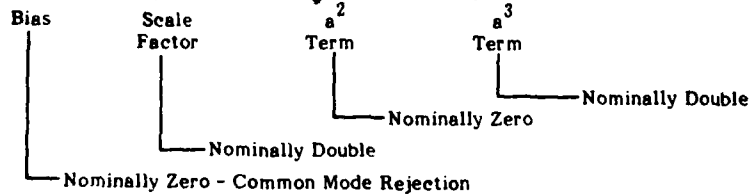
$$f_1 = K_{01} + K_{11}a + K_{21}a^2 + K_{31}a^3 \quad (1)$$

BEAM 2 OUTPUT

$$f_2 = K_{02} - K_{12}a + K_{22}a^2 - K_{32}a^3 \quad (2)$$

DIFFERENCE OUTPUT

$$f_1 - f_2 = \underbrace{K_{01} - K_{02}}_{\text{Bias}} + \underbrace{(K_{11} + K_{12})a}_{\text{Scale Factor}} + \underbrace{(K_{21} - K_{22})a^2}_{a^2 \text{ Term}} + \underbrace{(K_{31} + K_{32})a^3}_{a^3 \text{ Term}} \quad (3)$$



a = Input Acceleration

The advantages of this dual beam push-pull mechanization are:

- The difference frequency and hence accelerometer bias is low. The tolerance on the match of the individual beam K_0 will determine the bias.
- The scale factor is twice that of the individual beam scale factor.
- The difference frequency a^2 term is nominally zero to reduce vibration effects and increase linearity.
- The difference frequency a^3 term is nominally doubled, but is very small.
- Differencing results in common mode rejection to greatly reduce thermal effects.

The common mode rejection feature greatly reduces the effects of bias error sources that similarly affect the individual beams such as thermal effects. Examples of VBA data illustrate that the difference frequency is at least an order of magnitude more stable than the individual beam frequencies. This is attributed to the beams being in very close physical proximity and therefore experiencing the same environment. This residual temperature effect on bias is a result of the mismatch between individual beam temperature characteristics, kept small by careful selection of beam pairs.

The effectiveness of the common mode rejection principle is shown in Figure 2. It is obvious from this example that the randomness of the difference frequency, in equivalent input acceleration, is at least an order of magnitude less than that of the individual beams. Similar to scale factor, the residual temperature effect on bias is very predictable and therefore also modelable for heaterless operation.

SECTION III LOW COST VBA DESIGN APPROACH

1. VBA TECHNOLOGY BASELINE

Prior to this program, Kearfott had directed its development efforts toward a high accuracy VBA instrument intended for strategic applications. As a result of these efforts, Kearfott now has several capabilities applicable to the low-cost VBA:

- Force-sensitive crystal resonator design techniques were developed which make extensive use of finite element analysis.
- Quartz crystal selection, fabrication, processing, plating and testing techniques were developed.
- VBA assembly facilities and procedures were developed, including high vacuum techniques.
- VBA test procedures were developed, which included automatic data acquisition and reduction using an HP21MX Computer capable of monitoring 12 frequency signals simultaneously.

2. LOW-COST TACTICAL VBA APPROACH

Preliminary experiments and investigations indicated that the dual beam VBA had good potential for low-cost tactical applications. To realize this potential, technology development efforts were expended which:

- Increase sensitivity by using more of the beam force measuring range.
- Introduce a proof mass damping mechanism to protect the beams from shock and vibration and simplify the design.
- Develop a saturating oscillator which has the potential for low cost and high reliability.

Details on development approaches that realized these goals are described next.

3. INCREASED SENSITIVITY

The VBA, designed for high accuracy strategic applications, had no internal means of damping the beam-proof mass mechanism. Vibration protection depends on keeping the natural frequency of the beam-mass system high (>2000 Hz), and then providing an external vibration isolator with a lower (≈ 900 Hz) break frequency to assure adequate input vibration attenuation at the natural frequency. Keeping the natural frequency high was accomplished by keeping the mass of the proof mass low and keeping the axial stiffness of the beam high.

Both of these actions result in lower acceleration sensitivity since a low mass proof mass results in lower forces and a stiff beam results in lower frequency-force sensitivity.

The sensitivity of the low-cost VBA was increased by increasing the mass of proof mass. The actual amount of sensitivity increase depends on size, linearity and other considerations, but for the 10 g full scale VBA developed under this program, the factor was about 3. This resulted in a 16 g proof mass.

This increase in sensitivity will proportionately reduce thermal crystal aging and other effects on bias. However, unless measures were taken, increasing sensitivity also will decrease the natural frequency and increase susceptibility to shock and vibration. To compensate for this, a beam protection mechanism and proof mass damping mechanism was devised.

4. PROOF MASS DAMPING MECHANISM

Proof mass damping was accomplished by a squeeze-film gas gap between the proof mass and housing. This is a proven damping mechanism that has been successfully used in many accelerometers. Sufficient damping can be introduced to achieve a critical or near-critical damping ratio and the scale factor can be greatly increased. The resonant frequency of the beam-mass system can be reduced to about 300 to 400 Hz. Enough compliance can be built into the resonator so that mechanical stops can be used to protect the beam from vibration and shock overload. This gas damping approach is the most simple and results in lower cost.

The equations describing the action of a gas damping mechanism are included as Appendix B. They are for an ideal arrangement and do not account for the effects of nonsymmetry, the central resonator mounting hole or the effects of $c_1 \neq c_2$, all shown schematically in Figure 2; c_2 was made longer than c_1 because there is more motion at the c_2 point. The plan was to assemble a unit and then vibrate it with various gases and gas pressures to empirically establish a performance baseline. The initial values selected were:

Radius $R = 1.14$ cm
Gaps $c_1 = 0.00254$ cm, $c_2 = 0.00381$ cm
Beam Spring Rate $K_B = 5.77 (10^4)$ dyne/cm
Proof Mass $m = 16$ g

The performance goals were:

Natural frequency (undamped) $f_N = 300$ Hz
Damping ratio = on the order of one

Vibration test results for various gases and gas pressures are presented in Section 4.

5. COMPLIANT RESONATOR

The previous resonator designs for the high accuracy VBA are axially very stiff because of the high natural frequency requirements. For the low-cost VBA under development an entirely new resonator was needed, one that was axially compliant. The resonator design arrived at is illustrated in Figure 3. The only characteristics retained from the previous resonator designs were the vibrating beam geometry, the isolator structure and mounting structure, were completely changed. Because of mounting requirements and vibration isolation requirements, the resonator is a rather complicated structure with many degrees of freedom. If not properly designed, the vibration frequency of one of these degrees of freedom will be close to the fundamental frequency of the vibrating beam. This can cause activity dips which are a well-known effect in the crystal industry. Activity dips are characterized by a very erratic vibrational frequency and a loss in Q . The vibration isolator must also be carefully designed. The vibration isolator isolates the bending moment and shear reactions at the root of the beam, and prevents vibrational energy from escaping to the mounting surface. Excessive escaping vibrational energy will result in a decreased resonator Q . In the design of the resonator, extensive use is made of finite

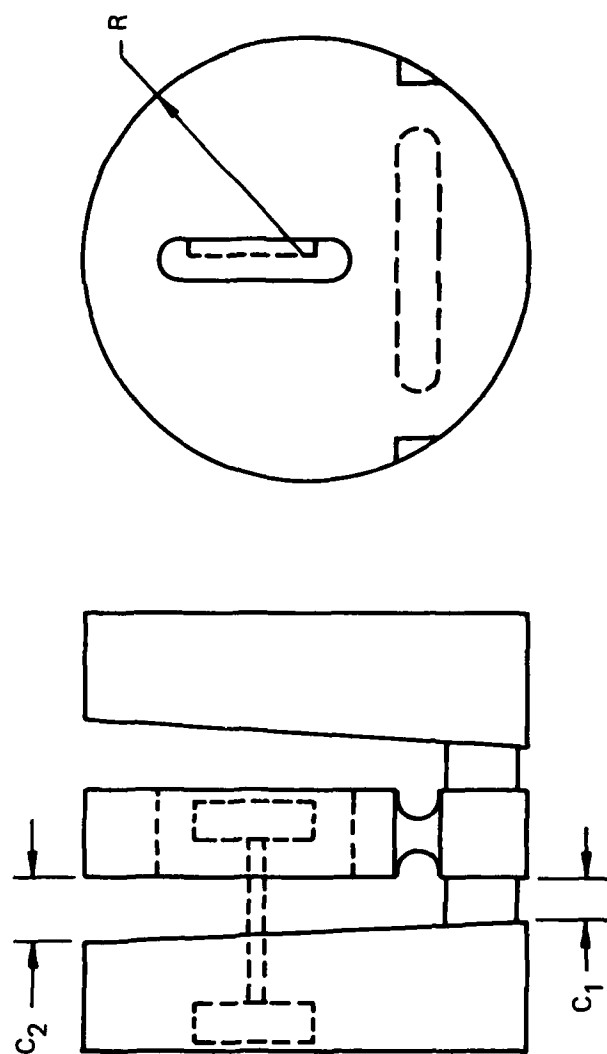


FIGURE 2. DAMPING GAP GEOMETRY SCHEMATIC

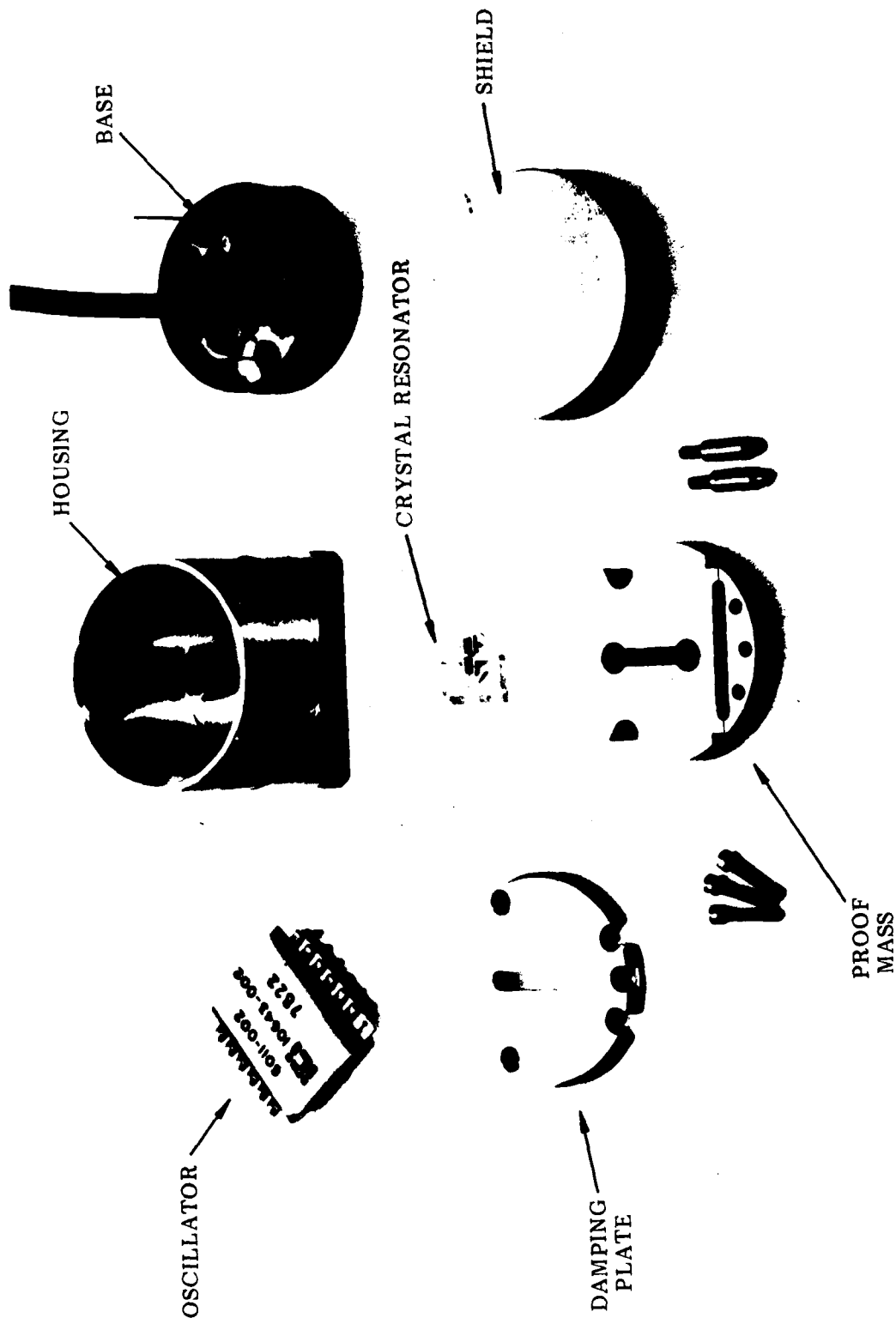


FIGURE 3. BREADBOARD ACCELEROMETER PIECE PARTS

element analysis where a candidate beam design is broken up into more than 100 separate elements. The model is then analytically subjected to an axial loading and the dimensions of the isolator springs are adjusted to obtain the correct axial compliance. Using this procedure, the value of 5.77×10^7 dyne/cm was arrived at in order to obtain a 300 Hz natural frequency with the 16 g proof mass. The finite element model is then subjected to a mode frequency analysis where the vibrational characteristics of the various degrees of freedom are determined. An example of the results obtained from this analysis is presented in Appendix C. The illustrations presented in Appendix C are computer generated graphics, and illustrate the various modes and frequency of vibration that can occur in the resonator structure. The mode and frequency predictions of this analysis method have been found to be very helpful and very accurate in determining the resonator vibrational characteristics. Observe that mode 12 is that of the fundamental beam vibration which is predicted to occur at 40 kHz where indeed it actually does. The lower frequency modes allow a check on the behavior of the vibration isolation system. The analysis is also used as a criterion to be sure that the various modes are at least 8 to 10 kHz away from the 40 kHz fundamental to avoid an activity dip problem.

6. ACCELEROMETER DESIGN APPROACH

Details on each of the piece parts illustrated in Figure 3 follows.

The base serves as both the bottom damping plate and the attachment point for the housing end of the resonator structure. It includes the two headers which communicate with the resonator electrodes. Also included is a copper exhaust tube. Through this tube, the device is evacuated during bake out and back filled with a predetermined pressure of gas. The design of this piece, as well as the other pieces, is very simple and should present no future manufacturing problems.

The proof mass is also illustrated, although from the view it was photographed from the flexure joints are not readily visible. Since the proof mass of this VBA, as well as other VBA's, is relatively heavy compared to conventional accelerometers, the flexures are easier to fabricate. This is because a lapping procedure is not needed to bring them down to very small dimensions. The thinnest flexure dimension used for the proof mass was 0.0012 inches. The flexures were used in the as-ground condition and did not require any additional lapping. The top and bottom surfaces of the proof mass serve as the damping surfaces. The upper end of the resonator is mounted the central opening of this proof mass.

The damping plate serves just that function.

As a pre-assembly, the proof mass is sandwiched between the base and the damping plate. The gaps are set by the circular shims shown. This three piece assembly is then inserted into the housing, after which a seal is made using a high temperature epoxy. The units assembled under this program are essentially breadboard units. To facilitate these assemblies, epoxy was liberally used. The crystal was epoxy mounted to the assembly, and then the base sealed to the housing by a bead of epoxy. This approach resulted in easy assembly to allow quick evaluation of the compliant resonator and the damping mechanism, since these two items were a radical departure from previous high accuracy VBA's.

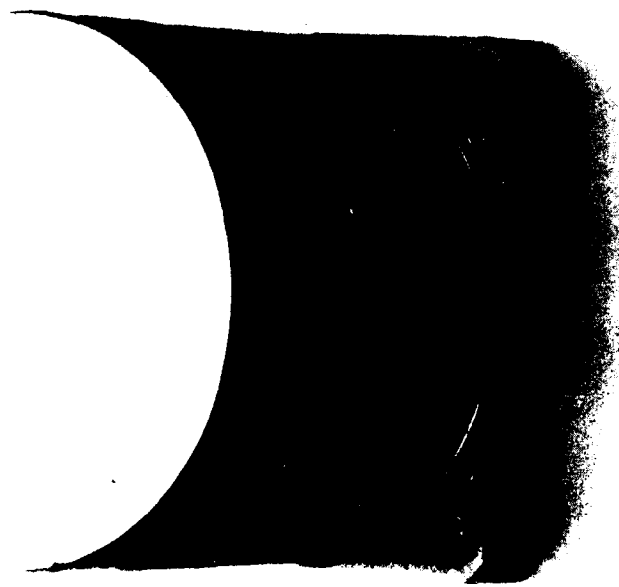
The saturating oscillator is also illustrated. This particular one was available in flat pack form and was used during most of the tests. It is cemented to the bottom portion of the base after the exhaust tube is pinched off and tucked into its recess.

An example of a complete assembly is illustrated in Figure 4. To make a complete dual beam VBA package, two of these assemblies are needed. The base of each assembly has recessed screw holes so that they can be easily mounted back to back. It is in this back-to-back condition that the devices were tested.

Liberal use of epoxy, however, is a shortcoming of this present design because:

- The ultimate in crystal stability is not obtained until a bake out at least 200°C can be obtained. The epoxy limited this to 100°C .
- The crystals being epoxied into place is also a serious shortcoming. Because of temperature changes and changes in load the epoxy has a somewhat plastic behavior. This results in creeping changes in the boundary conditions of the beam and results in the trends observed during tests.

For future development units it will be a goal to have an all-welded assembly. Means of achieving this all-welded assembly capable of a full 200°C bake out are presented in Section 6.



45637

FIGURE 4. ASSEMBLED BREADBOARD ACCELEROMETER

SECTION IV TEST RESULTS

1. NOMINAL BIAS AND SCALE FACTOR

The nominal scale factors of the individual resonators of units LC1 and LC3 are 88 and 89 Hz/g respectively. This results in a difference frequency scale factor of nominally 177 Hz/g.

The nominal bias frequencies of the individual resonators of units LC1 and LC3 are 40,856.7 and 40,507.2 Hz respectively. This results in a nominal difference frequency of 349.5 Hz, which is equivalent to (after dividing by 177) 1.97 g bias. It is characteristic of the VBA to have a high but very stable bias. Bias on production units can be reduced by better matching of individual resonators.

2. BIAS STABILITY

The major deviations in design approach of the low-cost VBA over the previous high accuracy VBA were:

- The introduction of gas damping, which means that the resonators, which formerly operated in a high vacuum, would now have to operate in a fraction of an atmosphere of the gas to be chosen.
- The former high accuracy unit used rather expensive linear oscillators. The low cost units operated with relatively inexpensive and simple saturating type oscillators.

One of the first tests conducted was to compare the behavior of the unit to these two new operating conditions. The test results are presented in Figure 5. Figure 5A is an example of short term stability obtained on unit LC4 which was operating under an evacuated condition with a resonator Q of about 40,000 and using one of the relatively expensive linear oscillators. Figure 5B is a similar unit LC3 operating in 1/20 of an atmosphere of neon which resulted in a resonator Q of 12,000. The oscillator used here was of the saturating type. Very little, if any, short term performance degradation was realized by going to these new conditions. Note that the test results presented in Figure 5 are for individual accelerometer halves tested separately. Therefore, there is no benefit of common mode rejection of thermal errors.

Figure 6 is an example of bias stability obtained over a longer period of time. Figure 6A is a plot showing how the drifts of the individual resonators varied during the approximately 20 hour period. As mentioned in Section II, the actual VBA output is taken as the difference frequency between these two individual frequencies. This difference frequency is plotted in Figure 6B. Note that bias stabilities of well under $1\mu\text{g}$ are being realized. Also note that this is raw data and has not been compensated for any effects at all. These tests were run in the +1 g position so that the drift error effects illustrated are those of both bias and scale factor. The temperature of the room monitored during the period of the test appears in Figure 6C. Because of thermal insulation and temperature control, the resonators experience only about one-tenth of these room temperature variations. Note that the periodic movement of the beam frequencies of Figure 6 is well correlated with the changes in room temperature of Figure 6C. Note, however, that these variations are absent from the difference frequency plot of Figure 6B. This is a typical example of the common mode rejection features obtained from the dual beam

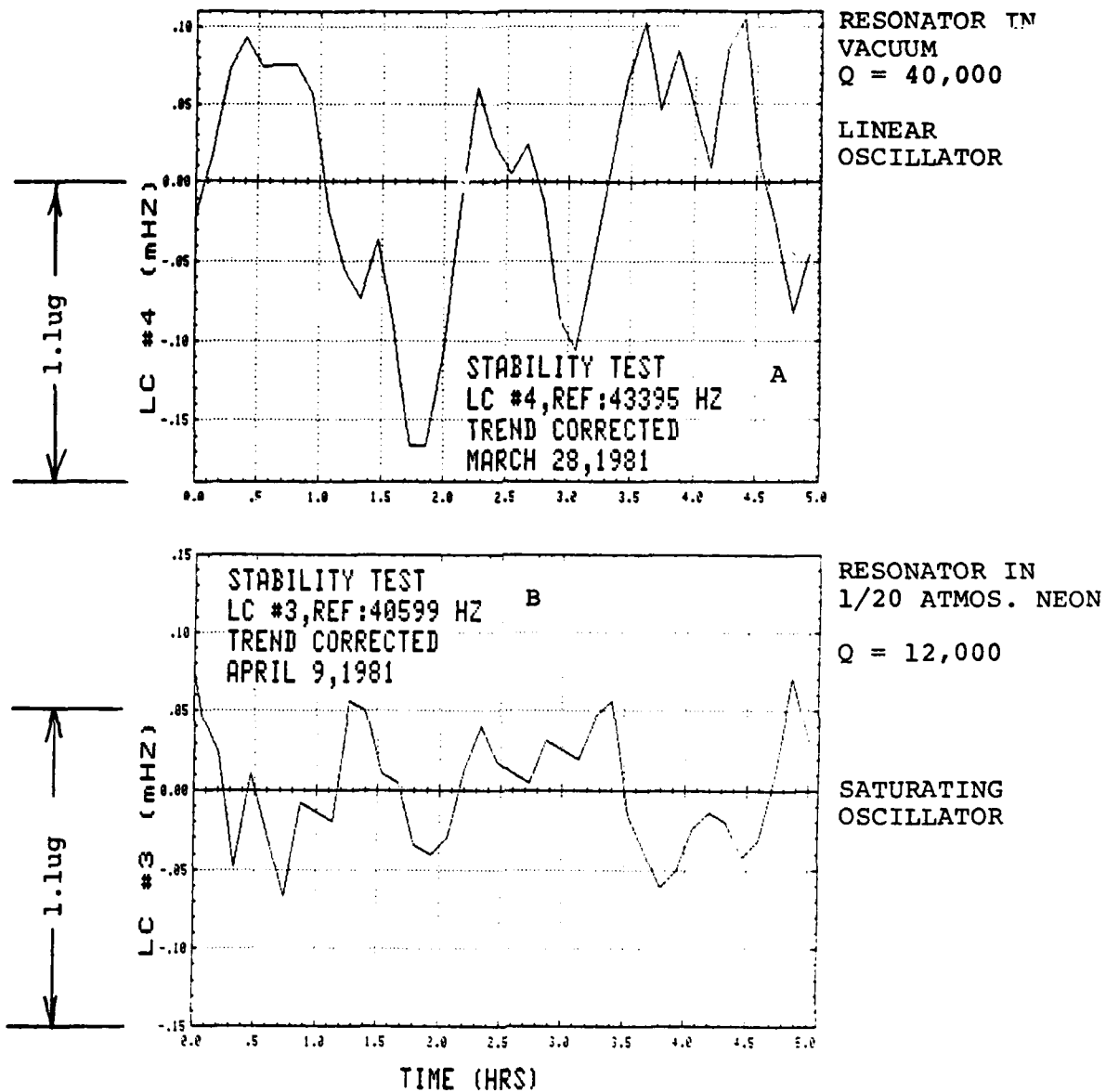


FIGURE 5. LOW COST VBA
 SHORT TERM BIAS STABILITY INDIVIDUAL RESONATOR

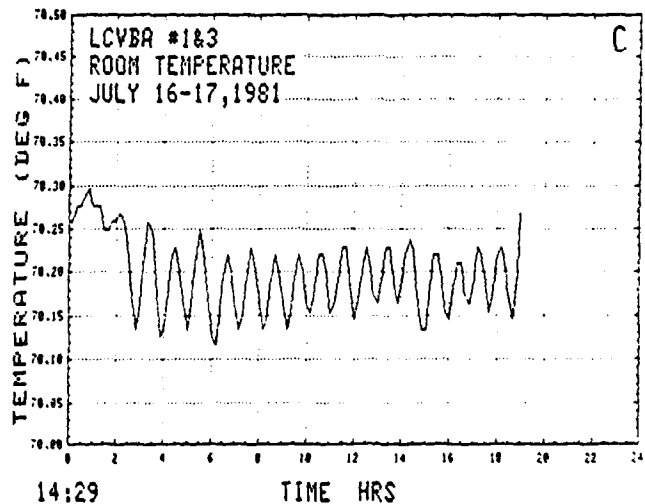
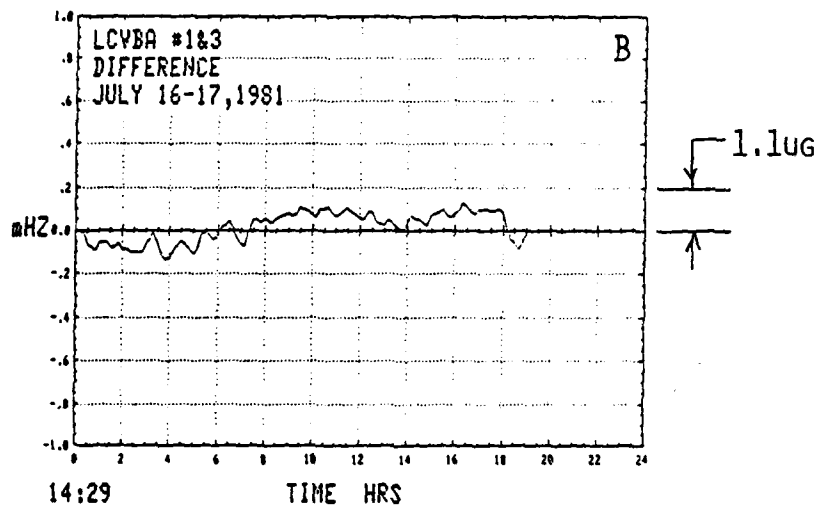
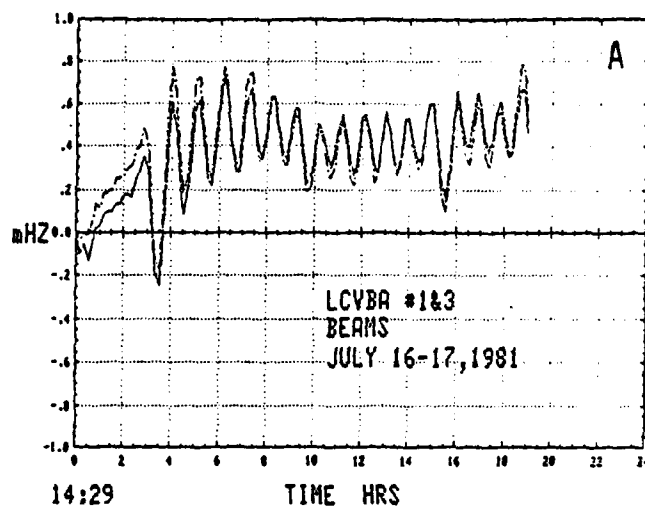


FIGURE 6. LOW COST VBA
INDIVIDUAL RESONATOR AND DIFFERENCE FREQUENCY

design. The combination of doubling the scale factor and common mode rejection has improved the bias stability by about one order of magnitude.

Figure 7 is a typical example of a longer drift run. However, note that the difference frequency is trend corrected for this example. It has been characteristic of the low-cost VBA's under test to exhibit first order trends which are very predictable. The difference frequency trend during this test was about $10\mu\text{g}/\text{day}$. It is these trends that will be corrected on the future designs by eliminating the epoxies and changing to an all-welded design so that the crystals can receive benefit of 200°C bake out.

3. BIAS THERMAL SENSITIVITY

A goal of the low-cost VBA program is to eventually provide an accelerometer which can operate over a wide temperature range without heater control. With respect to bias, the dual beam approach depends on a good thermal match between the temperature vs. frequency variation of the two individual resonators. (The bias temperature sensitivity model is presented in Appendix E.) Since the output is taken as the difference frequency, a perfect match will result in a zero bias temperature sensitivity. It has been found during the course of oscillator development that a change in the value of the trim resistor in the oscillator circuit will change the frequency of the resonator slightly. This is an action similar to "crystal pulling" used to final trim frequency standard crystals. It became apparent that if the trim resistor could be replaced with a thermistor-resistor network designed so that the temperature sensitivity of this circuit would compensate for the temperature sensitivity of the resonator, it may be possible to force a match between the two resonators. This experiment was tried and the results are presented in Figure 8. Figures 8A, B and C show the before compensation results. This was a dynamic test whereby the temperature change was induced by simply turning off the heaters. As a result, a dynamic thermal condition exists. Figure 8A and B indicate that there is about an 8% mismatch in the linear temperature coefficient of the individual resonators.

Figures 8D, E and F show the results of the same experiment run after the thermistor-resistor temperature compensation network was substituted for the oscillator trim resistor. Figure 8E indicates that now the temperature vs. time traces of the two beams are virtually superimposed.

A comparison of Figures 8C and F illustrates that the best straight line slope of temperature vs. bias has been reduced from an original $30\mu\text{g}/^\circ\text{F}$ down to about $1\mu\text{g}/^\circ\text{F}$ over the 30°F temperature range of the experiment.

The results of this experiment demonstrate that very low bias temperature sensitivity is achievable. For production units, the procedure will be even more effective since a large number of low-cost VBA "halves" will be available to initially obtain a lower thermal mismatch than the 8% of LC1 and LC3 breadboard units.

4. SCALE FACTOR STABILITY

It is estimated that the scale factor stability is better than 1 ppm, exclusive of thermal sensitivity (to be discussed in Section IV, para. 5). The following analysis is offered as a rationale for this estimate.

To describe the bias frequency and the force-frequency effects of an individual resonator, Equation (4) is taken from Appendix A. Note that just the bias and scale factor effects are considered and the terms are as defined in Appendix A.

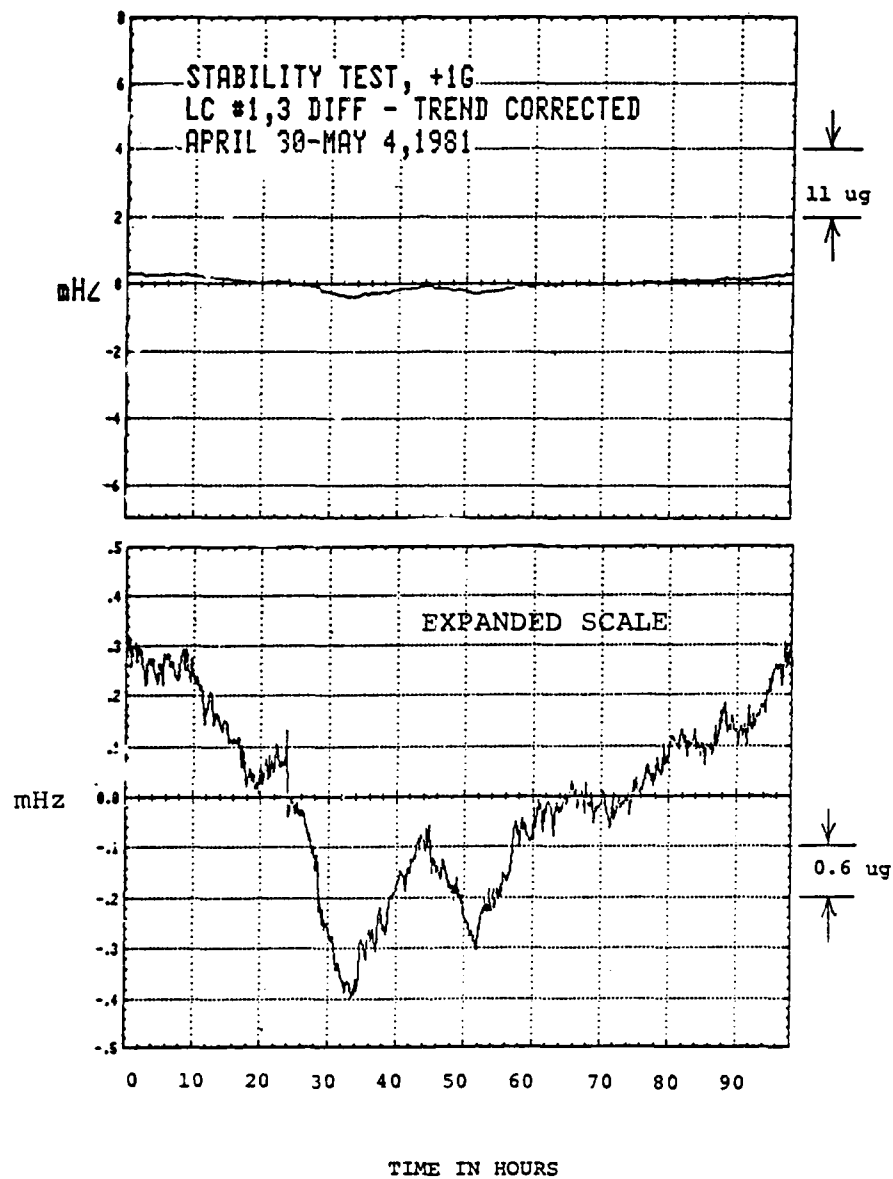


FIGURE 7. LOW COST VBA BIAS STABILITY

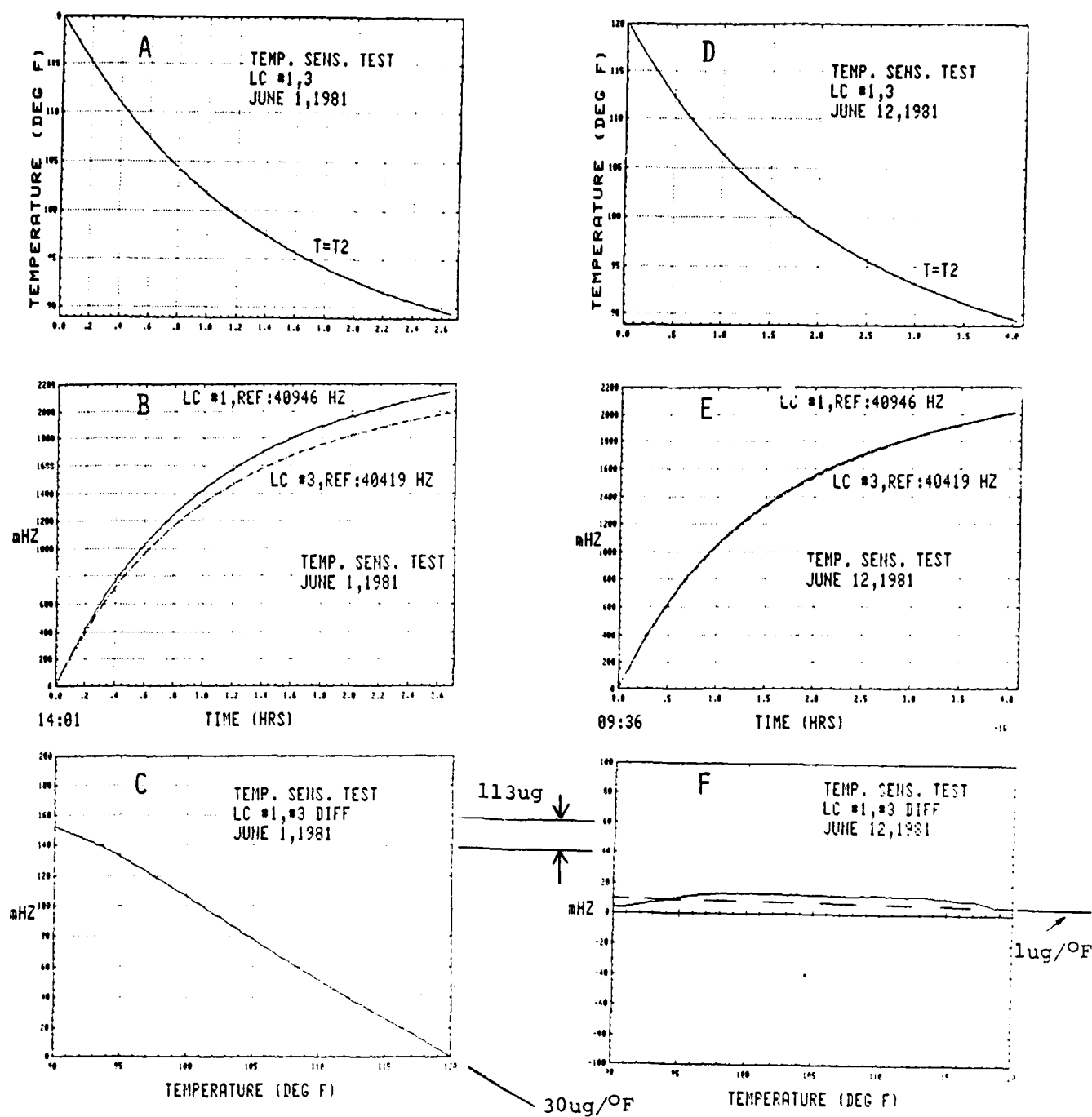


FIGURE 8. BIAS TEMPERATURE SENSITIVITY
COMPENSATION EXPERIMENT

$$\omega = a_0 \frac{t}{\ell^2} \sqrt{\frac{E}{\rho}} \left[1 + a_1 \left[\frac{\ell^2}{Eb + t^3} \right] T \dots \right] \quad (4)$$

In Equation (5), the tension term is replaced by a mass times acceleration term (mg) and Equation (4) is then rearranged.

$$\omega = \underbrace{a_0 \frac{t}{\ell^2} \sqrt{\frac{E}{\rho}}}_{\text{Bias Frequency}} + \underbrace{a_0 a_1 \frac{m}{bt^2} \sqrt{\frac{1}{E\rho}}}_{\text{Scale Factor}} g \quad (5)$$

Equation (5) describes for the individual resonator how both bias and scale factor are dependent on various characteristics such as beam boundary conditions, beam geometry and material properties. Note that both bias and scale factor are dependent on these various characteristics to approximately the same order of magnitude. That is, a 1 ppm change of any characteristic will change the bias or the scale factor by 0.5 ppm to 2 ppm. Now, for example, assume the a_0 term, which is dependent on the boundary conditions, changes by 1 ppm due to creep of the epoxy joint which fastens the beam to either the proof mass or the base. This 1 ppm change of a_0 results in a 1 ppm change in the bias frequency and also a 1 ppm change in scale factor. For the individual resonator experiencing 1 g, the nominal value of the bias term is 40,000 Hz, while the nominal value of the scale factor term is 88 Hz. The 1 ppm change of a_0 therefore causes a 0.04 Hz change in the bias term and just a 0.000088 Hz change in the scale factor term.

The conclusion indicated is that instability sources on individual resonators are common to both bias and scale factor to about the same degree. But, since the bias is much greater than the scale factor (about 450:1 at 1 g). Virtually all instabilities experienced during testing can be attributed to the bias.

Because of the performance limitation caused by epoxy creep and the inability to achieve a high temperature bake out as described in Section 7, individual resonator frequency instabilities of about 0.1 ppm are being realized. This indicates that one or a combination of several terms of Equation (5) are on the order of 0.1 ppm unstable. By the reasoning presented in the previous paragraph, this infers that the scale factor is about 0.1 ppm unstable.

5. SCALE FACTOR TEMPERATURE SENSITIVITY

A series of four position tests were performed over the temperature range of 85°F to 135°F. The dual beam VBA model equations for this procedure appear in Appendix D. From experience on previous VBA designs, we normally expect a slope of scale factor vs. temperature on the order of five to ten ppm/°F for an individual resonator. Because of the two beam mechanization of frequency differencing, the VBA scale factor is nominally twice that of the individual resonator scale factor and does not receive the benefit of common mode rejection. Therefore, even though the scale factor is double that of the individual resonator, the temperature sensitivity on a ppm/°F basis remains the same and therefore we would normally expect five to ten ppm/°F scale factor temperature sensitivity which will be very repeatable and very modelable. For this series of tests, however, one of the units, LC1, had a -7.0 ppm/°F scale factor slope while LC2 had a +6.6 ppm/°F slope. The reason why one scale factor had a negative slope and the other a positive slope is not currently known. The implication is that for this particular case, there was a common mode rejection mechanism over this temperature range of scale factor. Therefore the scale factor sensitivity of the difference frequency was less than 1 ppm/°F. This residual scale factor temperature sensitivity will also be very repeatable and very modelable. In production units, this scale factor common mode rejection may not be achieved. In any event, the scale factor temperature sensitivity is expected to be no greater than 10 ppm/°F.

6. NONLINEARITY

The same four position test procedure of Appendix D also gives us some indication of nonlinearity, although the test conditions were rather crude due to the bias instability. For LC1 and LC3 the Hz/g² coefficients were -0.146 and -0.178 respectively. For a 16 g proof mass, this translates to a force sensitivity of -5.94 (10⁻¹⁰) Hz/dyne² (for LC1) and -7.24 (10⁻¹⁰) Hz/dyne² (for LC3). Both these values are somewhat higher than the -4.44 (10⁻¹⁰) Hz/dyne² analytically predicted in Table 2-7 of Appendix A. It is not presently known why there was a deviation between individual resonators and what has been theoretically predicted. However, the test procedure used had shortcomings because of the bias instability, and determining this coefficient involves small differences of large numbers.

However, it is encouraging that the correct sign and order of magnitude was obtained. In production units there will be a large number of individual VBA halves to choose from. Also it is anticipated that future VBA's will not have as heavy a proof mass. In the dual beam mechanization the nonlinearity terms do receive benefit of the cancellation so that for an 8 g proof mass a VBA g² coefficient of about 4 μg/g² will be achieved for a 1% mismatch of individual resonator g² coefficients. By trimming, this can be brought down to on the order of 1 μg/g² or less. This trimming is accomplished very simply by changing slightly the mass of one of the proof masses. In summary then, production units will achieve high linearity by first making a careful match of the individual g² coefficients, and then trimming slightly the mass of one of the proof masses to bring the g² coefficient nominally to zero.

The g^2 coefficients were determined from multi-position test data over the range of 85 to 135°F and to the accuracy of the test there was no detectable temperature sensitivity of the g square coefficient. This is not surprising since the resonator theory presented in Appendix A shows that the nonlinear terms as the scale factor and bias are dependent on the same characteristics, such as beam boundary conditions, beam geometry and quartz material properties. Therefore, the sensitivity of the g^2 coefficient should also be on the order of one to ten ppm/°F.

7. ALIGNMENT STABILITY

As a result of the multi-position tests comes the alignment term. Although there was no attempt to align the devices, some insight was gained into the type of stability that we could expect over the temperature range. By nature of the VBA construction the alignment is simply a matter of the differential expansion between the quartz and the material of the VBA body itself. Therefore, an alignment sensitivity of temperature on the order of 1 μ rad/°F will result for each ppm/°F mismatch between quartz and the material body. It is planned to make a match of better than 1/2 ppm/°F in these expansion characteristics. Therefore an alignment stability with temperature on the order of 1/2 μ rad/°F should be expected on each unit. The actual alignment achieved during the four position test for LC1 and LC3 were 3.8 (10^{-3}) radian and -1.2 (10^{-4}) radian, respectively. The test data was not accurate enough to actually measure a slope and confirm the 1/2 to 1 μ rad/°F sensitivity expected.

8. VIBRATION TESTS

One of the first units assembled was subjected to vibration tests, before it was sealed, so that some evaluation of the damping mechanism could be gained. The test was run on a single unit so therefore there is no benefit of common mode rejection. The object of the test was to determine what the natural frequency and maximum transmissibility was and also to determine if there were any unusual resonances. Figure 9 is a good example of the type of response that was obtained. The test was run by placing the output of the oscillator into a frequency discriminator and then plotting the output of the discriminator. Figure 9 shows that the system behaves as a classical second order system having a resonant rise at the natural frequency. It was a design goal to place this frequency at 300 Hz. It came in at about 250 Hz. On future designs, this frequency is easily altered by adjusting the stiffness of the compliant resonator or the mass of the proof mass or both. The resonant frequency was found to be relatively insensitive to pressure. This is contrary to the analysis of Appendix B, which accounts for the gas spring effects. Transmissibility was greater (damping lower) than expected however, which agrees with Appendix B.

A series of vibration tests was performed at various absolute pressure levels with various gases. The results of these tests are plotted in Figure 10. The damping achieved is relatively insensitive to pressure down to 1 to 2 in Hg absolute. As the table in Figure 10 shows, the value of damping is proportional to the viscosity of the gas used. It was fortunate to find that very little absolute pressure is needed to achieve the desired damping. This is fortunate because the lower that gas pressure, the better the Q of the resonators. This is pointed out in Section IV, para. 9 where the effects of gas on resonator performance is discussed. Because of these test results, the remaining units were all filled with 1.5 in Hg absolute of neon. This limited the maximum transmissibility to about 1.5.

LOW COST VBA - LC #1
 DAMPING INVESTIGATION
 SINE VIBRATION INPUT
 28" Hg VACUUM BACK FILL AIR
 3/9/81 ROOM TEMPERATURE

$$\text{TRANSMISSIBILITY} = \frac{g_{\text{OUT}}}{g_{\text{IN}}} = 3$$

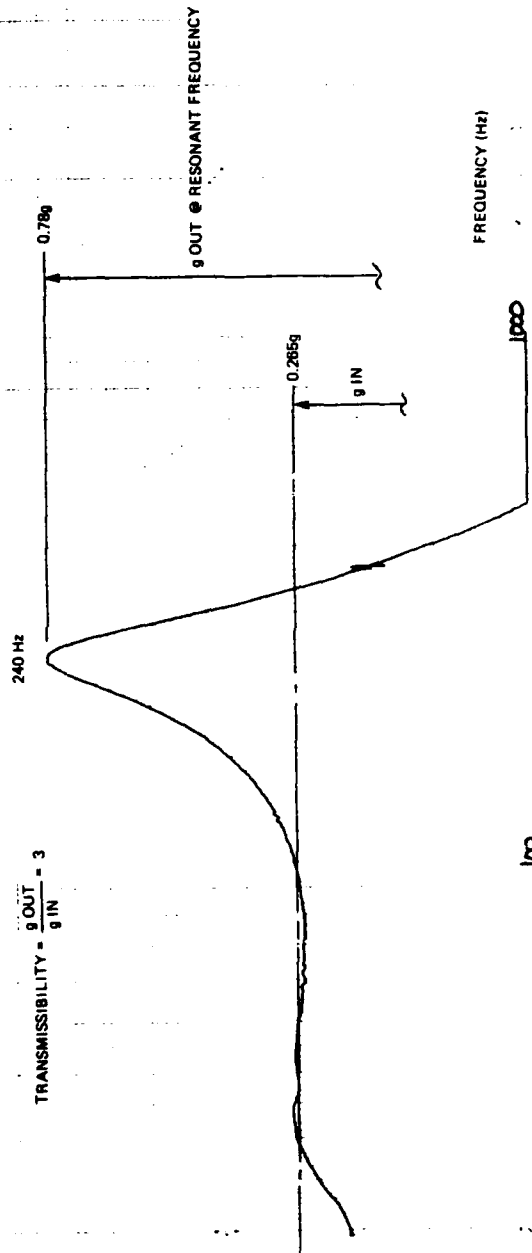


FIGURE 9. LOW COST VBA VIBRATION TEST

LC VBA GAS DAMPING

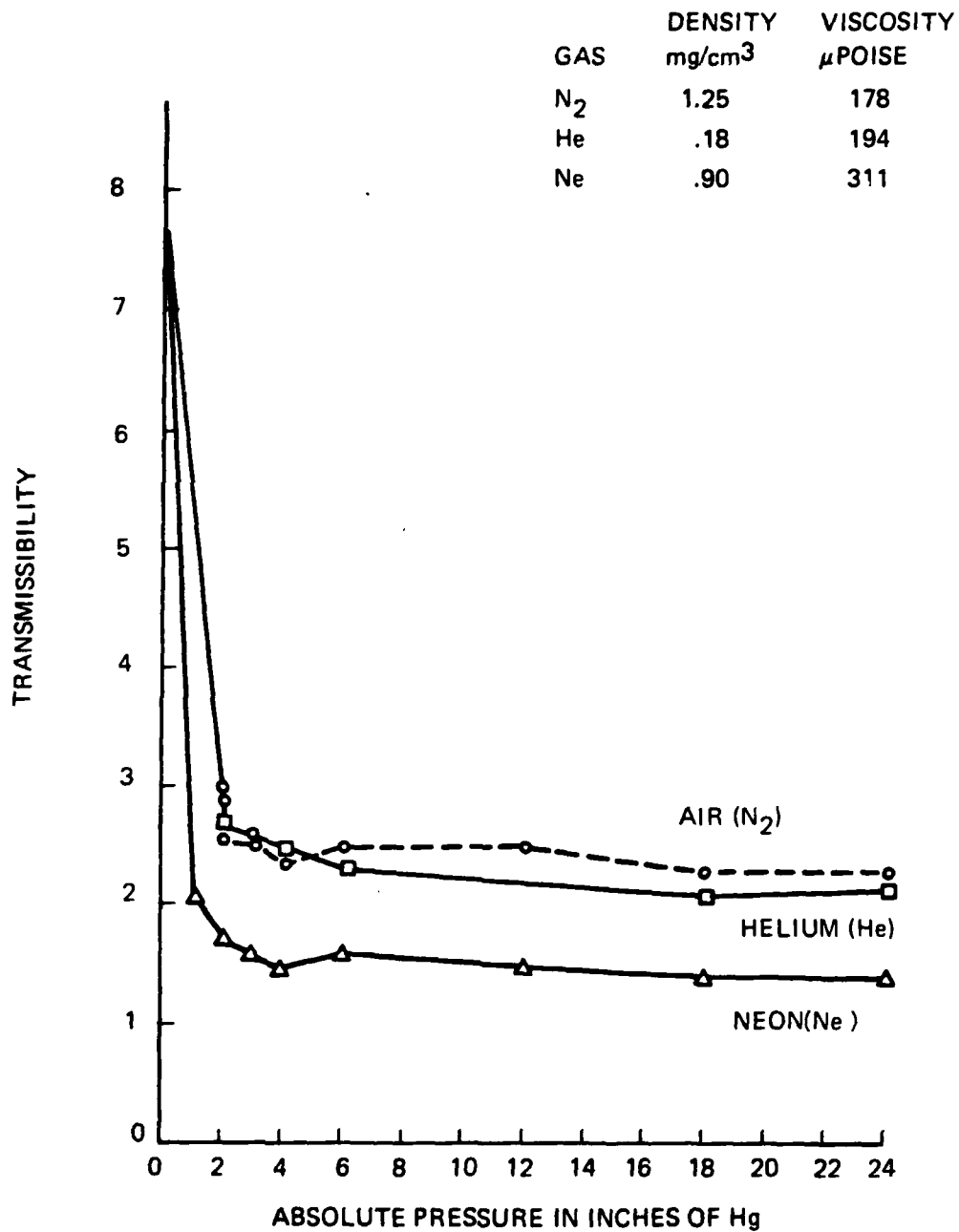


FIGURE 10. TRANSMISSIBILITY
VS
ABSOLUTE PRESSURE
FOR
VARIOUS GASES

Future development studies and tests are recommended to determine the ideal gas or gas mixture which will result in both high resonator Q and the desired damping.

9. RESONATOR-GAS EFFECTS

Figure 11 summarizes the gas effects on resonator operation. Figure 11A is a plot of gas density vs viscosity. As pointed out earlier, a gas of high viscosity provides the most effective damping while a gas of low density results in the least gas effects on resonator operation. From Figure 11A it can be seen that the gases which offer the most favorable viscosity to density ratios are neon and helium. Figure 11B is a plot of resonator Q vs gas absolute pressure. From this plot two things are apparent. First, it can be seen that helium has the least effect on resonator Q. Second, the relationship of Q to pressure becomes very nonlinear at low pressure. The reason for this is not known, however, it is suspected that at low pressures, the mean free path of the gas becomes commensurate with the resonator vibration amplitude. This is the extent to which this phenomena has been investigated. Figure 11C is a plot of resonator frequency change vs gas absolute pressure. This effect has been found to be linear and different for the three gases investigated. The pressure-frequency sensitivity appears to be approximately proportional to the gas density. This observation is reasonable since it is concluded that this frequency-pressure sensitivity is a mass effect. The gas immediately surrounding the vibrating beam is also set into motion and therefore the added mass of the gas increases the effective density of the quartz. It is not surprising, then, that a gas such as helium with a very low density would have the least effect. The data presented in Figure 11, along with the vibration test results presented in Section IV, para. 8 indicate that the 1/20 of an atmosphere of neon used may not be the ideal condition. Helium, or perhaps a mixture of helium and neon, may be the best choice to bring about the best combination of resonator performance (as indicated by high Q) and proof mass damping, (shown by low transmissibility). Neon was used in the breadboard accelerometers because they used epoxy seals and it was feared that helium might leak through these seals. However, future designs will be completely welded assemblies which should solve any possible helium containment problem. We plan to do further development work in this area.

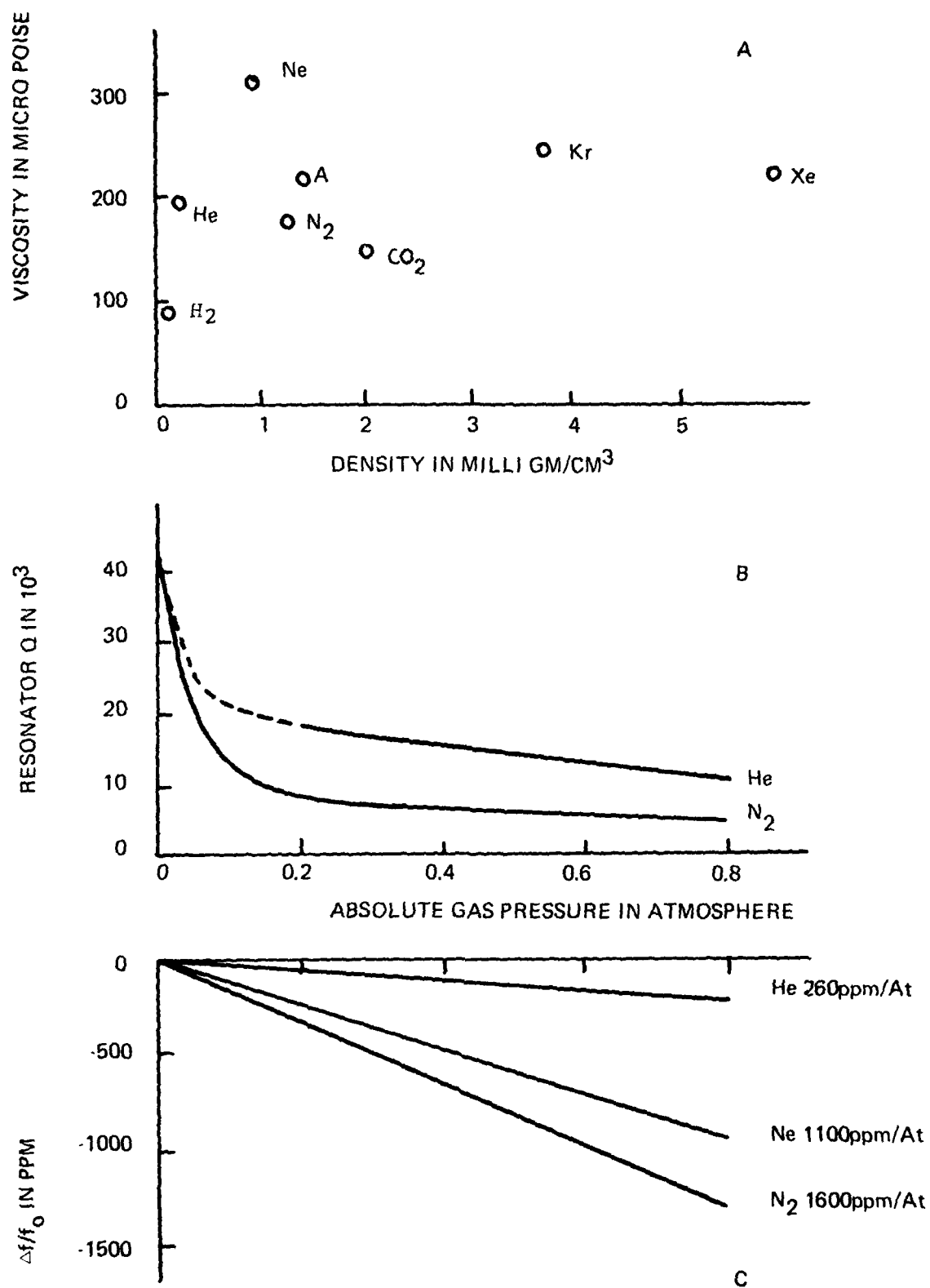


FIGURE 11. RESONATOR GAS EFFECTS

SECTION V OSCILLATOR ELECTRONICS

1. BACKGROUND

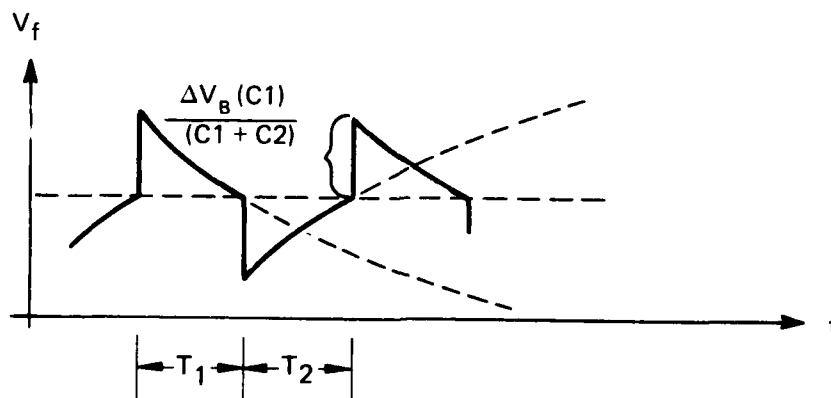
We have addressed the need for a low cost, highly reliable oscillator design to complement the dual beam low cost VBA approach. Included in this effort is a review of future packaging and system interface requirements that will optimize cost and performance. We will take full advantage of the commercial quartz crystal oscillator manufacturer's approach, utilizing low cost digital integrated circuits as basic oscillator building blocks. Experience gained as a result of extensive linear oscillator design work will be applied, both in the recommended packaging approach, and analytical/empirical design verification.

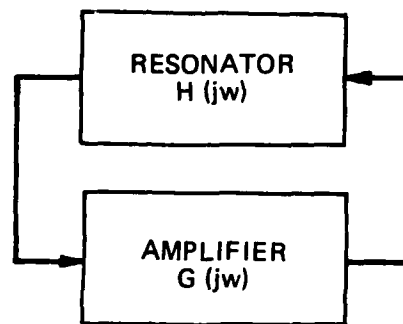
2. DESIGN APPROACH

To combine performance with low cost, it is necessary to synthesize a simplistic oscillator design, utilizing available I.C. technologies. Previous experience with linear oscillators highlighted the need for low power dissipation to aid integral mounting with the instrument. An ideal I.C. technology combining speed and low power is CMOS. The basic oscillator design approach is to satisfy the Barkhausen conditions for oscillation. Figure 12 is a block diagram illustrating the basic loop criteria to sustain oscillation requiring a loop gain of unity and zero degrees phase shift. A schematic diagram of the basic oscillator circuit is shown in Figure 13. The crystal resonator is being operated in its series resonant mode at nominally 40 kHz. A configuration of the gated oscillator variety is used whereby the open loop period of oscillation is determined by the supply voltage, CMOS threshold voltage and feedback RC time constant. The closed loop frequency is determined by the resonator feedback element which, for a high Q device, has a large rate of change of phase W/R to frequency. Initial calibration errors or environmentally induced component drifts will therefore produce a small frequency pull to correct for same. This characteristic will be put to good use in a temperature compensation circuit to be described later.

3. THEORY OF OPERATION

The basic oscillator design is a form of gated timing circuit. Referring to the schematic of Figure 13, the switching operation occurs around the threshold voltage of the logic devices used. Capacitors C_1 and C_2 form a capacitive divider network which will apply a portion of the step voltage change at V_B to the input of A_{IA} . The voltage at V_f will decrease with a time constant proportional to R_{ext} . When the logic threshold voltage of A_{IA} is reached, both the V_A and V_B will exhibit a reverse polarity voltage step which will decay with the same time constant. A diagram of this switching action follows.





$$G(j\omega) H(j\omega) = 1 + j0$$

FIGURE 12. BARKHAUSEN'S CRITERION FOR S.S. OSCILLATION

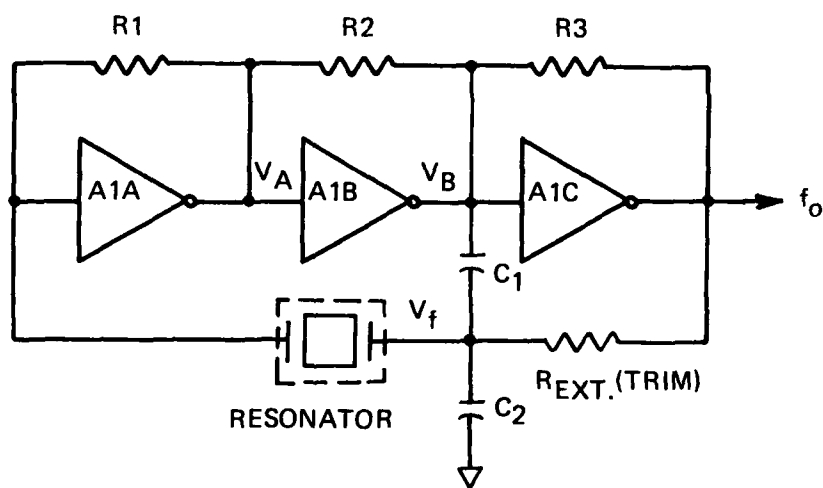


FIGURE 13. SATURATING OSCILLATOR SCHEMATIC

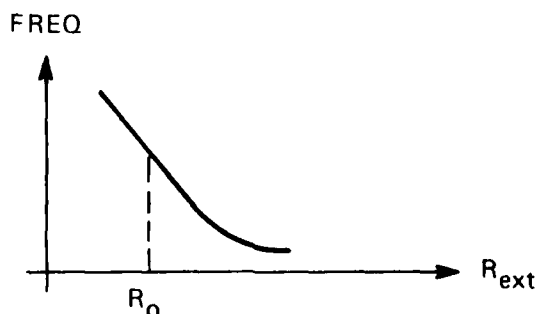
The sum of the switching periods $T_1 + T_2$ are set with the external trim resistor (R_{ext}) and should be close to the resonator's series resonant period. The high Q resonator tuned circuit will pull the closed loop frequency near its series resonant point. The hybrid used also contains a current regulator diode in series with the B line to minimize the effects of line voltage and circuit power consumption changes on the critical frequency determining parameters.

4. TEMPERATURE COMPENSATION

As described in Appendix E, the temperature sensitivity of the resonator bias frequency can be modeled as a downward sloping parabola centered around a frequency at which the temperature coefficient is zero (i.e., Zero Temperature Coefficient (ZTC) or turnover point). A perfect match of two resonators with the same ZTC point and the same second order coefficients would produce a difference frequency with a ZTC over the full military environment. In practice the second order coefficients of two resonators match quite well with compensation required for the different ZTC points. It can be shown that adding a function which linearly varies with temperature to a parabolic function can shift the latter's ZTC point. Varying the gated time constant resistance (R_{ext}) linearly as a function of temperature will produce a linear change in output oscillator frequency with temperature in the present digital oscillator configuration (see Figure 5-2). What remains to be done is to determine the scale factor of this frequency vs temperature characteristic and to design a resistance network to satisfy these conditions. The choices are metallic positive T/C resistors or a linearized version of the negative temperature coefficient thermistors. The latter configuration was chosen due to the more compatible resistance values at the temperatures of interest.

In practice, an existing commercial hybrid module was used for the basic oscillator section which, together with accompanying discrete trim components, was integrally mounted on the low cost instruments. A schematic of this brassboard configuration is shown in Figure 14. It should be noted that only one of the two oscillators require the linear temperature compensation network. The resonator with the lower ZTC point is compensated.

When driving this resonator with a saturating type of oscillator, in the series resonant mode, the change of frequency vs R_{ext} is as follows:



For a reasonable range of external resistance the frequency change curve is linear. Without compensation the beam frequency may be accurately modeled as:

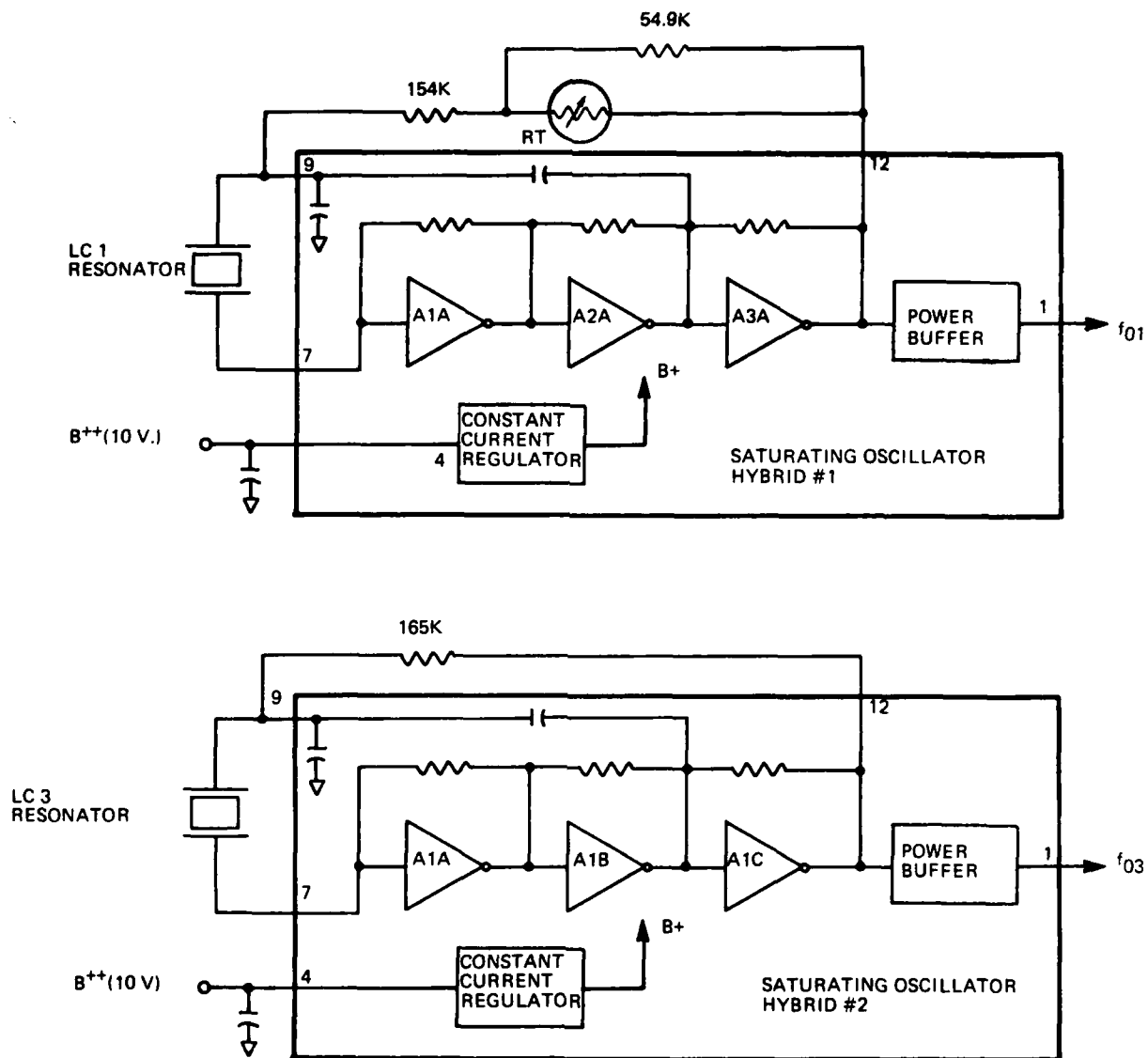


FIGURE 14. LOW COST VBA BRASSBOARD SCHEMATIC

$$f(T) = A_0 + A_1T + A_2T^2 \quad (6)$$

Completing the square of Equation (6) gives:

$$f(T) = A_0 - \frac{A_1^2}{4A_2} + A_2 \left(T + \frac{A_1}{2A_2} \right)^2 \quad (7)$$

The inflection point, or ZTC point of Equation (7) is at

$$T_{ZTC} = \frac{-A_1}{2A_2}$$

With the addition of a linear resistance change vs temperature, using the R_{ext} connection, a linear KT term is added to Equation (6) giving:

$$f'(T) = A_0 + A_1T + A_2T^2 + KT \quad (8)$$

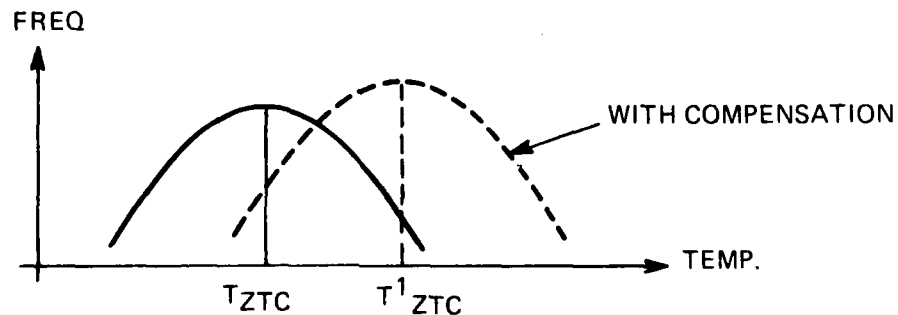
Again completing the square gives:

$$f'(T) = A_0 - \frac{(A_1 + K)^2}{4A_2} + A_2 \left(T + \frac{(A_1 + K)}{2A_2} \right)^2 \quad (9)$$

Therefore the compensated beam has a ZTC point at

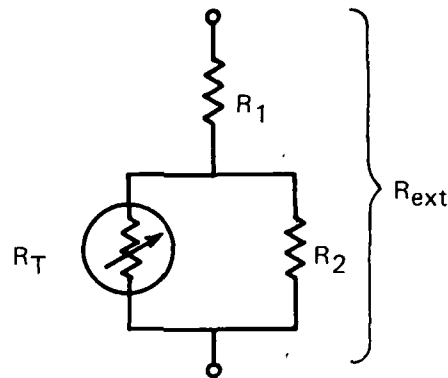
$$\begin{aligned} T'_{ZTC} &= - \frac{(A_1 + K)}{2A_2} \\ \Delta T_{ZTC} &= \frac{-K}{2A_2} \end{aligned} \quad (10)$$

Thus, linear temperature compensation has the effect of shifting a given resonator's ZTC temperature. It should be noted that the second order coefficient, A_2 , is preserved by the compensation. Graphically the impact of compensation is as follows:



This compensation technique provides a means for matching the ZTC temperature of two separate resonators. Only one of the two resonators need be compensated and providing we have a match of the second order coefficients the difference frequency shall be virtually constant over temperature.

To provide this compensation a passive load resistance network must be implemented which varies as a linear function of temperature and is substituted for R_{ext} in Figure 13. A linearizing thermistor configuration is as follows:

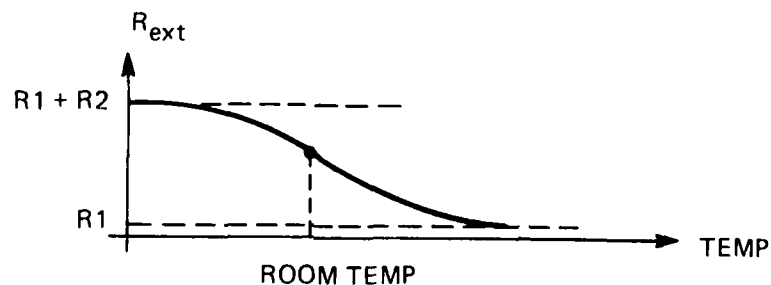


The expression for R_{ext} is:

$$R_{ext} = R_1 + R_T // R_2 \quad (11)$$

$$R_{ext} = R_1 + \frac{R_T R_2}{R_T + R_2} \quad (12)$$

Graphically the resistance vs temperature characteristic of the network is:



A large portion of the curve centered about the midpoint (room temperature) is linear.

The thermistor R_T is an exponential function of temperature and can be approximated with a series expansion resulting in the following expression for R_{ext} :

$$R_{ext} \approx R_1 + \frac{R_0 R_2}{R_0 + R_2} + \frac{R_0 R_2^2}{(R_0 + R_2)^2} a \Delta T \quad (13)$$

where R_0 = Room Temp. resistance of thermistor
 a = Temperature coefficient of thermistor

$$\text{Let } R_0' = R_1 + \frac{R_0 R_2}{R_0 + R_2} \quad (14)$$

$$K_R = \frac{R_0 R_2^2}{(R_0 + R_2)^2} a \quad (15)$$

Rewriting Equation (13) gives:

$$R_{ext} = R_0' + K_R \Delta T \quad (16)$$

The above equation behaves as a linear function of temperature over a sizeable temperature range.

5. EXPERIMENTAL RESULTS

The temperature compensation of accelerometer bias using this technique was demonstrated, as described in Section 4. The procedure was:

- o The temperature sensitivity of the individual resonators of LC1 and LC3 was determined. This data appears in Figure 8 A and B with the resultant temperature sensitivity of the difference frequency which appears in Figure 8 C.
- o Using this data and the procedure described, the characteristics of the R_{ext} circuit was determined and then installed.
- o The temperature tests of Figure 8 were then repeated for these new conditions. As Figures 8 E and F demonstrate, the procedure was very effective with the bias temperature sensitivity being reduced to the order of $1 \mu g/^{\circ}F$ over the limited temperature range of the experiment.

6. RECOMMENDED FUTURE ACTIVITIES

Future activities should include a further refinement of the linear temperature compensation scheme whereby the full military temperature range (i.e., $-55^{\circ}C$ to $+71^{\circ}C$) is addressed. Compliance over this environment will make the low cost VBA a prime candidate for future strapdown systems.

Short term stability testing of these LC1, LC3 units revealed that package size and physical proximity played an important part in the results. When a discrete equivalent circuit was used for breadboard evaluations, there was a 10/1 degradation in peak to peak

drift. One of the major contributors to this instability is humidity changes which will affect interlead capacitances. From analytical studies conducted on a linear oscillator, the resonator drive lead capacitance had the highest sensitivity factor. It should be noted that a change in lead-to-lead capacitance has a direct effect on the value of the resonator's electrode capacitance (i.e., $C_0 = 1.5$ pf. nom). As the value of R_M increases the sensitivity also increases. A solution to this problem is to develop a small, low cost hybrid module that is mounted directly to the low cost VBA unit. With careful layout and short stiff interconnect system this hybridized version will optimize performance. A preliminary study on parabolic temperature compensation is included in Appendix H. This type of compensation will essentially make each resonator insensitive to temperature variations, thereby increasing yield. A cost and size trade-off study would be conducted as part of this effort.

SECTION VI VBA RELIABILITY/MAINTAINABILITY PREDICTION

1. INTRODUCTION

A reliability prediction was generated to comply to para. 4.3 of the Statement Of Work for the VBA Accelerometer Study Program. Maintainability aspects of the design are also addressed herein. The Reliability Prediction was performed for a single beam accelerometer for an Airborne Fighter application. The prediction considers both inhabited and uninhabited flight environments. This prediction is based upon the latest design configuration and utilizes the failure rates of MIL-HDBK-217C-1 and the failure rates derived from Kearfott field performance data on similar components in inertial instruments. MIL-HDBK-217C-1 environmental 'K' factors were used to adjust failure rates for Inhabited and Uninhabited Flight, where applicable, and MIL-STD-756A environmental K-factors for parts not included in MIL-HDBK-217C-1.

Four different VBA ambient operational temperatures were also considered for this analysis.

2. RESULTS AND CONCLUSIONS

The prediction analysis results are summarized in Table 1. The failure rate for the Uninhabited Fighter application varies from 5.7047 f/10⁶ to 6.6357 f/10⁶ hours for the four ambient temperatures considered (55°C, 60°C, 65°C and 70°C). This translates to a Mean Time Between Failure (MTBF) of 175,293 to 150,699 hours with increasing temperature.

The failure rate for Inhabited Fighter application varies from 5.0667 f/10⁶ to 5.7161 f/10⁶ hours with ambient temperature increasing from 50°C to 70°C. This translates to an MTBF of 197,366 to 174,945 hours.

The hybrid oscillator is the predominant influencing factor in the change in both the failure rate and MTBF with temperature and environments.

The VBA accelerometer is a sealed component. Therefore, it has no maintainability requirements.

3. DISCUSSION

a. SINGLE BEAM ACCELEROMETER

(1) Parts

The parts comprising the single beam accelerometer, quantity used, and sources of the failure rate data are listed below in Table 2. For the purposes of this analysis, a military equivalent of the hybrid oscillator was considered.

(2) Failure Rates

Failure rates were obtained from MIL-HDBK-217C-1, and also derived from Kearfott field performance data on similar parts, where MIL-HDBK-217C-1 failure rate data was not available. The failure rates of the following VBA parts are based upon a field evaluation of 2,938 Kearfott Single Axis Accelerometers which accumulated 6,822,759 equivalent

TABLE 1. RELIABILITY PREDICTION ANALYSIS RESULTS FOR SINGLE VBA

AMBIENT TEMPERATURE	RELIABILITY PREDICTION			
	UNINHABITED AIRCRAFT ENV.		INHABITED AIRCRAFT ENV.	
	FAILURE RATE ($f/10^6$ HRS)	MTBF (HRS)	FAILURE RATE ($f/10^6$ HRS)	MTBF (HRS)
55°C	5.7047	175,293	5.0667	197,366
60°C	5.9570	167,869	5.2420	190,768
65°C	6.2640	159,641	5.4560	183,285
70°C	6.6357	150,699	5.1761	174,945

laboratory environment operating hours. These accelerometers were used on 14 different programs for missiles, aircraft, and space applications.

TABLE 2. PARTS AND (FAILURE RATE) SOURCE OF DATA

PART	QUANTITY	SOURCE OF DATA (FAILURE RATE)
HYBRID OSCILLATOR	1	MIL-HDBK-217C-1
THERMISTER	1	MIL-HDBK-217C-1
RESISTOR, COMP. (R)	1	MIL-HDBK-217C-1
CRYSTAL	1	MIL-HDBK-217C-1
CONNECTOR	1	MIL-HDBK-217C-1
FLEXURE	1	KEARFOTT DATA
FEED-THRU	2	KEARFOTT DATA
SEAL	4	KEARFOTT DATA

<u>PARTS</u>	<u>FAILURE RATE</u>
Flexure	0.2565 f/10 ⁶ h
Seal	0.0321 f/10 ⁶ h
Feed-through	0.0641 f/10 ⁶ h

MIL-STD-756A environmental adjustment 'K' factors were applied to the laboratory failure rates for these parts to obtain the equivalent fighter aircraft environment failure rate.

(3) Reliability Prediction Calculation

Reliability predictions were performed for airborne fighter aircraft at four different MVA ambient operational temperatures (similar to Kearfott Single Axis accelerometer application) of 55°C, 60°C, 65°C, and 70°C for both Inhabited Flight and Uninhabited Flight environment.

The MTBF's and failure rates for each ambient temperature have been calculated for both Inhabited and Uninhabited Flight. The prediction details are presented in Tables 3 and 4, respectively.

TABLE 3. ENVIRONMENT - AIRBORNE, INHAB, FTR

QUALITY - VHA

		AMBIENT TEMPERATURE =						55C	60C	65C	70C
PART TYPE	APPL	QUAL	QTY	STRESS	ENV	FAIL RATE	FAIL RATE	FAIL RATE	FAIL RATE	FAIL RATE	FAIL RATE
HYBRID	USL	LIN	1	**	2.80	0.7973	0.9725	1.1864	1.4464	1.7164	1.9964
TIEMISTOR			1	10	1.00	0.5000	0.5000	0.5000	0.5000	0.5000	0.5000
RES COMP PC	(R)		1	10	5.70	0.0003	0.0004	0.0004	0.0005	0.0005	0.0005
CRYSTAL			1	**	1.00	0.2000	0.2000	0.2000	0.2000	0.2000	0.2000
CLAMP, MAND SOLDER	15CONN		1	**	6.00	0.2340	0.2340	0.2340	0.2340	0.2340	0.2340
FLEXURE			1	**	6.50	1.6672	1.6672	1.6672	1.6672	1.6672	1.6672
FLED-TRPO			2	**	6.50	0.8333	0.8333	0.8333	0.8333	0.8333	0.8333
SLAL			4	**	6.50	0.8346	0.8346	0.8346	0.8346	0.8346	0.8346

SUBASSEMBLY FAILURE RATE = 5.0667 5.2420 5.4560 5.7161

RELIABILITY

MTBF (MEAN TIME BETWEEN FAILURE) (HOURS)			
MTBF	MTBF	MTBF	MTBF
197,265	190,768	183,287	174,945

TABLE 4. ENVIRONMENT - AIRBORNE, UNINHAB, FTR

Subassembly - VPA

		AMBIENT TEMPERATURE =							
		55C				60C			
		65C				70C			
PART TYPE	APPL QVAL QTY STRESS ENV	FAIL RATE				FAIL RATE			
HYBRID	LIN 0	1	**	4.20	1.1770	1.4292	1.7361	2.1076	
TERMINATOR		1	10	1.00	0.6800	0.6800	0.6800	0.6800	
RES COMP RC	(R)	1	10	11.00	0.0006	0.0007	0.0008	0.0010	
CRYSTAL		1	**	1.00	0.2000	0.2000	0.2000	0.2000	
COND. MAINT SOLDER	15COND	1	**	8.00	0.3120	0.3120	0.3120	0.3120	
FLEXURE		1	**	6.50	1.6672	1.6672	1.6672	1.6672	
FLEX-TIM U		2	**	6.50	0.8333	0.8333	0.8333	0.8333	
SLAL		4	**	6.50	0.8346	0.8346	0.8346	0.8346	
SUB-ASSEMBLY FAILURE RATE =		5.7047				5.9570			
		6.2640				6.6357			
RELIABILITY		MTBF				MTBF			
MTBF (MEAN TIME BETWEEN FAILURE (HOURS))		175,293				167,869			
		159,641				150,699			

b. DUAL BEAM ACCELEROMETER

Based on engineering discussions, it has been determined that the Dual Beam Accelerometer complexity will be twice that of the Single Beam Accelerometer which results in a failure rate twice that of the single beam listed at any particular ambient temperature in Tables 3 and 4. This results in a MTBF equal to one-half that listed in the respective tables.

c. MAINTAINABILITY

The single and dual beam accelerometers are sealed components; therefore, they have no maintainability requirements. The replaceable items would be returned to the depot for repair.

SECTION VII FUTURE DEVELOPMENT AREAS

In this section, the recommended tasks for future development are made. Because the dual beam approach offers the best immediate potential, we recommend that future efforts proceed along these lines. The individual areas of effort to achieve the ultimate goals are described below.

1. GLASS FRIT

This effort is intended to eliminate the use of epoxy in installing the crystal resonators into the VBA. Initial development work has been performed as part of another program to achieve a quartz to metal bond using a low melting temperature glass (glass frit). Sample joints have been made of quartz to monel. Monel has been found to be a good choice for this joint because it is a good expansion coefficient match to quartz and it also forms the proper oxide that promotes wetting by the melted glass. The monel/quartz assembly will be fabricated in a sequence of operations as illustrated in Figure 15. Figure 15 illustrates how a low melting temperature glass will form the joint between the quartz and monel. The monel can then, in turn, be welded to the VBA assembly. This joint will then be capable of withstanding the 200°C bakeout needed to achieve the bias stability goals. The joint will not exhibit the plastic-like behavior of the epoxy, but will result in very stable beam boundary conditions.

2. ALL-WELDED ASSEMBLY

Future VBA builds should be of an all-welded design so that a 200°C bakeout can be achieved and organics can be completely eliminated from the assembly. It is estimated that improved resonator mounting, as described in the previous paragraph, along with high temperature bakeout and better resonator matching, can reduce the frequency difference trends to significantly less than 1 μ g per day. The all-welded design effort will consist of redesigning the VBA assembly joints to eliminate the epoxy seals and replace them with EB welds.

3. GAS DAMPING

The VBA's evaluated as part of this program are filled with 1/20 of an atmosphere of neon. There is some indication that helium or perhaps a mixture of helium and neon will provide a better combination of high resonator Q and high proof mass damping. Part of this effort will be to further analyze the damping mechanism and perform various other experiments to further evaluate the effects of gas pressure and gas viscosity on the resonator and the proof mass damping mechanism.

4. MINIATURIZATION

The envelope of the breadboard VBA is too large to make the VBA interchangeable with currently available accelerometers in many applications. The present size is dictated by the present geometry of the beams used. It is suggested that a miniaturization effort be undertaken with the goal of achieving a dual beam VBA design including electronics having an overall length of about 1 inch and a diameter of 1 inch or less. This effort will include the design and evaluation of a miniature resonator followed by the design of a miniaturized version of the dual beam VBA.

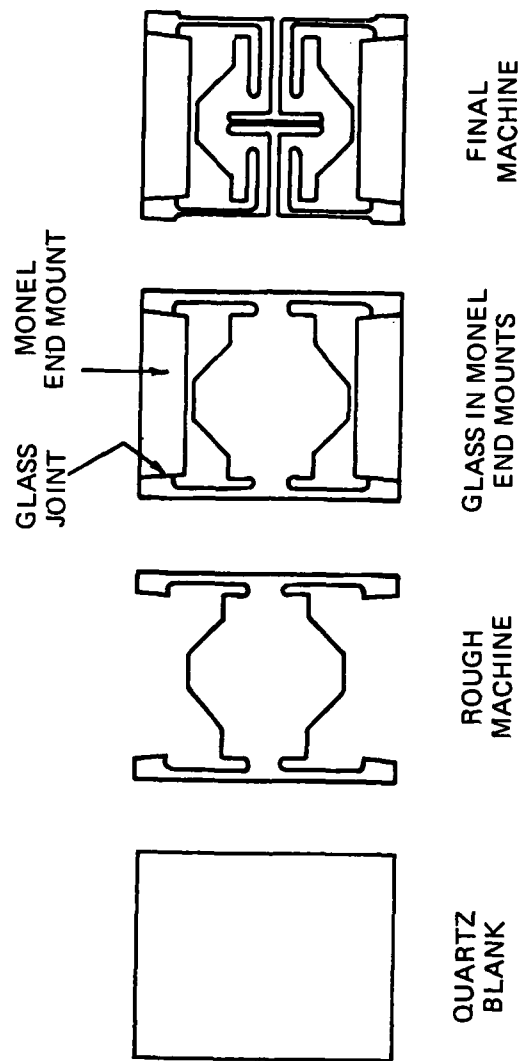


FIGURE 15. GLASS FRIT JOINT

5. HYBRID OSCILLATOR

During the course of development tests both hybrid and discrete component versions of various oscillators were evaluated. It was discovered that the small hybrid oscillators performed at least an order of magnitude better than the discrete component versions of the same oscillators. This performance improvement of hybrids over discrete component versions is attributed to the reduction of stray capacitance effects by an order of magnitude or more. For both performance and envelope purposes it is suggested that a small hybrid version of the oscillator design to be selected be developed and mounted within the VBA body.

6. RESONATOR GEOMETRY IMPROVEMENT

The present resonator machining processes result in a beam geometry which is not completely symmetrical in cross section and also not completely symmetrical at the beam root. It can be shown that these non-symmetrical conditions makes the resonator more susceptible to instabilities of the beam boundary conditions. It is therefore suggested that the resonator fabrication procedure be improved to result in more favorable resonator geometry.

7. FINITE ELEMENT ANALYSIS

Using finite element analysis has been a great advantage in determining resonator static and dynamic behavior. Some preliminary work has also been performed in using finite element analysis to also predict and adjust the temperature-frequency characteristics of the resonator. Presently we are able to analytically predict the shape of the resonator frequency vs. temperature characteristics, but we are not able to predict the turnover (ZTC) temperature. This is because the stresses and strains at the root of a vibrating beam are very complicated and it is in the root where the major portion of the vibration strain energy is concentrated. A detailed finite analysis program is available which considers the entire quartz compliance tensor. It is also capable of performing coordinate transformations of this tensor which result when different angular cuts of quartz are used. This program is also capable of running in double precision which is needed to resolve small frequency changes experienced due to the temperature changes in the various terms of the compliance tensor. It is believed that by using this analysis method, a prediction of the turnover temperature vs. crystal cut can be made. The goal of this effort will be to increase the turnover temperature to a more favorable temperature and also determine a crystal cut which has the lowest temperature-frequency sensitivity.

8. NON-PRISMAL RESONATOR GEOMETRY

To date only prismatic resonator geometries have been used since they are the simplest to analyze and to machine. However, the analysis capability and the machining capability is at hand to analyze and machine resonators with non prismatic beams. There is some evidence to show that non prismatic beams will have a higher force- frequency sensitivity and also be less sensitive to changes in resonator boundary conditions. Higher scale factor and improved bias stability should result.

9. LINEARITY IMPROVEMENT

It has been discovered that subtle changes in the way the axial load is applied to the resonator can affect the resonator linearity. By design, a resonator loading mechanism can be devised which will tend to cancel the second order frequency-force sensitivity.

The net result will be a resonator frequency-force sensitivity that is much more linear than the present resonators. This improvement will make the task of matching and trimming individual resonators and proof masses, in order to null out the g^2 effects that much easier.

DOCUMENT NO _____

REV A

ENGINEERING TECHNICAL REPORT

APPENDIX A

VIBRATING FLEXURE BEAM IN TENSION MATH MODEL

BY

W. C. Albert

March 1979

SINGER
AEROSPACE & MARINE SYSTEMS

THE SINGER COMPANY • KEARFOTT DIVISION • 1166 MCBRIDE AVENUE • LITTLE FALLS, N. J. 07424

TABLE OF CONTENTS

1. INTRODUCTION

2. BEAM ANALYSIS CONSIDERING FLEXURE, TENSION & LINEAR DISPLACEMENT

- 2.1 Procedure
- 2.2 Assumed Beam Deflection
- 2.3 Flexure Potential Energy $(PE)_M$
- 2.4 Tension Potential Energy $(PE)_T$
- 2.5 Linear Kinetic Energy $(KE)_L$
- 2.6 Determine Beam Resonant Frequency (ω_B)
- 2.7 Typical Beam Tension Coefficients

LIST OF SYMBOLS

C_1, C_2, C_3, C_4 , Coefficients of beam equation determined from boundary conditions

M = Bending Moment

V = Shear Reaction

PE = Potential Energy

KE = Kinetic Energy

I = Section Moment of Inertia

ρ = Density

\dot{y} = Time derivative of y

m = Mass

$\dot{\theta}$ = Time derivative of θ

a_0, a_1, a_2, a_3 = Beam power series coefficients

G = Shear Modulus

$(l, t, b)_B$ = Length, thickness, and width of beam (B)

E = Elastic Modulus $8.61 (10^{11})$ dyne/cm² for quartz

ω = Beam vibrational frequency in rad/sec

N = Beam vibration mode ($N = 1$ for fundamental)

y = Beam amplitude

y' = dy/dx (beam slope)

y'' = d^2y/dx^2 (beam curvature)

y''' = d^3y/dx^3

x = Location along beam length

Other symbols as defined in various illustrations and text.

1. INTRODUCTION

In determining the vibrational characteristics of a quartz resonator, piezoelectric effects are neglected. This is justified because of the high Q (about 40,000) of the resonating system. The analysis, therefore, considers only Hook's Law and Newton's Law.

The analysis uses the Rayleigh Method which has been modified to include beam tension effects. The reason is that the Rayleigh Method is easy to follow and it agrees well with experimental data and more rigorous analytical methods. It also more easily adapts itself to non-prismal shapes and can also be used to assess the effects of shear and rotary inertia which is usually neglected in flexure beam analysis.

2. BEAM ANALYSIS CONSIDERING FLEXURE, TENSION AND LINEAR DISPLACEMENT

2.1 Procedure

The Rayleigh Method will be used and the basic steps are as follows:

1. Assume a beam deflection shape that is reasonable.
2. Assume harmonic motion.
3. Determine and then equate the maximum potential energy of the vibrating system to the maximum kinetic energy.
4. Solve for the resonant frequency of the system. This can be done since the kinetic energy term will include the resonant frequency term.

The analysis of this section will consider only the potential energy due to flexure and tension and only the kinetic energy due to linear velocity. The effects of shear and rotation are neglected in the analysis but are commented upon later.

2.2 Assumed Beam Deflection

The assumed deflection will be that of a fixed-fixed vibrating beam where tension effects are considered to have a negligible effect on the deflection shape. The deflection shape for the first five modes is shown in Figure 2-1. The general expression for these shapes is given in Reference 1 and also in other vibration literature as Equation (2-1).

$$y = C_1 \sinh kx + C_2 \cosh kx + C_3 \sin kx + C_4 \cos kx \quad (2-1)$$

MODE NUMBER

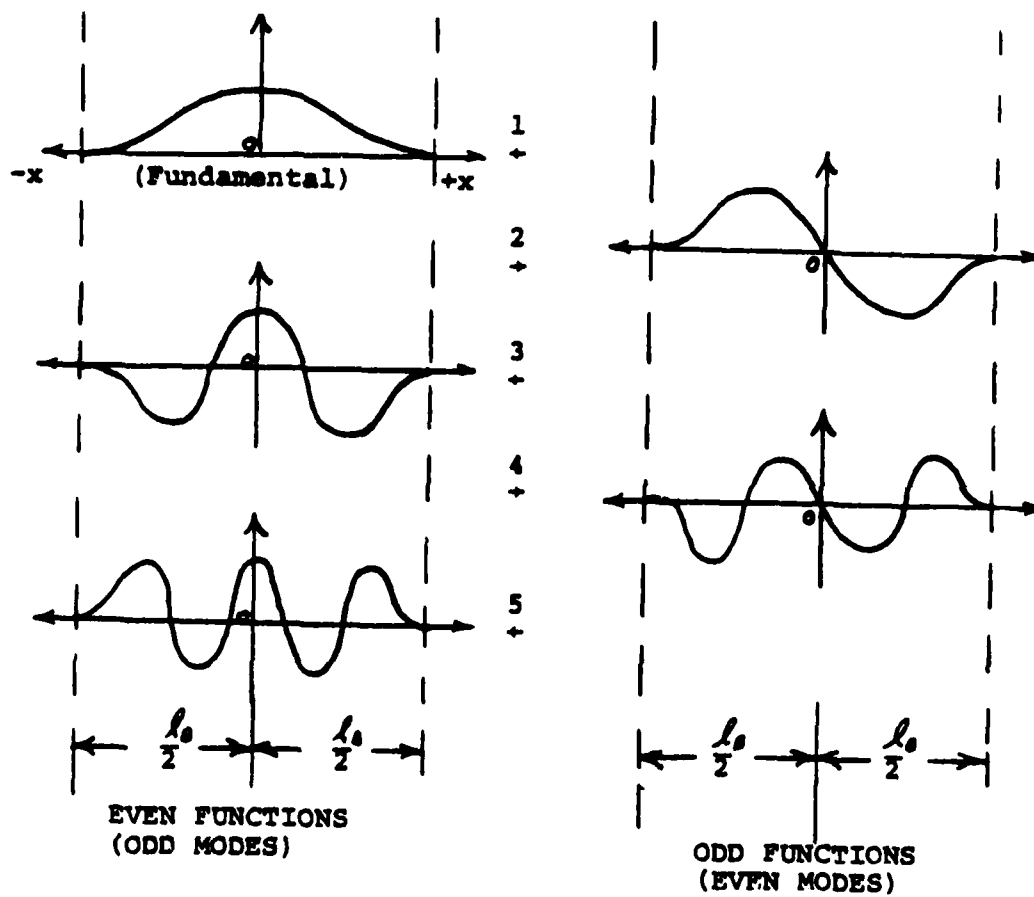


FIGURE 2-1
BEAM DEFLECTION CURVES
FOR MODES 1 THROUGH 5

2.2 (cont'd)

From odd and even symmetry of Figure 2-1 it can be seen that the coefficients C_1 and C_3 will be zero of odd modes (even functions, $N = 1, 3, 5, \dots$) and the coefficients C_2 and C_4 will be zero for the even modes (odd functions, $N = 2, 4, 6, \dots$). The remaining coefficients are evaluated for the boundary conditions of zero deflection ($y = 0$) and zero slope ($dy/dx = 0$) at the beam ends ($x = \pm l/2$). Equation (2-1) then reduces to Equations (2-2) and 2-3). The values of Table 2-1 will satisfy the boundary conditions for the various modes.

For odd modes (even functions)

$$y = C_2 \left[\frac{C_2}{C_4} \cosh kx + \cos kx \right] \quad (2-2)$$

For even modes (odd functions)

$$y = C_3 \left[\frac{C_3}{C_1} \sinh kx + \sin kx \right] \quad (2-3)$$

TABLE 2-1. BOUNDARY CONDITIONS FOR MODES OF OPERATION

MODE	MODE (M)	k	C_2/C_4	C_1/C_3
1	FUNDAMENTAL	1.0037 ($3\pi/2l_B$)	.1328	----
2		.9999 ($5\pi/2l_B$)	----	.0278
3		1.0000 ($7\pi/2l_B$)	-.00580	----
4		1.0000 ($9\pi/2l_B$)	----	-.00120
5		1.0000 ($11\pi/2l_B$)	-.000250	

2.2 (cont'd)

Note that an approximation for k is

$$k \approx \frac{(2n+1)\pi}{2l_b}$$

Also note that the actual values of C_3 and C_4 will depend on the beam vibration amplitude.

Tables 2-2, 3 and 4 include the successive differentiations of Equations (2-2 and 3) with respect to x (y' , y'' and y''') along with values at various locations along the beam for modes 1, 2 and 3. These functions are plotted in Figures 2-2, 3 and 4.

TABLE 2-2

MODE 1 CHARACTERISTIC

$$y = C_4 \left[\frac{C_2}{C_4} \cosh kx + \cos kx \right] \quad y'' = C_4 k^2 \left[\frac{C_2}{C_4} \cosh kx - \cos kx \right]$$

$$y' = C_4 k \left[\frac{C_2}{C_4} \sinh kx - \sin kx \right] \quad y''' = C_4 k^3 \left[\frac{C_2}{C_4} \sinh kx + \sin kx \right]$$

$$k = 1.0037 \frac{(3\pi/2)}{L}$$

$$\frac{C_2}{C_4} = .1328$$

x =	0	$\frac{L}{16}$	$\frac{8}{8}$	$\frac{3L}{16}$	$\frac{L}{4}$	$\frac{5L}{16}$	$\frac{3L}{8}$	$\frac{7L}{16}$	$\frac{L}{2}$
.1328 cosh kx	.133	.139	.137	.180	.237	.306	.403	.534	.713
.1328 sinh kx	0	.040	.003	.134	.196	.276	.380	.518	.701
cos kx	1.000	.957	.830	.632	.379	.093	-.202	-.478	-.713
sin kx	0	.291	.557	.775	.926	.996	.979	.878	.701
y/C ₄	1.133	1.096	.987	.820	.616	.399	.201	.056	0
y'/kC ₄	0	-.251	-.474	-.641	-.730	-.720	-.599	-.360	0
y''/k ² C ₄	-.867	-.818	-.673	-.444	-.142	.213	.605	1.012	1.426
y'''/k ³ C ₄	0	.221	.640	.909	.122	1.272	1.399	1.396	1.402
(y/C ₄) ²	1.284	1.201	.974	.672	.379	.159	.040	.003	0
(y'/kC ₄) ²	0	.065	.225	.411	.533	.518	.359	.130	0
(y''/k ² C ₄) ²	.752	.669	.453	.197	.020	.045	.366	1.024	2.033
(y'''/k ³ C ₄) ²	0	.110	.410	.826	1.299	1.618	1.847	1.949	1.966

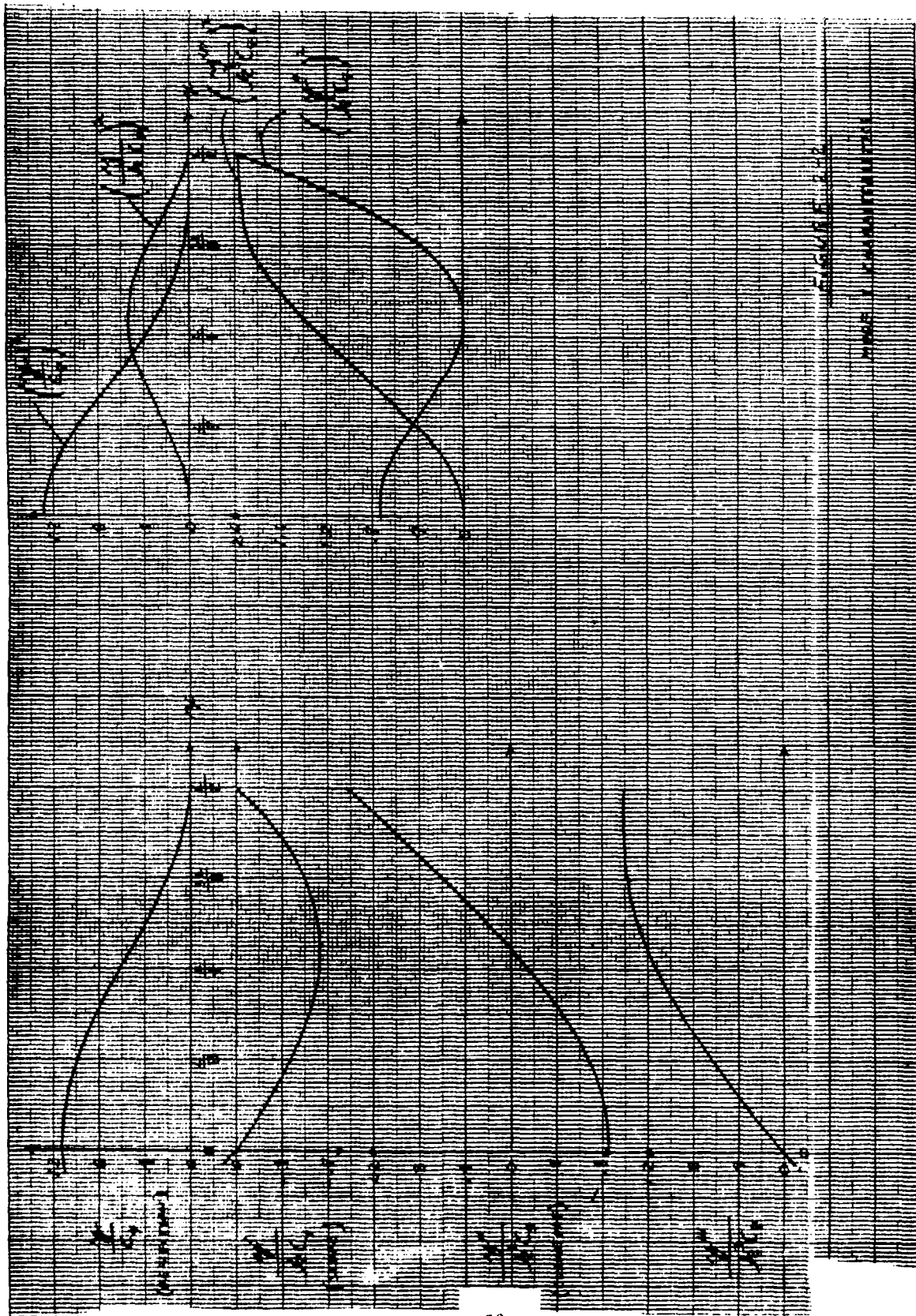


FIGURE 2-2. MODE 1 CHARACTERISTICS

TABLE 2-3

MODE 2 CHARACTERISTICS

$$y = C_3 \left[\frac{C_1}{C_3} \sinh kx + \sin kx \right] \quad y'' = C_3 k^2 \left[\frac{C_1}{C_3} \sinh kx - \sin kx \right]$$

$$y' = C_3 k \left[\frac{C_1}{C_3} \cosh kx + \cos kx \right] \quad y''' = C_3 k^3 \left[\frac{C_1}{C_3} \cosh kx - \cos kx \right]$$

$$k = \frac{(5\pi/2)}{l}$$

$$\frac{C_1}{C_3} = .0278$$

$x =$	0	$\frac{l}{18}$	$\frac{l}{9}$	$\frac{l}{6}$	$\frac{l}{4}$	$\frac{l}{3}$	$\frac{l}{2}$	$\frac{7l}{18}$	$\frac{l}{2}$
.0278 cosh kx	.028	.031	.042	.064	.101	.163	.265	.432	.705
.0278 sinh kx	0	.014	.032	.057	.097	.161	.264	.431	.705
cos kx	1.000	.882	.535	.098	-.383	-.772	-.980	-.957	-.707
sin kx	0	.471	.831	.995	.924	.634	.195	-.290	-.707
y/C_3	0	.485	.863	1.052	1.021	.795	.460	.141	0
y'/kC_3	1.020	.913	.597	.162	-.282	-.609	-.724	-.525	0
y''/k^2C_3	0	-.457	-.799	-.938	-.827	-.473	.069	.721	1.412
y'''/k^3C_3	-.972	-.881	-.513	-.034	.484	.935	1.245	1.389	1.412
$(y/C_3)^2$	0	.235	.749	1.107	1.042	.632	.212	.020	0
$(y'/kC_3)^2$	1.037	.833	.356	.026	.079	.370	.524	.276	0
$(y''/k^2C_3)^2$	0	.209	.638	.880	.684	.224	.003	.520	1.993
$(y'''/k^3C_3)^2$.945	.724	.263	.001	.234	.874	1.550	1.929	1.993

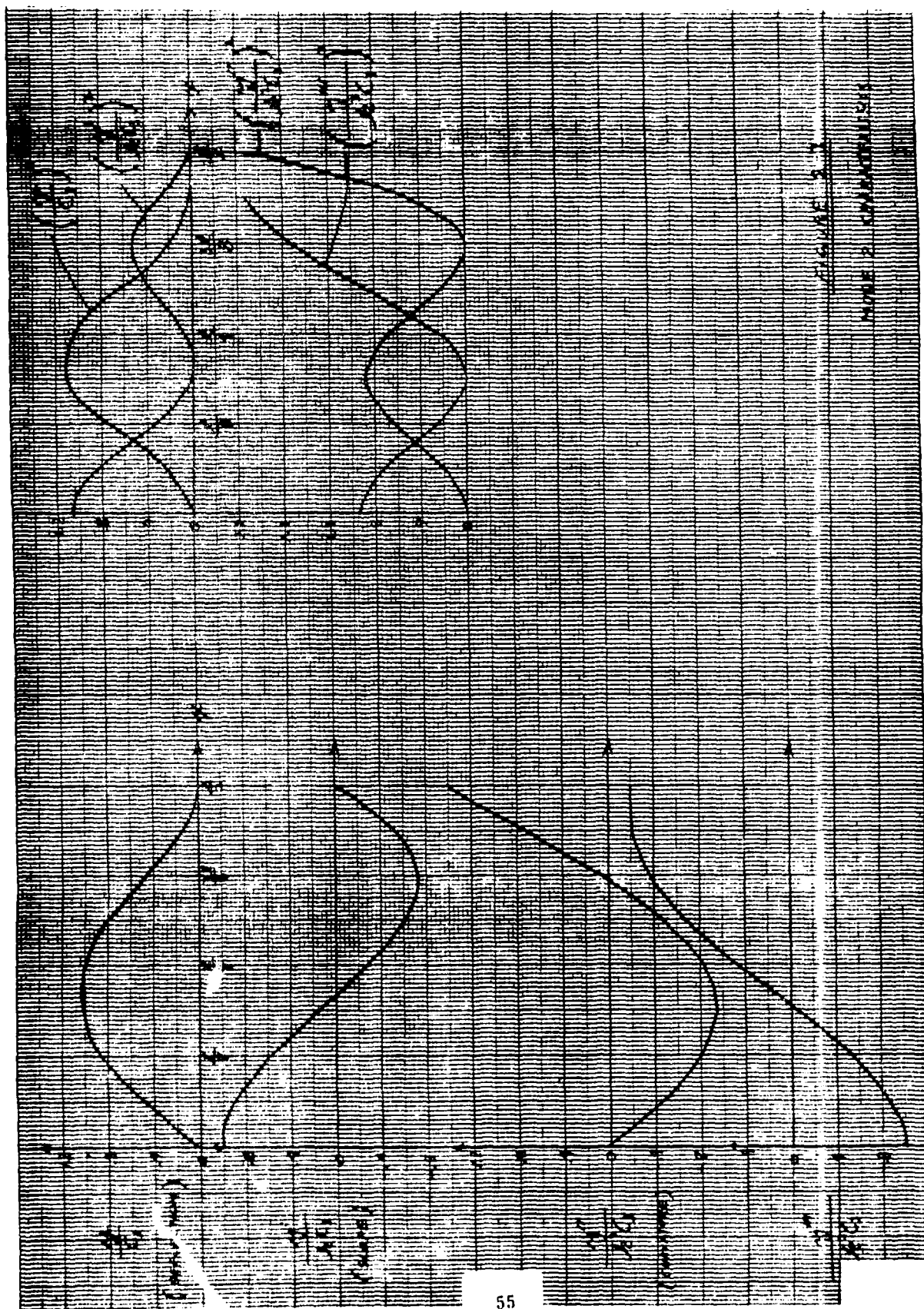


FIGURE 2-3. MODE 2 CHARACTERISTICS

TABLE 2-4

MODE 3 CHARACTERISTICS

$$y = C_4 \left[\frac{C_2}{C_4} \cosh kx + \cos kx \right] \quad y'' = C_4 k^2 \left[\frac{C_2}{C_4} \cosh kx - \cos kx \right]$$

$$y' = k C_4 \left[\frac{C_2}{C_4} \sinh kx - \sin kx \right] \quad y''' = C_4 k^3 \left[\frac{C_2}{C_4} \sinh kx + \sin kx \right]$$

$$k = \frac{(7\pi/2)}{l}$$

$$\frac{C_2}{C_4} = -.00580$$

x =	0	$\frac{l}{10}$	$\frac{l}{8}$	$\frac{3l}{10}$	$\frac{l}{4}$	$\frac{7l}{10}$	$\frac{3l}{8}$	$\frac{7l}{10}$	$\frac{l}{2}$
.00580 cosh kx	.0058	.007	.012	.023	.043	.090	.129	.356	.708
.00580 sinh kx	0	.004	.020	.022	.043	.090	.179	.356	.708
cos kx	1	.773	.198	-.471	-.924	-.957	-.555	.098	.707
sin kx	0	.634	.981	-.082	.383	-.290	-.831	-.995	-.707
y/C ₄	.994	.766	.183	-.494	-.969	-1.047	-.734	-.258	0
y'/C ₄ k	0	-.638	-1.001	-.094	-.426	.200	.652	.639	0
y''/C ₄ k ²	-1.006	-.780	-.207	.448	.879	.867	.376	-.454	-1.415
y'''/C ₄ k ³	0	.630	.961	.860	.338	-.380	-1.010	-1.351	-1.415
(y/C ₄) ²	.988	.587	.033	.244	.939	1.096	.538	.066	0
(y'/kC ₄) ²	0	.407	1.002	.817	.183	.040	.425	.408	0
(y''/k ² C ₄) ²	1.012	.608	.043	.201	.773	.732	.141	.206	2.002
(y'''/k ³ C ₄) ²	0	.397	.923	.740	.114	1.144	1.020	1.825	2.002

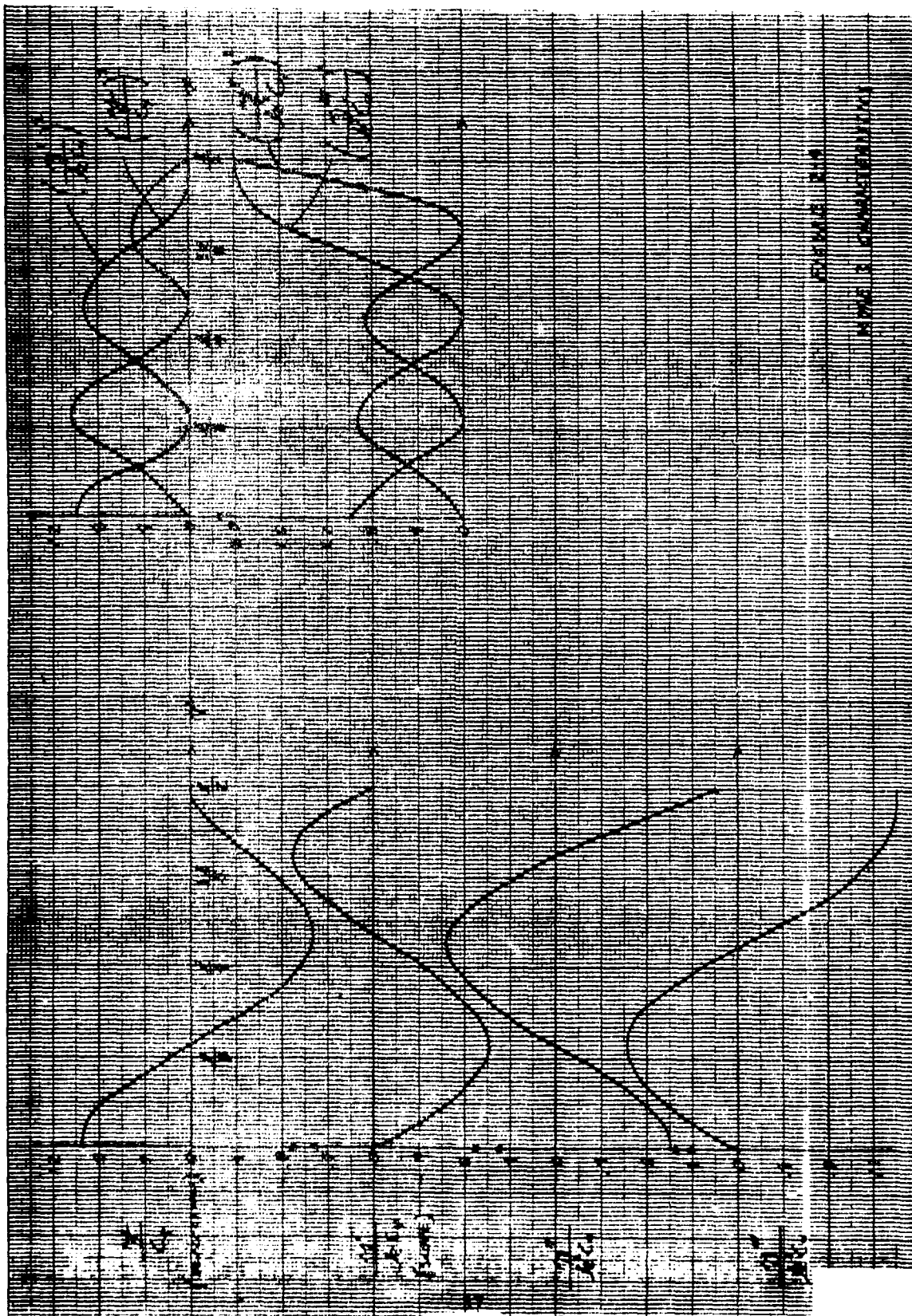
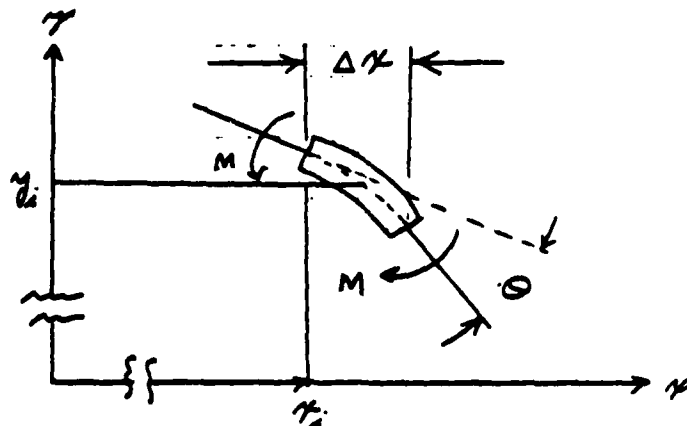


FIGURE 2-4. MODE 3 CHARACTERISTICS

2.3 Flexure Potential Energy (PE)_M

A small increment of the deflected beam is illustrated in Figure 2-5.



BENDING MOMENT EFFECT
FIGURE 2-5

The potential energy of a system which has a linear spring rate is $1/2$ the spring rate times the square of the deflection. Therefore, the incremental potential energy of the dx beam element is:

$$\Delta(PE)_M = \frac{(M/\theta)\theta^2}{2} \quad (2-5)$$

From strength of materials comes the following two expressions which relate bending angle (θ) to bending moment (M) and bending moment to curvature (y'').

$$\theta = \frac{M \Delta x}{EI} \quad \text{and} \quad M = EI y'' \quad (2-6, 7)$$

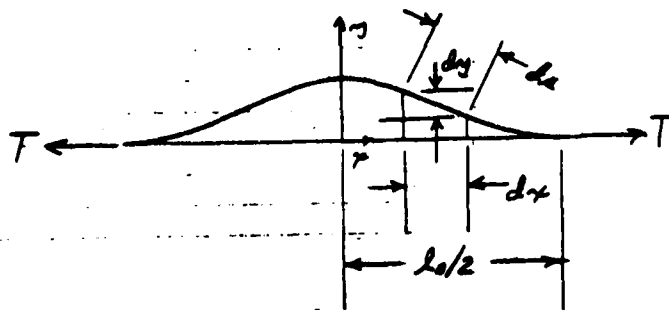
2.3 (cont'd)

Making the indicated substitutions will give the following expression for the total flexure potential energy for 1/2 the beam.

$$(PE)_M = \frac{EI}{2} \int_{x=0}^{L/2} (\gamma'')^2 dx \quad (2-8)$$

2.4 Tension Potential Energy (PE)_T

Tension potential energy is determined by considering the beam as a string under tension as shown in Figure 2-6.



TENSION EFFECT
FIGURE 2-6

The potential energy, in this case the change in potential energy, is the tension force (\$T\$) times the change in length (\$ds - dx\$) of the "string" as it deflects from its zero position to its deflected position. The incremental potential energy of the \$dx\$ beam element is:

$$\Delta(PE)_T = T(ds - dx) \quad (2-9)$$

2.4 (cont'd)

From Figure 2-6 is derived the following expression for ds along with its approximation using the binomial expansion.

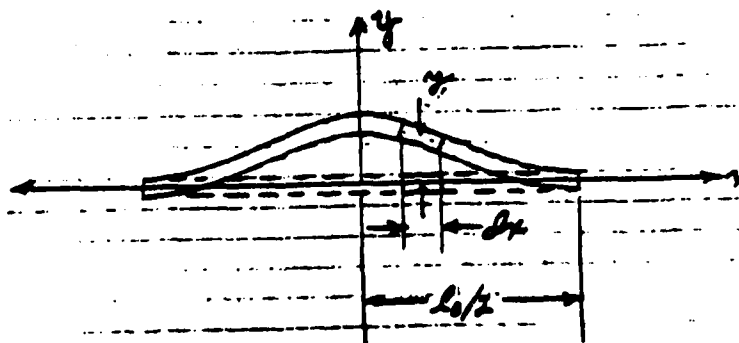
$$ds = [(dx)^2 + (dy)^2]^{1/2} = dx \left[1 + \left(\frac{dy}{dx} \right)^2 \right]^{1/2} \approx dx \left[1 + \frac{1}{2} \left(\frac{dy}{dx} \right)^2 \right] \quad (2-10)$$

Substituting Equation (2-10) into (2-9) results in the following expression for the total tension potential energy for 1/2 the beam.

$$(PE)_T = \frac{T}{2} \int_{x=0}^{L_0/2} (y')^2 dx \quad (2-11)$$

2.5 Linear Kinetic Energy (KE)_L

A small increment of the deflected beam is illustrated in Figure 2-7.



LINEAR MOMENTUM EFFECT
FIGURE 2-7

2.5 (cont'd)

The element dx is at rest at maximum deflection and has maximum velocity in the y direction when $y=0$. For such a system the maximum incremental kinetic energy is $1/2$ the mass times the square of maximum linear velocity.

$$\Delta(KE)_L = \frac{\Delta M (\dot{y})_{\max}^2}{2} \quad (2-12)$$

For the element dx experiencing harmonic motion:

$$\Delta M = \rho b t dx \quad \dot{y}_{\max} = y \omega \quad (2-13, 14)$$

Making the indicated substitutions results in the following expression for the total linear kinetic energy for $1/2$ the beam.

$$(KE)_L = \frac{\omega^2 \rho b t}{2} \int_{x=0}^{L/2} y^2 dx \quad (2-15)$$

2.6 Determine Beam Resonant Frequency (ω_B)

As stated in Steps 3 and 4 of section 2.1, the beam resonant frequency is determined by equating maximum kinetic energy to maximum potential energy and solving for ω_B as follows.

From $\Sigma KE = \Sigma PE$

$$(KE)_L = (PE)_M + (PE)_T \quad (2-16)$$

Substituting Equations (2-8, 11 and 15) into (2-16)

$$\frac{\omega^2 \rho b t}{2} \int_{x=0}^{L/2} y^2 dx = \frac{EI}{2} \int_{x=0}^{L/2} (y'')^2 dx + \frac{T}{2} \int_{x=0}^{L/2} (y')^2 dx \quad (2-17)$$

Solve for ω

$$\omega = \left[\frac{EI \int (\psi'')^2 dx + T \int (\psi')^2 dx}{\rho b t \int \psi^2 dx} \right]^{1/2} \quad (2-18)$$

2.6 (cont'd)

Note that symmetry allows the limits of integration to be over the whole or half the beam. For simplicity, the limits of integration are omitted.

The bias frequency (ω_0) is determined for the condition $T = 0$.

$$\omega_0 = \left[\frac{EI}{\rho b t} \frac{\int (\psi'')^2 dx}{\int (\psi^2) dx} \right]^{1/2} \quad (2-19)$$

Or for $I = bt^3/12$

$$\omega_0 = \left[\frac{t^2 E}{12 \rho} \frac{\int (\psi'')^2 dx}{\int (\psi^2) dx} \right]^{1/2} \quad (2-20)$$

Equation (2-18) now becomes::

$$\omega = \omega_0 \left[1 + \frac{T}{\omega_0^2 \rho b t} \frac{\int (\psi')^2 dx}{\int \psi^2 dx} \right]^{1/2} \quad (2-21)$$

Using the binomial expansion

$$\begin{aligned} \omega = \omega_0 \left\{ 1 + \frac{1}{2} \left[\frac{1}{\omega_0^2 \rho b t} \frac{\int (\gamma')^2 dx}{\int \gamma^2 dx} \right] T \right. \\ \left. - \frac{1}{8} \left[\frac{1}{\omega_0^2 \rho b t} \frac{\int (\gamma')^2 dx}{\int \gamma^2 dx} \right]^2 T^2 \right. \\ \left. + \frac{1}{16} \left[\frac{1}{\omega_0^2 \rho b t} \frac{\int (\gamma')^2 dx}{\int \gamma^2 dx} \right]^3 T^3, \dots \right\} \end{aligned} \quad (2-22)$$

The expansion of Equation (2-22) carried to the cubic T term is usually sufficient. If needed, the next two terms of the series are:

$$\begin{aligned} - .039 \left[\frac{1}{\omega_0^2 \rho b t} \frac{\int (\gamma')^2 dx}{\int \gamma^2 dx} \right]^4 T^4 \\ + .0273 \left[\frac{1}{\omega_0^2 \rho b t} \frac{\int (\gamma')^2 dx}{\int \gamma^2 dx} \right]^5 T^5 \end{aligned} \quad (2-22)'$$

Additional terms may be obtained by further applying the expansion.

2.6 (cont'd)

Equation (2-22) can be expressed in another form.

$$w = a_0 \frac{F_0 \sqrt{E}}{L^2 \rho} \left[1 + a_1 \left[\frac{L^2}{E A L^2} \right] T - a_2 \left[\frac{L^2}{E A L^2} \right]^2 T^2 + a_3 \left[\frac{L^2}{E A L^2} \right]^3 T^3 \dots \right] \quad (2-23)$$

The a_N coefficients are determined from Equation (2-22) and the integral values of Table 2-5.

TABLE 2-5
INTEGRAL VALUES

MODE INTEGRAL	1	2	3
$\int y^2 dx$	$.254 C_0^2 L$	$.249 C_0^2 L$	$.250 C_0^2 L$
$\int (y')^2 dx$	$3.06 C_0^2 / L$	$11.6 C_0^2 / L$	$24.9 C_0^2 / L$
$\int (y'')^2 dx$	$127 C_0^2 / L^3$	$949 C_0^2 / L^3$	$3650 C_0^2 / L^3$
$\int (y''')^2 dx$	$6370 C_0^2 / L^5$	$1.03(10^5) C_0^2 / L^5$	$692(10^5) C_0^2 / L^5$

Note: Limits of integrals are $x=0$ to $x=L/2$.

Integrals were evaluated using Simpson's rule on the values of Tables (2-2, 3, 4).

2.6 (cont'd)

To demonstrate the effectiveness of the Rayleigh method, coefficients a_0 thru a_3 were evaluated for Mode 1 and found to be 6.45, .145, .010 and .0015 respectively. This compares well to the accepted values of 6.45, .148, .012 and .0018 respectively that were determined by a very rigorous and hard to follow solution of the differential equation of a vibrating flexure beam under tension.

This is good agreement considering the graphical integrations. Other coefficients are given in Table 2-6.

TABLE 2-6. COEFFICIENTS OF EQUATION (2-23)

MODE NO. \ COEFF.	a_0	a_1	a_2	a_3
1	6.45	.148	$-1.2(10^{-3})$	$1.8(10^{-5})$
2	17.8	.122	$-7.7(10^{-3})$	$1.0(10^{-3})$
3	34.9	.044	$-8.5(10^{-3})$	$3.3(10^{-5})$

FOR $\omega = \text{Rad/sec}$

2.7 Typical Beam Tension Coefficients

Typical beam dimensions and quartz properties are:

$$\begin{aligned} l &= .173 \text{ in} &= .439 \text{ cm} \\ b &= .040 \text{ in} &= .102 \text{ cm} \\ t &= .0052 \text{ in} &= .0132 \text{ cm} \\ E &= 8.61 (10^{11}) \text{ dyne/cm}^2 \\ \rho &= 2.65 \text{ gm/cm}^3 \end{aligned}$$

From these values the expressions are evaluated.

$$\frac{t}{l^2} \sqrt{\frac{E}{\rho}} = 3.90 \times 10^4 \text{ sec}^{-1}$$

$$\frac{l^2}{E b t^3} = 9.55 \times 10^{-7} \text{ dyne}^{-1}$$

For the beam frequency expressed as the power series of Equation (2-23), typical frequency-tension coefficients are given for Modes 1, 2 and 3 in Table 2-7.

$$f = k_0 + k_1 T + k_2 T^2 + k_3 T^3 + \dots \quad (2-28)$$

TABLE 2-7. BEAM FREQUENCY-TENSION COEFFICIENTS

MODE NO \ COEFF.	k_0 kHz	k_1 Hz/dyne	k_2 Hz/dyne ²	k_3 Hz/dyne ³
1	40	$5.7(10^{-3})$	$-4.4(10^{-10})$	$6.3(10^{-17})$
2	110	$12.8(10^{-3})$	$-7.8(10^{-10})$	$9.7(10^{-17})$
3	216	$8.5(10^{-3})$	$-1.5(10^{-10})$	$0.6(10^{-17})$

REFERENCES

- (1) Church, A.H., Mechanical Vibrations,
New York: Wiley, (1957) p 202

ENGINEERING TECHNICAL REPORT

APPENDIX B
SQUEEZE FILM GAS DAMPING
FOR THE
LOW COST VBA

BY
W. C. ALBERT

ABSTRACT

The introduction of squeeze film gas damping to the basic VBA design approach has the potential of greatly simplifying the design, reducing the size, increasing the ruggedness and increasing the scale factor. This report is an analysis of the frequency sensitivity effects of gas damping. It is concluded that there will be some increase in vibration transmissibility (up to 20%) at some frequencies but this is considered tolerable. The analysis also shows that serious resonance problems can be avoided as long as the damping corner frequency can be kept high compared to the undamped natural frequency of the system. This frequency ratio for the design analyzed was 7.

January 1980

SINGER
AEROSPACE & MARINE SYSTEMS

THE SINGER COMPANY • KEARFOTT DIVISION • 1150 MCBRIDE AVENUE • LITTLE FALLS, N. J. 07424

TABLE OF CONTENTS

	<u>Page No.</u>
1. INTRODUCTION	1
2. DAMPING GAP DESIGN	2
3. FREQUENCY EFFECTS OF SQUEEZE FILM DAMPING	5
4. CONCLUSIONS	10
5. REFERENCES	11

ACKNOWLEDGEMENT

The help of John DeCotiis in the preparation of this analysis is gratefully acknowledged.

LIST OF SYMBOLS

X_C	= Case displacement
X_m	= Proof mass displacement
m	= Proof mass mass
K_B	= Resonator spring rate
K_D	= Gas film spring rate (frequency sensitive)
D_O	= Gas film damping coefficient neglecting frequency sensitivity
D_D	= Gas film damping coefficient considering frequency sensitivity
W_N	= Undamped natural frequency neglecting frequency effects
W_{ND}	= Undamped natural frequency considering frequency effects
W_C	= Damping corner frequency
ζ_O	= Damping ratio neglecting frequency effects
ζ_D	= Damping ratio considering frequency effect
μ	= Gas viscosity
P	= Gas pressure
R	= Damping gap radius
C	= Damping gap (squeeze film) thickness
k	= W_C/W_N
tr	= Transmissibility neglecting frequency effects
tr_D	= Transmissibility considering frequency effects

1. INTRODUCTION

Squeeze film gas damping is being considered for the low cost version of the VBA. Because of gas compressibility effects, the gas film also has spring-like characteristics. This spring term increases with input vibration frequency. Conversely, the damping characteristics of the gas film decreases with increasing frequency. This behavior of the gas film alters the response of the VBA which would otherwise be a simple second order system.

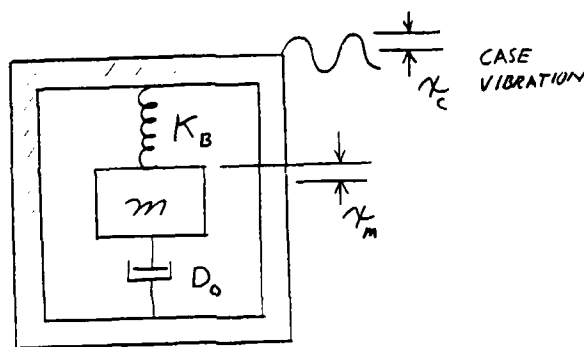
This analysis determines how the transmissibility of the system to case vibration is altered by these effects. The following procedure was used.

1. When the frequency sensitivity effect on spring rate and damping are ignored, the VBA becomes a simple passive second order system. For these conditions the damping gap physical characteristics are determined for a damping ratio of one (critical damping) and a undamped natural frequency of 300 Hz.
2. The corner frequency (3 db point) at which the damping term is turning into a spring term is then determined.
3. Determined next is how this corner frequency alters the natural frequency, damping coefficient and damping ratio. How these characteristics vary with input frequency and corner frequency are plotted in Figure 3-2.
4. From the values determined in Step 3, the transmissibility of the system is determined and plotted in Figure 3-3.

2. DAMPING GAP DESIGN (Neglecting Frequency Effects)

2.1 Step 1

The analysis of this section will neglect, temporarily, the frequency dependence of the damping and spring rate terms. The spring rate and damping coefficients are constants



SECOND ORDER SYSTEM
FIGURE 2-1

and the problem reduces to a simple second order system as illustrated in Figure 2-1. For this system, the undamped natural frequency and the damping ratio are described by equations (2-1) and (2-2) respectively. Note these are standard relationships (Reference 2).

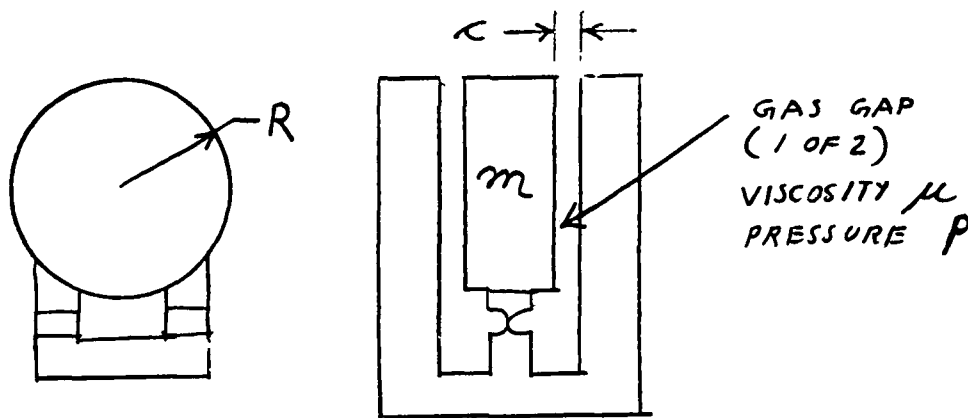
$$\omega_N = \sqrt{\frac{K_B}{m}}$$

(2-1)

$$D_o = 2 \zeta_o m \omega_N$$

(2-2)

The double squeeze film damping gap is shown schematically in Figure 2-2. The expression for the damping coefficient of such an arrangement (again temporarily neglecting frequency effects) is described approximately by Equation 2-3 (Reference 1).



DAMPING MECHANISM
FIGURE 2-2

$$D_o = \frac{9 \mu R^4}{c^3} \quad (2-3)$$

When Equation (2-2 and 3) are combined the following expression is obtained.

$$c^3 = 4.5 \frac{\mu R^4}{\zeta_o m \omega_N} \quad (2-4)$$

The damping gap c is determined for the following typical Low Cost VBA design conditions.

$$\mu = 300 (10^{-6}) \text{ poise (Neon)}$$

$$R = 0.9 \text{ cm}$$

$$m = 10 \text{ gm}$$

$$\omega_N = 300 \text{ Hz } (1.88 (10^3) \text{ rad/sec})$$

$$\zeta_o = 1$$

The result is a c dimension of $3.61 (10^{-3}) \text{ cm} = 1.42 (10^{-3}) \text{ inches}$.

This is considered a reasonable gap for manufacturing purposes.

2.2 Step 2

The expression for the corner frequency in terms of gas properties and gap dimensions is given by Equation (30) (Reference 1).

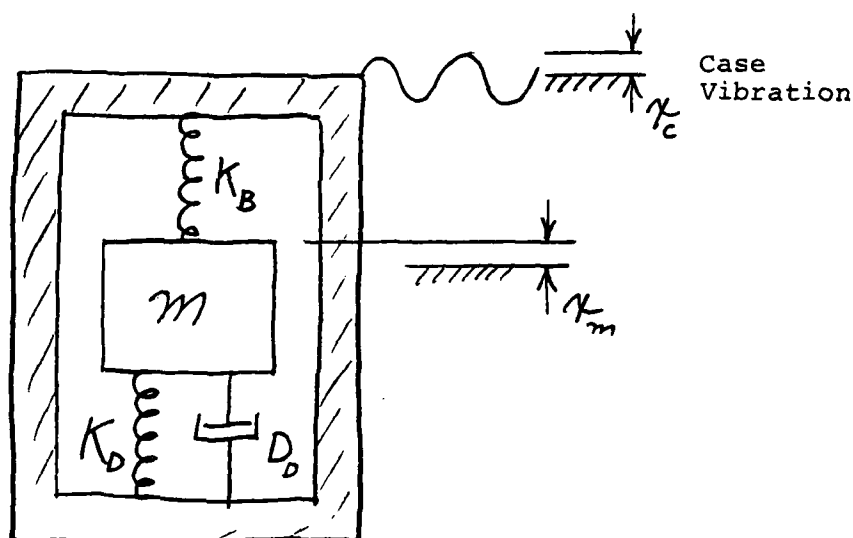
$$\omega_c = \frac{\kappa^2 P}{2.07 \mu R^2} \quad (2-5)$$

For the typical conditions of Section 2 and a pressure of 1/2 atmosphere ($P = 5(10^5)$ dyne/cm²), $\omega_c = 1.3(10^4)$ rad/sec = $2(10^3)$ Hz.

3. FREQUENCY EFFECTS OF SQUEEZE FILM DAMPING

3.1 Step 3

It is characteristic of a squeeze film gap to behave as a pure damper at low frequencies and then transform into a pure spring at high frequencies. This section will include these effects by modifying the simple system of Figure 2-1 into that of Figure 3-1



GAS SPRING EFFECTS
FIGURE 3-1

D_D is the damping coefficient term which also includes the frequency effects. It is described by Equation 3-1 (Reference 1)

$$D_D = \frac{D_o}{1 + \left(\frac{\omega}{\omega_c}\right)^2} \quad (3-1)$$

K_D is the spring effect of the gas compressibility which is described by Equation 3-2 (Reference 1).

$$K_D = \frac{D_o \frac{\omega^2}{\omega_c}}{1 + \left(\frac{\omega}{\omega_c}\right)^2} \quad (3-2)$$

At a particular input vibration frequency, the system of Figure 3-1 will behave as if it had an overall spring rate and damping coefficient determined at that particular frequency. This apparent natural frequency is:

$$\omega_{ND} = \sqrt{\frac{K_D + K_D}{m}} \quad (3-3)$$

and after Equation (2-1, 2) and (3-2) are substituted into (3-3) and rearranged:

$$\omega_{ND} = \omega_N \sqrt{1 + 2 S_o \frac{\omega^2}{\omega_N \omega_c} \left[1 + \left(\frac{\omega}{\omega_c}\right)^2 \right]} \quad (3-4)$$

Letting $W_C = k W_N$, Equation (3-1) and (3-4) become respectively:

$$\frac{D_D}{D_o} = \frac{1}{1 + \frac{1}{k^2} \left(\frac{\omega}{\omega_N}\right)^2} \quad (3-5)$$

$$\frac{\omega_{ND}}{\omega_N} = \sqrt{1 + \frac{2 S_o k^2}{1 + k^2 \left(\frac{\omega}{\omega_N}\right)^2}} \quad (3-6)$$

Both these expressions are plotted in Figure 3-2.

The apparent damping ratio will also change with input frequency.

The expression used for damping ratio are:

$$\zeta_o = \frac{D_o}{2 m \omega_n} \quad (3-6) \quad \zeta_o = \frac{D_o}{2 m \omega_{no}} \quad (3-7)$$

Therefore:

$$\frac{\zeta_o}{\zeta_o} = \frac{D_o/D_o}{\omega_{no}/\omega_n} \quad (3-8)$$

Equation (3-8) is also plotted in Figure 3-2.

The effects of D_D , K_D and W_c on the transmissibility of the system of Figure 3-1 will be determined next.

3.2 Step 4

From vibration analysis (Reference 2) the expression for the transmissibility of the system of Figure 2-1 is

$$\tau_o = \frac{1 + (2 \zeta_o \frac{\omega}{\omega_n})^2}{\sqrt{[1 - (\frac{\omega}{\omega_n})^2]^2 + (2 \zeta_o \frac{\omega}{\omega_n})^2}} = \frac{\tau_m}{\tau_c} \quad (3-9)$$

This expression is next modified to account for the frequency sensitivity of the damping and spring coefficients of Figure 3-1.

$$\tau_o = \frac{1 + (2 \zeta_o \frac{\omega}{\omega_{no}})^2}{\sqrt{[1 - (\frac{\omega}{\omega_n})^2]^2 + (2 \zeta_o \frac{\omega}{\omega_{no}})^2}} = \left(\frac{\tau_m}{\tau_c} \right)_o \quad (3-10)$$

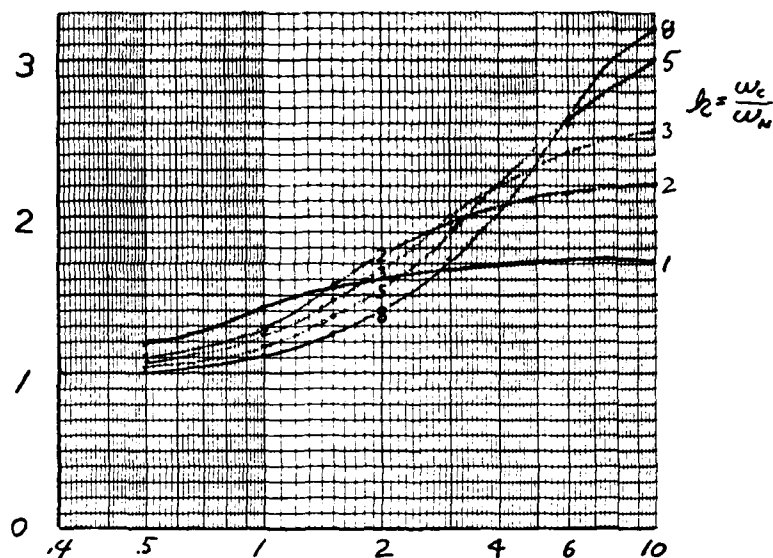
This expression was evaluated and plotted for $\zeta_o = 1$ and various values of k in Figure 3-3.

GAS SPRING EFFECTS ON COEFFICIENTS
FIGURE 3-2

$$\frac{\omega_{ND}}{\omega_N}$$

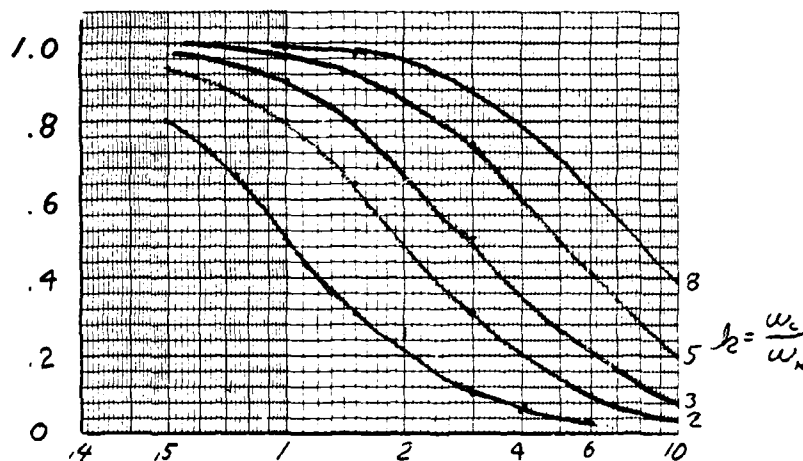
$$= \sqrt{1 + \frac{2 \zeta_0 k}{1 + k^2 \left(\frac{\omega}{\omega_N}\right)^2}}$$

$$\zeta_0 = 1$$



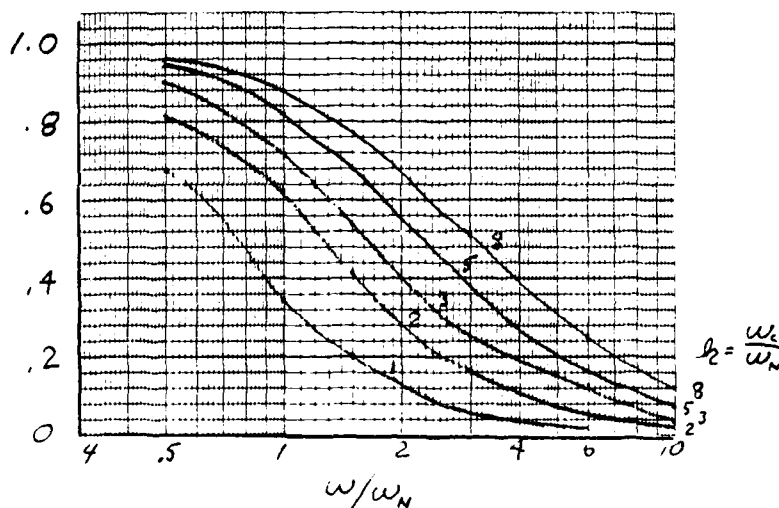
$$\frac{D_0}{D_0}$$

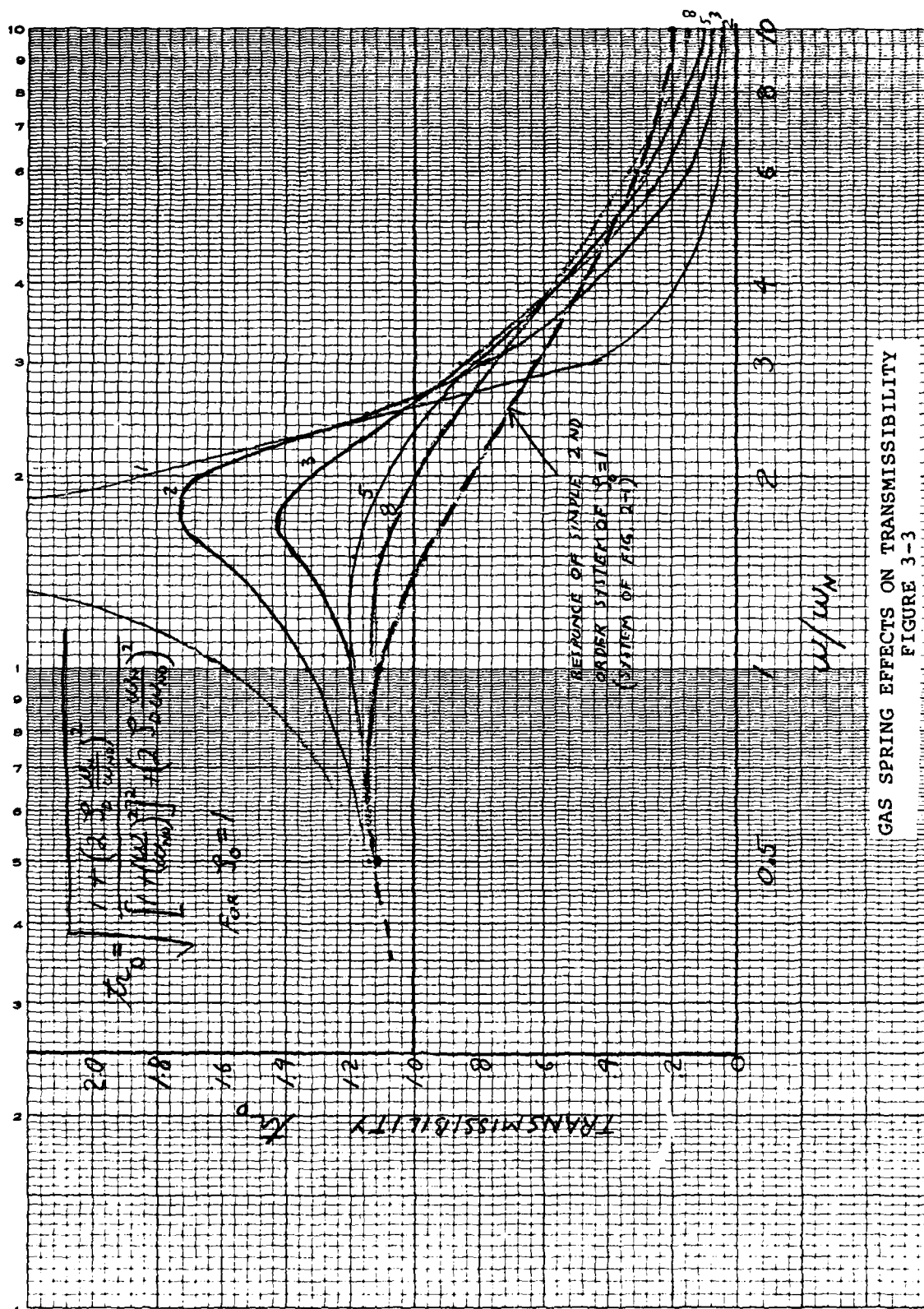
$$= \frac{1}{1 + \frac{1}{k^2} \left(\frac{\omega}{\omega_N}\right)^2}$$



$$\frac{\zeta_0}{\zeta_0}$$

$$= \frac{D_0/D_0}{\omega_{ND}/\omega_N}$$





GAS SPRING EFFECTS ON TRANSMISSIBILITY
FIGURE 3-3

4. CONCLUSIONS

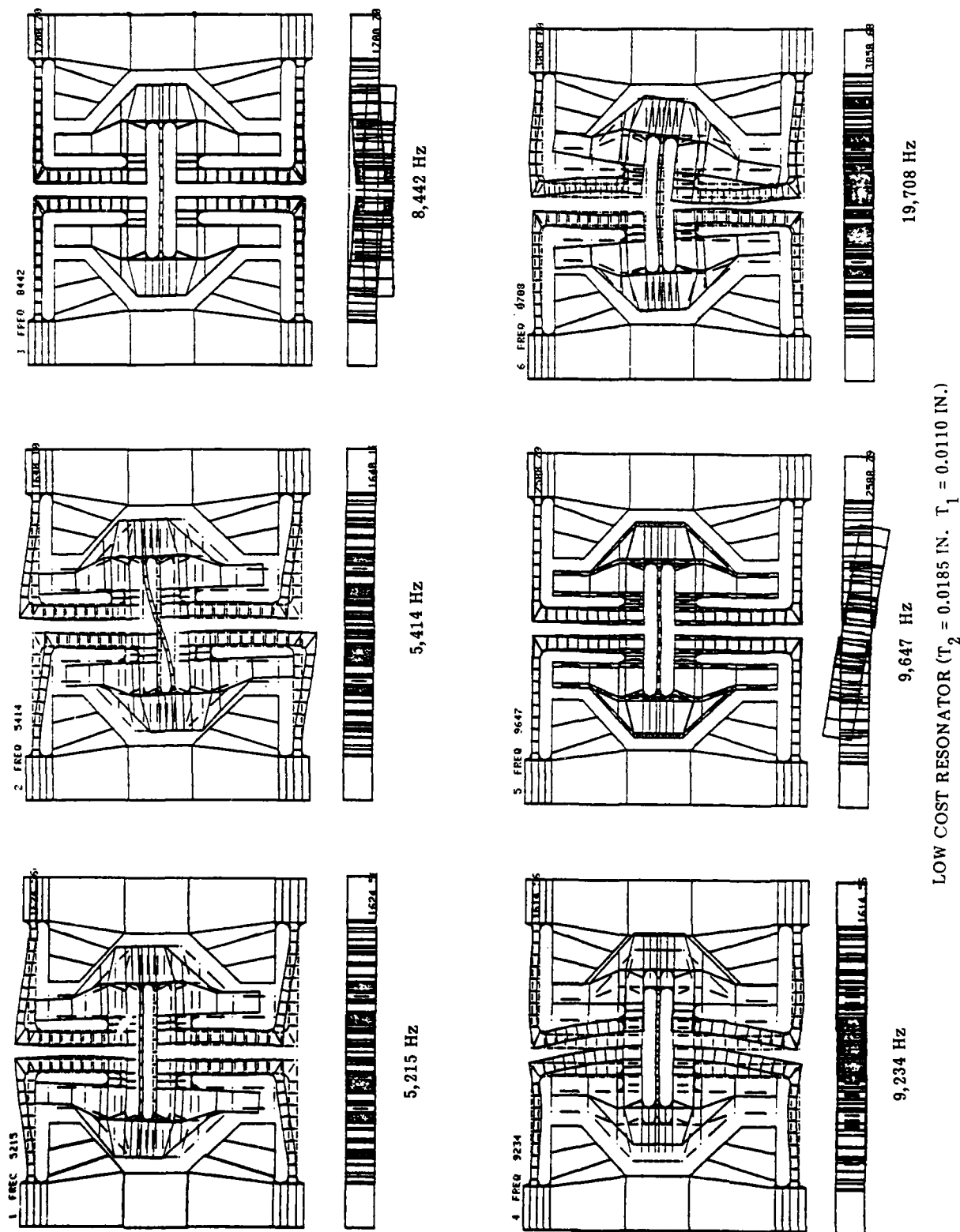
From the equations developed and the plots of Figures 3-2 and 3-3, it can be seen that the frequency sensitivity of squeeze film damping has the following effect:

1. The apparent undamped natural frequency increases with increasing input vibrational frequency. This is due to the squeeze film acting as a spring at high frequencies.
2. The damping coefficient decreases with increasing frequency.
3. The apparent damping ratio decreases with increasing frequency.
4. If W_C is near W_N , The system will behave as an underdamped system even though it is designed for critical damping at low frequencies. If W_C is large compared to W_N , then the system behaves more like a critically damped system although the resonant frequency will be higher. For the proposed squeeze film damped VBA, the ratio of W_C to W_N is about 7 and therefore the transmissibility will never exceed 1.2 as illustrated by Figure 3-3. Figure 3-3 also shows the response of the system neglecting the frequency sensitive effects.

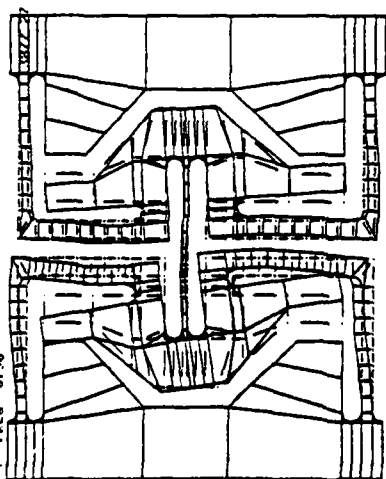
5. REFERENCES

1. A Study of Squeeze-Film Damping, W. S. Griffin, H. H. Richardson, S. Yamanami, Journal of Basic Engineering, June, 1966.
2. Church, A. H., Mechanical Vibration, John Wiley, 1957.

APPENDIX C RESONATOR MODE FREQUENCY ANALYSIS

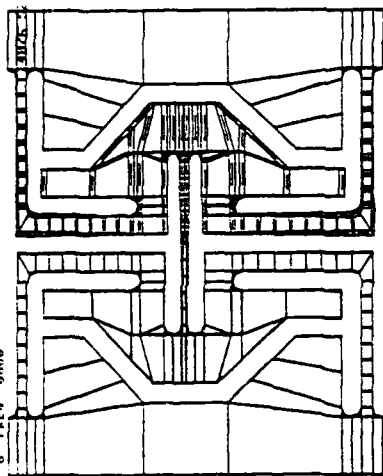


7 FREQ 0790



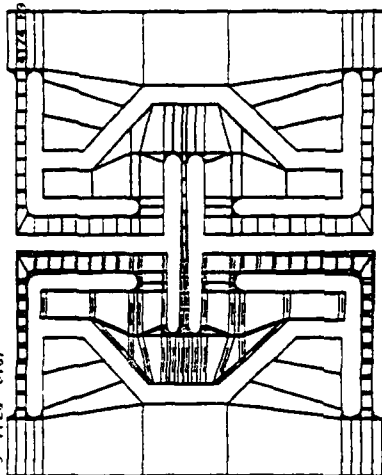
19,790 Hz

8 FREQ 0860



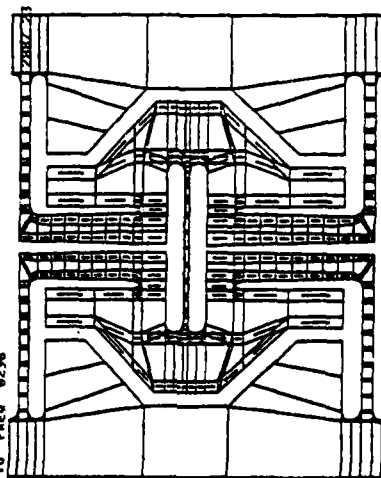
19,860 Hz

9 FREQ 0107



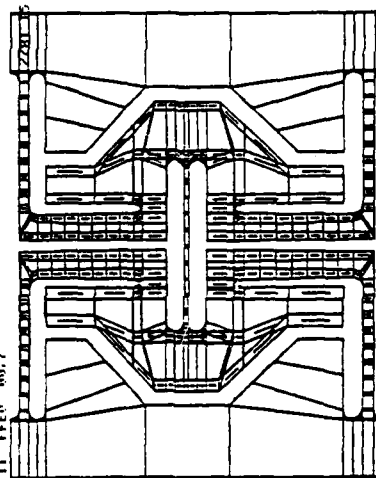
20,107 Hz

10 FREQ 0296



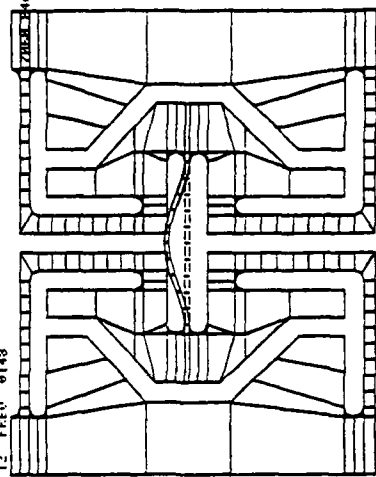
22,296 Hz

11 FREQ 0077

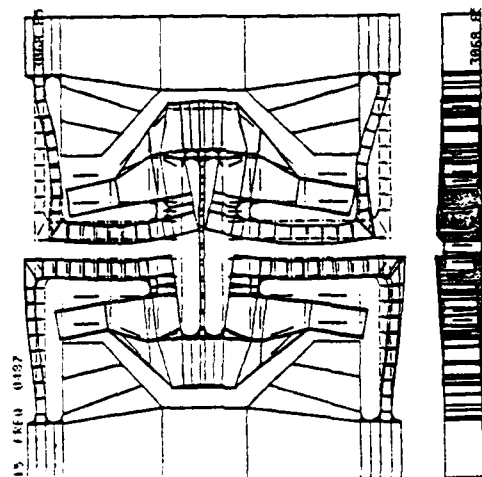


26,077 Hz

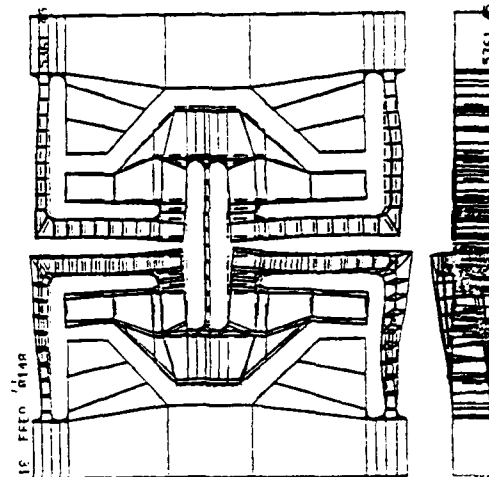
12 FREQ 0143



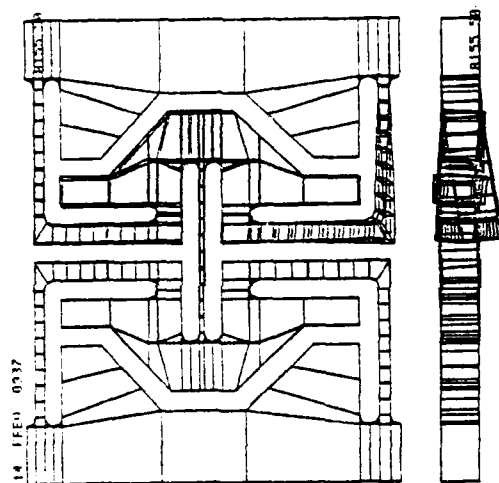
40,148 Hz



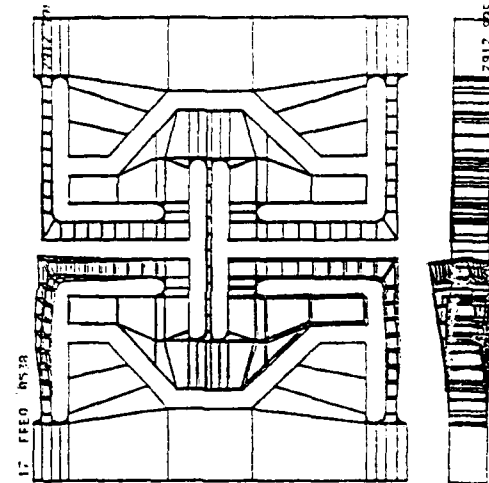
64,487 Hz



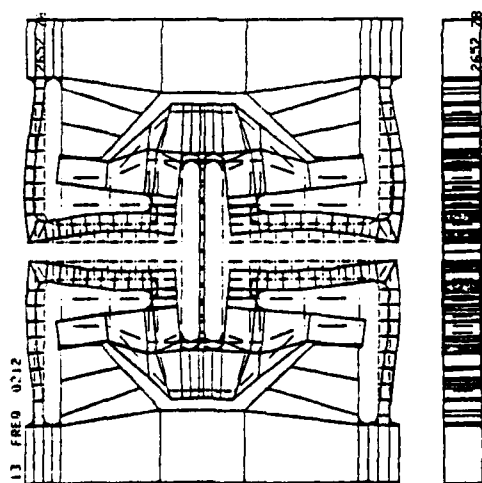
79,148 Hz



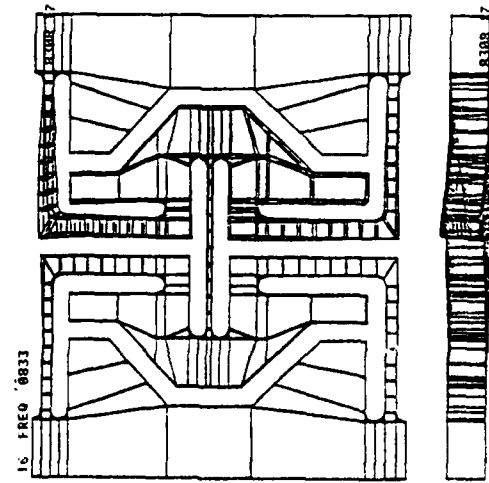
62,937 Hz



75,538 Hz



49,212 Hz



72,833 Hz

APPENDIX D DUAL BEAM VBA FOUR POSITION TEST

Figure D-1 is a schematic representation of the Dual Beam VBA test arrangement. For a four position test just bias, scale factor, nonlinearity and misalignment are considered. Therefore, for Beam 1, the assumed output model and input acceleration are, respectively:

$$f_1 = f_{01} + k_{11} g + k_{21} g^2 \quad (D.1)$$

and

$$g = G \sin (\theta + \theta_{M1}) \quad (D.2)$$

Similarly, for Beam 2

$$f_2 = f_{02} + k_{12} g + k_{22} g^2 \quad (D.3)$$

$$g = G \sin (\theta + 180^\circ + \theta_{M2}) \quad (D.4)$$

Where

- | | | |
|---------------------------------|---|---|
| f_{01} and f_{02} | = | Bias frequencies of Beams 1 and 2, respectively, in Hz |
| k_{11} and k_{12} | = | First order scale factors of Beams 1 and 2, respectively, in Hz/g |
| k_{21} and k_{22} | = | Nonlinearity of beams 1 and 2, respectively, in Hz/g ² |
| θ_{M1} and θ_{M2} | = | Misalignment of VBA halves 1 and 2, respectively, in radians. |

Readings are taken at $\theta = 0^\circ, 90^\circ, 180^\circ$ and 270° . It is assumed that misalignment effects on the g^2 effects are a secondary effect on a secondary effect and therefore negligible. It is also assumed that the misalignment effects are negligible for the $\theta = 90^\circ$ and $\theta = 270^\circ$ positions. The model now reduces to the following for Beam 1 at the four positions:

$$(f_1)_0 = f_{01} + k_{11} G \theta_{M1} \quad (D.5)$$

$$(f_1)_{90} = f_{01} + k_{11} G + k_{21} G^2 \quad (D.6)$$

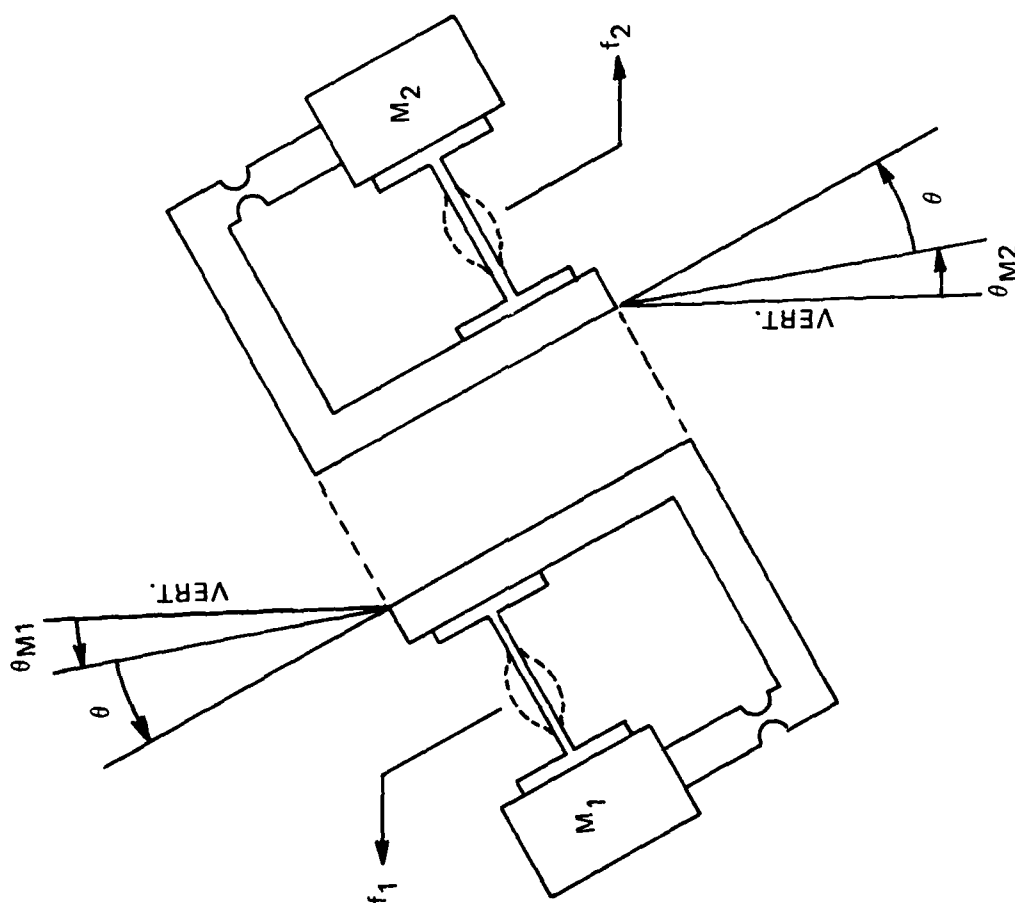
$$(f_1)_{180} = f_{01} - k_{11} G \theta_{M1} \quad (D.7)$$

$$(f_1)_{270} = f_{01} - k_{11} G + k_{21} G^2 \quad (D.8)$$

A similar set of equations is also obtained for Beam 2.

By summing and differencing Equations (D.5) through (D.8), the following expressions for the various coefficients are obtained:

$$f_{01} = \frac{(f_1)_0 + (f_1)_{180}}{2} \quad (D.9)$$



DUAL BEAM VBA 4 POSITION TEST
FIGURE D-1

$$k_{11} = \frac{(f_1)_{90} - (f_1)_{270}}{2g} \quad (D.10)$$

$$k_2 = \frac{(f_1)_{90} + (f_1)_{270} - 2f_{01}}{2g} \quad (D.11)$$

$$\theta_{M1} = \frac{(f_1)_0 - (f_1)_{180}}{(f_1)_{90} - (f_1)_{270}} \quad (D.12)$$

The Dual Beam VBA output is the difference frequency of the two beams, as described in Section 2. For the difference frequency the total VBA output model becomes:

$$f = K_0 + K_1 g + K_2 g^2 \quad (D.13)$$

Where

$$\text{Bias} = K_0 = f_{01} - f_{02} \text{ in Hz} \quad (D.14)$$

$$\text{Scale Factor} = K_1 = k_{11} + k_{12} \text{ in Hz/g} \quad (D.15)$$

$$\text{Nonlinearity} = K_2 = k_{21} - k_{22} \text{ in Hz/g}^2 \quad (D.16)$$

The input now is expressed

$$g = G \sin \left[\theta + \frac{\theta_{M1} + \theta_{M2}}{2} \right] \quad (D.17)$$

by Equation (D.17), which indicates that the misalignment effects become the average of the individual θ_M term.

From Equations (D.14) through (D.17), the following becomes apparent:

- The bias is nominally zero and the tolerance on the individual f_0 mismatches will determine its actual value. The important feature of common mode rejection is also achieved.
- The scale factor is nominally double that of the individual resonator.
- The nonlinearity is also nominally zero and the tolerance on the individual k_2 terms will determine the actual value. Additional zero trim of this term can also be achieved by changing slightly the mass of one of the proof masses.
- The net misalignment is the average of the individual misalignments. These terms can also be adjusted to zero by conventional means.

AD-A113 644

SINGER CO FAIRFIELD NJ KEARFOTT DIV F/G 17/7
NEW SENSOR CONCEPTS: LOW COST VIBRATING BEAM ACCELEROMETER. (U)
DEC 81 W C ALBERT F33615-80-C-1218

UNCLASSIFIED

KD-81-27

AFWAL-TR-81-1229

NL

2 of 2
AD-A
86-12

END

DATE

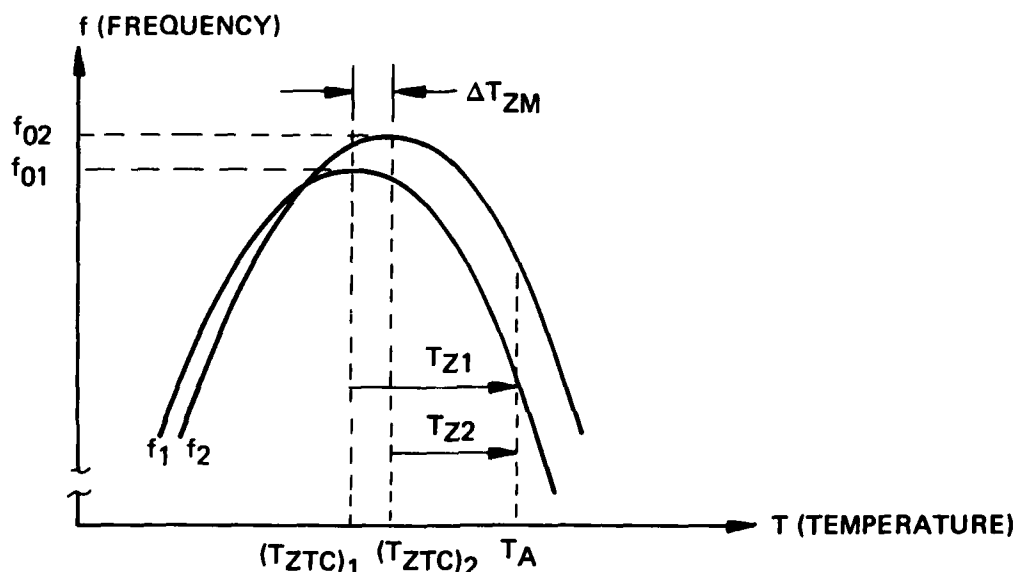
FILED

5-82

DTIC

APPENDIX E BIAS TEMPERATURE SENSITIVITY MODEL

For the dual beam VBA, a low bias temperature coefficient is achieved by matching the individual beam temperature sensitivities. The temperature coefficient of the proposed resonator, like that of all crystal resonators, is nonlinear. The proposed resonators have an empirically determined frequency vs temperature characteristic as illustrated in Figure E-1.



RESONATOR BIAS FREQUENCY VS TEMPERATURE
FIGURE E-1

The curve is described very well by a second order expression having the following typical form:

$$f = f_o + k_T T_Z^2 \quad (E.1)$$

The following definitions now apply to Figure E-1 and Equation (E.1).

T_{ZTC} is the Zero Temperature Coefficient (ZTC) temperature, sometimes called the turnover temperature, at which the resonator becomes virtually temperature insensitive. The temperature at which turnover occurs is adjustable to some extent by the proper selection of beam geometry and crystal axes rotation. Controlling the location of this point is a major area of investigation on the High Accuracy VBA Program. It is a

temperature-controlled device and is being designed so that its operating temperature coincides with the ZTC temperature. This will make the High Accuracy VBA virtually temperature insensitive for small temperature variations.

ΔT_{ZM} is the mismatch of individual resonator ZTC temperatures for the dual beam VBA. As the following analysis will show, it is convenient to use T_{Z1} and T_{Z2} as temperature differences to the accelerometer operating temperature T_A .

The VBA bias is the difference frequency $f_1 - f_2 = \Delta f$ and so from Figure E-1 considering just bias and bias thermal effects

$$\Delta f = f_1 - f_2 = f_{01} - f_{02} + k_{T1} T_{Z1}^2 - k_{T2} T_{Z2}^2 \quad (E.2)$$

$T_{Z1} + \Delta T_{ZM}$ is substituted for T_{Z2} and after expansion and rearranging, Equation (E.3) is obtained.

$$\Delta f = f_{01} - f_{02} + (k_{T1} - k_{T2}) T_{Z1}^2 - 2k_{T2} T_{Z1} \Delta T_{ZM} + k_{T2} \Delta T_{ZM}^2 \quad (E.3)$$

A change in accelerometer temperature T_A will essentially be a change in T_{Z1} since $(T_{ZTC})_1$ is a constant and so Equation (E.3) is differentiated with respect to T_{Z1} .

$$\frac{d(\Delta f)}{dT_{Z1}} = \frac{d(\Delta f)}{dT_A} = 2(k_{T1} - k_{T2}) T_{Z1} - 2k_{T2} \Delta T_{ZM} \quad (E.4)$$

To obtain the thermal sensitivity in terms of equivalent input acceleration (a) Equation (E.4) is divided by the accelerometer scale factor ($k_{11} + k_{22} \approx 2k_1$) (see Equation 2.3).

$$\frac{\Delta a}{\Delta T} = \frac{(k_{T1} - k_{T2}) T_{Z1}}{k_1} - \frac{k_{T2} \Delta T_{ZM}}{k_1} \quad (E.5)$$

Of the two remaining terms of Equation (E.5), the first is the result of a k_T mismatch between resonators and the second is the result of the ZTC mismatch. Because quartz is a well-ordered crystal material, the thermal characteristics are very consistent. An estimate of expected thermal sensitivity will be made for the following typical conditions:

$k_T = -1.3(10^{-3}) \text{ Hz}/^\circ\text{C}^2$. This is an experimentally determined coefficient.

$k_1 = 100 \text{ Hz/g}$. This is typical of the proposed scaling.

$(k_{T1} - k_{T2}) = 0.01 k_T$. It is estimated that this coefficient can be matched to 1% by proper selection.

$\Delta T_{ZM} = 0.25^\circ\text{C}$. It is estimated that a ZTC match of 0.25°C can be made by proper selection.

For a temperature controlled accelerometer application, the ZTC point and the operating temperature are designed to be coincident so that $T_{Z1} = 0$. For this condition only the ΔT_{ZM} term of Equation (E.5) remains and for the above typical conditions, $\Delta a/\Delta T = -3.2 \mu\text{g}/^\circ\text{C}$.

For no thermal control, the ZTC point is selected to be at the midpoint of the operating temperature range, so that the expected thermal deviation from this point is typically

$\pm 30^{\circ}\text{C}$. For the above typical conditions the T_{Z1} (thermal error) term of Equation (E.5) varies from 0 to $\pm 3.9\mu\text{g}/^{\circ}\text{C}$ at the extremes of the operating temperature range (0 and 60°C). This thermal error source, coupled with the ΔT_{ZM} term, indicates that the expected thermal sensitivity on bias will vary typically from zero to $-3.2 \pm 3.9 = +0.6$ to $-7.1\mu\text{g}/^{\circ}\text{C}$ over the operating temperature range of 0 to 60°C .

Because of the characteristics of quartz, the thermal error on bias will be very predictable and very repeatable for effective system modeling. To achieve the ultimate goal of $1\mu\text{g}/^{\circ}\text{C}$, a combination of resonator matching and system modeling is proposed.

APPENDIX F DUAL BEAM VBA CROSS AXIS SENSITIVITY

Cross-axis sensitivity is caused by a deflection of the proof mass due to mg_i forces as illustrated by Figure F-1. The T forces shown in the free body diagrams are the tension forces of the resonators represented by springs K. The F_H forces are those of the flexure.

From summation of forces in the input (i) direction the following expression for T_1 and T_2 are obtained.

$$T_1 = M_1 g_i - F_{Hi} \quad (F.1)$$

$$T_2 = -M_1 g_i - F_{Hi} \quad (F.2)$$

From the free body diagrams of Figure F-1, a summation of forces in the x direction, along with a summation of moments will indicate that

$$F_{Hi} = Mg_x \theta = Mg_x \frac{Mg_i}{\ell k} = \frac{M^2 g_x g_i}{\ell k} \quad (F.3)$$

Considering just the T_1 and T_2 effects on the beam frequency, and also considering that the dual beam VBA output is the difference of the two resonator frequencies, the following expression for the difference frequency is obtained.

$$\Delta f = f_1 - f_2 = k_{11} T_1 - k_{12} T_2 \quad (F.4)$$

Where k_1 and k_{12} are the first order frequency-tension sensitivities of resonators 1 and 2 respectively.

After combining Equations (F.1) through (F.4) the following is obtained

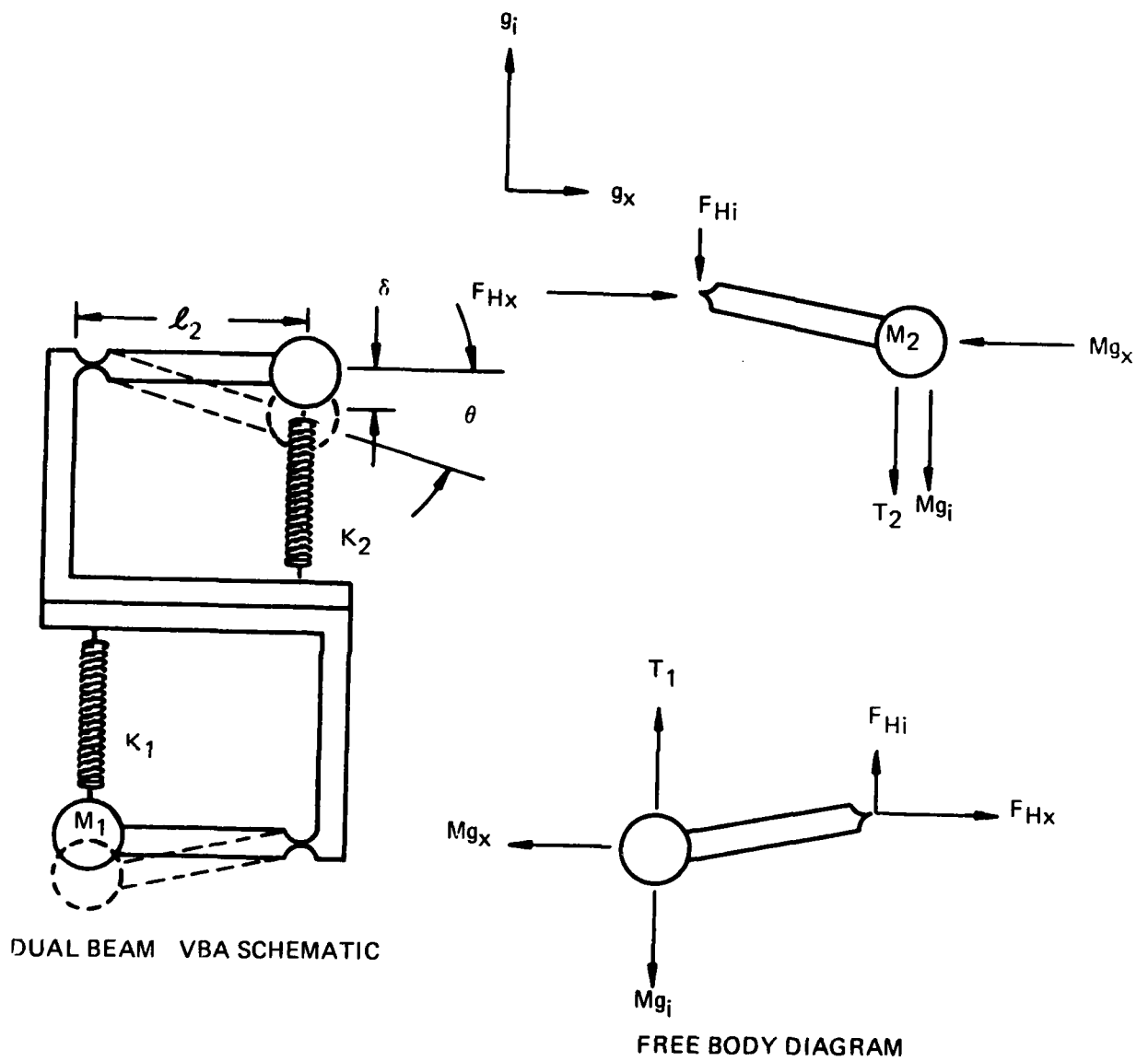
$$\Delta f = k_{11} \left(M_1 g_i - \frac{M_1^2 g_i g_x}{k \ell} \right) - k_{12} \left(-M_2 g_i - \frac{M_2^2 g_i g_x}{k \ell} \right) \quad (F.5)$$

For the $k_{11} \approx k_{12} \approx k_1$ and $M_1 \approx M_2 \approx M_1$ Equation (F.5) reduces to

$$\Delta f = 2 k_1 M g_i - k_1 \left[\left(\frac{M^2}{k \ell} \right)_1 - \left(\frac{M^2}{k \ell} \right)_2 \right] g_i g_x \quad (F.6)$$

Note that the $g_i g_x$ effects tend to cancel (common mode reject).

To obtain the difference frequency in terms of indicated acceleration, Equation (F.6) is divided by $2 k_1 M$ to yield the following



DUAL BEAM VBA CROSS AXIS SENSITIVITY
FIGURE F-1

$$g_{ind} = \frac{\Delta f}{2 k_1 M} = g_i - 1/2 \left[\left(\frac{M}{k \ell} \right)_1 - \left(\frac{M}{k \ell} \right)_2 \right] g_i g_x \quad (F.7)$$

Or considering just the $g_i g_x$ effects

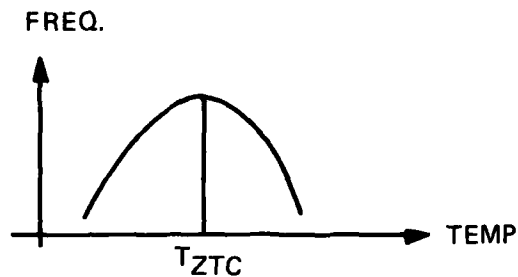
$$\frac{g_{ind}}{g_i g_x} = 1/2 \left[\left(\frac{M}{k \ell} \right)_1 - \left(\frac{M}{k \ell} \right)_2 \right] \quad (F.8)$$

For the typical values of $M = 9 \text{ g}$, $K = 8 (10^7) \text{ dyne/cm}$ and $\ell = 1 \text{ cm}$, $g_{ind}/g_i g_x = 0.06 \mu\text{g/g}^2$ per 1% mismatch of the $(M/K\ell)$ terms.

The $(M/k\ell)$ mismatch will be 10% or less and so no more than a $0.6 \mu\text{g/g}^2 g_x g_i$ error is expected.

APPENDIX G
LOW COST VBA - PARABOLIC TEMPERATURE COMPENSATION

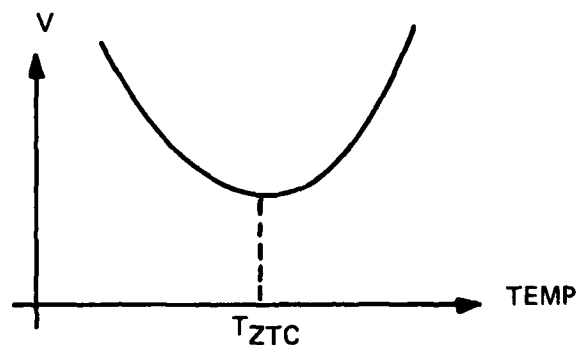
The frequency versus temperature characteristic of a typical beam possesses a parabolic signature



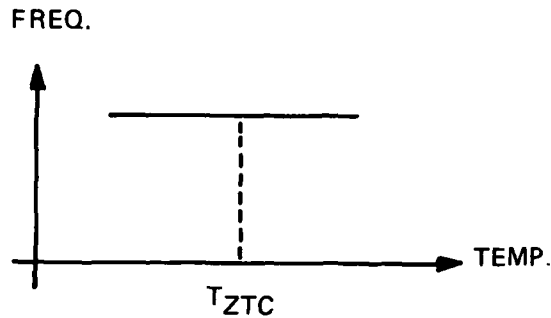
For a typical beam (Reference: "Saturating Oscillator Tests", an Engineering Technical Report by W. Albert), frequency may be related to supply voltage (provided the Constant Current Diode, CCD, is shorted)



Therefore, an effective temperature compensation for a single beam may be realized by parabolically varying the supply voltage with temperature



After compensation the frequency versus temperature characteristic becomes



To compensate, electronics must be designed which generate a beam supply voltage that varies as a parabolic function of temperature. In addition, the Turnover Temperature (T_{ZTC}) and Second Order Coefficient (SOC) of the electronics must be adjustable in order to cancel a particular beam's frequency versus temperature characteristic.

Consider the product of two linear functions of temperature:

$$\text{Let } G_1(T) = G_{01} + K_{G1} \Delta T$$

$$\text{and } G_2(T) = G_{02} + K_{G2} \Delta T$$

So, the product is

$$\begin{aligned} G_1(T) G_2(T) &= (G_{01} + K_{G1} \Delta T) (G_{02} + K_{G2} \Delta T) \\ &= G_{01} G_{02} + (G_{01} K_{G2} + G_{02} K_{G1}) \Delta T + K_{G1} K_{G2} (\Delta T)^2 \\ &= A_0 + A_1 \Delta T + A_2 (\Delta T)^2 \end{aligned}$$

$$\text{Where } A_0 = G_{01} G_{02}$$

$$A_1 = G_{01} K_{G2} + G_{02} K_{G1}$$

$$A_2 = K_{G1} K_{G2}$$

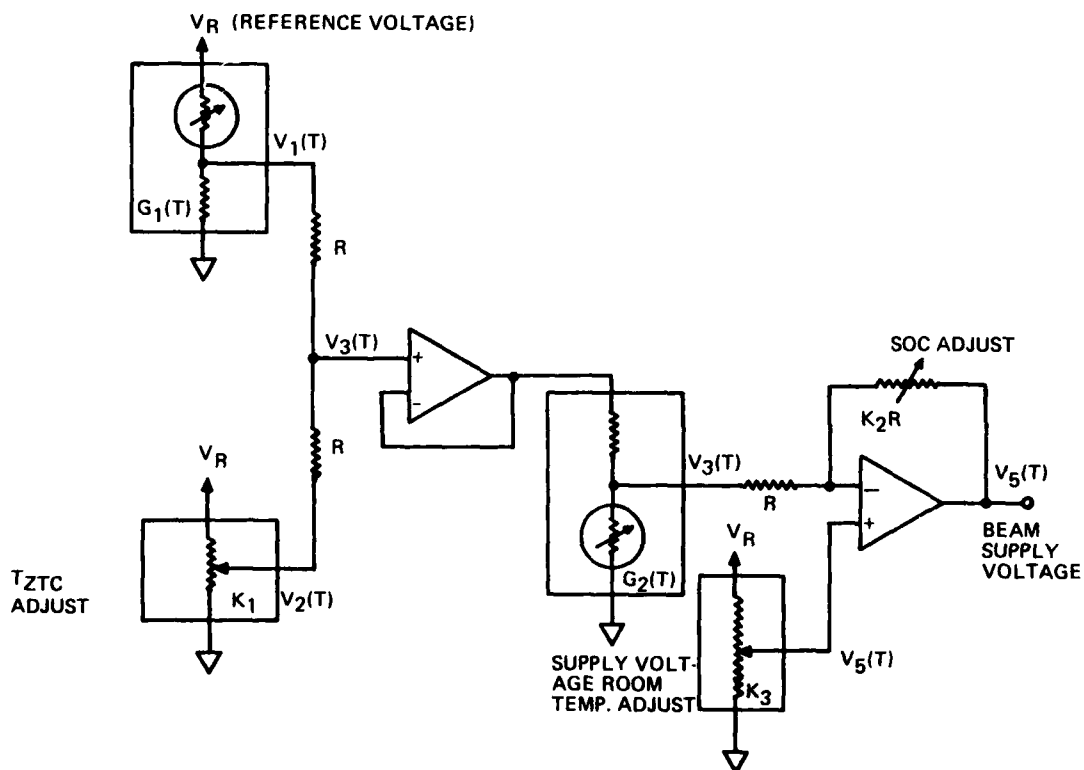
Note that a parabolic temperature characteristic is obtained. If one completes the square of the right-hand side of the above equation, the following expression results:

$$G_1(T) G_2(T) = A_0 - \frac{A_1^2}{4A_2} + A_2 \left(\Delta T + \frac{A_1}{2A_2} \right)^2$$

By inspection,

$$\begin{aligned} \text{Turnover Temp.} &= T_{ZTC} = \Delta T = -\frac{A_1}{2A_2} \\ \text{Second Order Coeff.} &= SOC = A_2 \end{aligned}$$

The following circuit is based on cascading linearly temperature sensitive voltage dividers created from conventional NTC thermistors to provide a beam supply voltage that varies parabolically with respect to temperature.



Where -

$$\left. \begin{aligned} G_1(T) &= G_0 + K_G \Delta T \\ G_2(T) &= G_0 - K_G \Delta T \end{aligned} \right\} \text{Thermistor Divider Gains}$$

Determine the beam supply voltage $V_s (T)$ -

$$G_1 (T) = G_0 + K_G \Delta T$$

$$\begin{aligned} V_1 (T) &= G_1 (T) V_R \\ &= G_0 V_R + K_G V_R \Delta T \end{aligned}$$

$$V_2 (T) = K_1 V_R$$

$$\begin{aligned} V_3 (T) &= \frac{1}{2} V_1 (T) + \frac{1}{2} V_2 (T) \\ &= \frac{1}{2} G_0 V_R + \frac{1}{2} K_G V_R \Delta T + \frac{1}{2} K_1 V_R \\ &= \frac{1}{2} G_0 V_R + \frac{1}{2} K_1 V_R + \frac{1}{2} K_G V_R \Delta T \end{aligned}$$

$$G_2 (T) = G_0 - K_G \Delta T$$

$$\begin{aligned} V_4 (T) &= G_2 (T) V_3 (T) \\ &= (G_0 - K_G \Delta T) \left(\frac{1}{2} G_0 V_R + \frac{1}{2} K_1 V_R + \frac{1}{2} K_G V_R \Delta T \right) \\ &= \frac{1}{2} V_R (G_0 - K_G \Delta T) (G_0 + K_1 + K_G \Delta T) \\ &= \frac{1}{2} V_R (G_0 (G_0 + K_1) + (G_0 K_G - G_0 K_G - K_1 K_G) \Delta T - K_G^2 (\Delta T)^2) \\ &= \frac{1}{2} V_R (G_0 (G_0 + K_1) - K_1 K_G \Delta T - K_G^2 (\Delta T)^2) \end{aligned}$$

$$V_5 (T) = K_3 V_R$$

$$\begin{aligned} V_s (T) &= -K_2 V_4 (T) + (K_2 + 1) V_5 (T) \\ &= -\frac{1}{2} K_2 V_R \left[G_0 (G_0 + K_1) - K_1 K_G \Delta T - K_G^2 (\Delta T)^2 \right] + (K_2 + 1) K_3 V_R \\ &= \left[K_3 (K_2 + 1) - \frac{1}{2} K_2 G_0 (G_0 + K_1) \right] V_R \\ &\quad + \left(\frac{1}{2} K_1 K_2 K_G V_R \right) \Delta T \\ &\quad + \left(\frac{1}{2} K_2 K_G^2 V_R \right) (\Delta T)^2 \end{aligned}$$

$$\therefore V_s (T) = A_0 + A_1 \Delta T + A_2 (\Delta T)^2$$

$$\text{Where } A_0 = \left[K_3 (K_2 + 1) - \frac{1}{2} K_2 G_0 (G_0 + K_1) \right] V_R$$

$$A_1 = \frac{1}{2} K_1 K_2 K_G V_R$$

$$A_2 = \frac{1}{2} K_2 K_G^2 V_R$$

Note: ΔT represents temperature deviation about Room Temp. (+25°C).

G01 represents divider G1's output at Room Temp.

The above circuit features simple adjustment of the Turnover Temperature, Second Order Coefficient and supply voltage at room temperature.

For example

$$\begin{aligned}\text{Turnover Temp.} = T_{ZTC} = \Delta T &= \frac{-A_1}{2A_2} = - \frac{\frac{1}{2}K_1 K_2 K_G V_R}{2 (\frac{1}{2}K_2 K_G^2 V_R)} \\ &= - \frac{K_1}{2K_G}\end{aligned}$$

Assuming K_G is fixed, the Turnover Temperature may be adjusted simply by varying divider K_1 .

Also,

$$\text{Second Order Coeff.} = \text{SOC} = A_2 = \frac{1}{2}K_2 K_G^2 V_R$$

Assuming K_G and V_R are fixed, the Second Order Coefficient may be adjusted by varying resistor K_2 .

Finally,

$$\begin{aligned}\text{Supply Voltage (@Room Temp.)} = V_s (\Delta T = 0) &= A_0 \\ &= [K_3 (K_2 + 1) - \frac{1}{2}K_2 G_O (G_O + K_1)] V_R\end{aligned}$$

Assuming G_O and V_R are fixed and K_1 and K_2 have been determined, then the supply voltage may be adjusted by varying divider K_3 .

Design Example

Assume the following fixed parameter values in the circuit

$G_O = 0.5$	(Divider Output at Room Temp (+25°C))
$K_G = 0.010^{\circ\text{C}}^{-1}$	(Corresponds to -4%/°C Negative Temp. Coeff.
$= 0.0056^{\circ\text{F}}^{-1}$	Thermistor Divider)
$V_R = 10.0 \text{ VDC}$	

Assume the following parameters for the beam to be compensated:

$$T_{ZTC} = \Delta T = -25^{\circ}\text{C} \quad (\text{Where } \Delta T \text{ represents Temp. Deviation about Room Temp. } (+25^{\circ}\text{C}))$$

$$\text{SOC} = -12 \text{ PPM}/^{\circ}\text{F}^2$$

$$f_0 = 40,000 \text{ Hz}$$

$$\frac{\Delta f}{\Delta V} = +2.9 \text{ Hz/VDC} \quad (\text{Supply sensitivity obtained from "Saturating Oscillator Tests" Report})$$

$$V_s = 5.0 \text{ VDC} \quad (\text{Supply voltage desired at Room Temp. } (+25^{\circ}\text{C}))$$

$$\text{Since, } T_{ZTC} = -\frac{A_1}{2A_2} = -\frac{K_1}{2K_G}, \text{ thus,}$$

$$\begin{aligned} K_1 &= -2T_{ZTC} K_G \\ &= -2 (-25^{\circ}\text{C}) (0.010^{\circ}\text{C}^{-1}) \end{aligned}$$

$$K_1 = 0.500 \text{ V/V}$$

Matching the Second Order Coefficients for the beam and supply voltage temperature characteristics via the supply sensitivity $\Delta f/\Delta v$ yields,

$$\frac{(\text{SOC}) (f_0)}{\Delta f / \Delta v} = -A_2 = -\frac{1}{2} K_2 K_G^2 V_R$$

$$\begin{aligned} \text{Thus, } K_2 &= -\frac{2(\text{SOC}) (f_0)}{(\Delta f / \Delta v) (K_G^2) (V_R)} \\ &= -\frac{2(-12 \text{ PPM}/^{\circ}\text{F}^2) (40,000 \text{ Hz})}{(+2.9 \text{ Hz/VDC}) (0.0056^{\circ}\text{F}^{-1})^2 (10.0 \text{ VDC})} \end{aligned}$$

$$K_2 = 1.056 \text{ } \Omega/\Omega$$

$$\text{Finally, } V_s = \left[K_3 (K_2 + 1) - \frac{1}{2} K_2 G_0 (G_0 + K_1) \right] V_R$$

$$\frac{V_s}{V_R} + \frac{1}{2} K_2 G_0 (G_0 + K_1) = K_3 (K_2 + 1)$$

$$\begin{aligned} \text{Thus, } K_3 &= \frac{1}{K_2 + 1} \left[\frac{V_s}{V_R} + \frac{1}{2} K_2 G_0 (G_0 + K_1) \right] \\ &= \frac{1}{1.056 + 1} \left[\frac{5.0 \text{ VDC}}{10.0 \text{ VDC}} + \frac{1}{2} (1.056) (0.5) (0.5 + 0.500) \right] \end{aligned}$$

$$K_3 = 0.372 \text{ V/V}$$

Therefore, in this typical example, realizable values are obtained for K_1 , K_2 and K_3 .

Evaluate A_0 -

$$\begin{aligned} A_0 &= \left[K_3 (K_2 + 1) - \frac{1}{2} K_2 G_0 (G_0 + K_1) \right] V_R \\ &= \left[(0.372) (1.056 + 1) - \frac{1}{2} (1.056) (0.5) (0.5 + 0.500) \right] 10 \text{ VDC} \\ \therefore A_0 &= 5.01 \text{ VDC} \end{aligned}$$

Evaluate A_1 -

$$\begin{aligned} A_1 &= \frac{1}{2} K_1 K_2 K_G V_R \\ &= \frac{1}{2} (0.500) (1.056) (0.010^{\circ\text{C}^{-1}}) (10.0 \text{ VDC}) \\ A_1 &= 0.0264 \text{ VDC}/^{\circ}\text{C} \end{aligned}$$

Evaluate A_2 -

$$\begin{aligned} A_2 &= \frac{1}{2} K_2 K_G^2 V_R \\ &= \frac{1}{2} (1.056) (0.010^{\circ\text{C}^{-1}})^2 (10.0 \text{ VDC}) \\ \therefore A_2 &= 5.28 \times 10^{-4} \text{ VDC}/^{\circ}\text{C}^2 \end{aligned}$$

Therefore,

$$V_S(T) = 5.01 + 0.0264 \Delta T + 5.28 \times 10^{-4} (\Delta T)^2$$

Note: V_S is in VDC when ΔT is in $^{\circ}\text{C}$. ΔT is referenced to Room Temp. ($+25^{\circ}\text{C}$).

So,

<u>T</u>	<u>ΔT</u>	<u>$V_S(T)$</u>
($^{\circ}\text{C}$)	($^{\circ}\text{C}$)	(VDC)
-50	-75	6.00
-25	-50	5.01
0	-25	4.68
+25	0	5.01
+50	+25	6.00
+75	+50	7.65

Supply voltage versus temperature appears as:

